THE UNIVERSITY *of* EDINBURGH

This thesis has been submitted in fulfilment of the requirements for a postgraduate degree (e.g. PhD, MPhil, DClinPsychol) at the University of Edinburgh. Please note the following terms and conditions of use:

- This work is protected by copyright and other intellectual property rights, which are retained by the thesis author, unless otherwise stated.
- A copy can be downloaded for personal non-commercial research or study, without prior permission or charge.
- This thesis cannot be reproduced or quoted extensively from without first obtaining permission in writing from the author.
- The content must not be changed in any way or sold commercially in any format or medium without the formal permission of the author.
- When referring to this work, full bibliographic details including the author, title, awarding institution and date of the thesis must be given.

Lattice Phenomenology of Minimal Walking Technicolor

Eoin Kerrane

A thesis submitted in fulfilment of the requirements
for the degree of Doctor of Philosophy
to the
University of Edinburgh
November 11, 2011

Abstract

As results from the Large Hadron Collider (LHC) begin to shed light on the physics of the electroweak scale, which has been of primary interest to theorists for many years, we have entered a phase where critical judgement of the many models of electroweak symmetry breaking (EWSB) that have been developed in recent years will be possible.

As this process continues, those models which are not additionally constrained by emerging data attract increased scrutiny and interest. In this respect, technicolor models, in which EWSB occurs dynamically through the spontaneous chiral symmetry breaking in a new strongly coupled sector, are the subject of growing research activity.

The focus of this work is a program of investigation of Minimal Walking Technicolor (MWT), a candidate theory for the new strongly coupled sector of a model of dynamical EWSB using Lattice Gauge Theory (LGT) techniques.

We have performed an improved comprehensive study of mesonic spectral observables within MWT, with emphasis on finite volume effects arising from finite temporal and spatial boundaries. Our results clarify the role of finite volume effects in such studies, while confirming the near-conformal behaviour of the theory in the infra-red, and indicating a relatively small value of the mass anomalous dimension, in agreement with other studies.

We also describe a calculation of the leading order hadronic vacuum polarisation contribution to the anomalous magnetic moment of the muon from a lattice simulation of 2+1 flavour lattice QCD using Domain Wall Fermions (DWF). We investigate in detail a number of systematic uncertainties involved in this calculation, determining how to effectively bring them under control, and obtain a result in close agreement with previous determinations from LGT studies, from calculations based on independent experimental data, and from experimental

measurements.

We present a preliminary calculation of the contribution to the electroweak S parameter from MWT, using a mixed-action simulation involving the DWF action used for the valence sector combined with gauge configurations generated using the Wilson fermion action for sea quarks.

Declaration

Except where otherwise stated, the research undertaken in this thesis was the unaided work of the author. Where the work was done in collaboration with others, a significant contribution was made by the author.

E. Kerrane
June 2010

Acknowledgements

I would like to record my thanks to all those who have helped me in the course of this work. In particular, the following:

Professor Luigi Del Debbio, Dr. Claudio Pica, Dr. Antonio Rago, Dr. Agostino Patella, Professor Biagio Lucini, Dr. Peter Boyle, Dr. James Zanotti and many others.

Sincere thanks go to my friends and colleagues who have supported me warmly throughout my time as a graduate student. Particular thanks to the members of The Edinburgh Samba School for helping me to remain human through these years.

Contents

Chapter 1

Introduction

1.1 Dynamical Electroweak Symmetry Breaking at the LHC

The Standard Model of particle physics [1, 2] has been established as the description of electroweak and strong interactions for many decades. Discounting gravity, it provides a quantitative explanation of the forces between all known fundamental particles. It has been verified repeatedly through experiment, and has accurately predicted the existence of several particles which were subsequently discovered. There has been no measurement or discovery which has contradicted the predictions of the Standard Model save the recent observation of neutrino oscillations [3].

There is, however, one element of the Standard Model, which has not yet been verified [4–6]. The Standard Model is usually considered to include an explanation for the breaking of the electroweak symmetry of nature, that is, the most naive mechanism, involving an elementary Higgs field. However, this model is certainly not the only such method that can be considered, and in fact involves some undesirable features.

As such, much effort has been devoted to formulating a more desirable mechanism, with some success. Many candidate models have been developed, with varying degrees of attractiveness. Considerable effort has gone into studying these models, and determining their phenomenological consequences and the constraints on their parameters which emerge from existing experimental data.

This effort has become more intense in recent years as the date of the

commencement of the operation of the LHC approached and continues to increase as the LHC has started to produce results which are already impacting the constraints on these models and promise to have sweeping implications as the gratifying large amounts of data being generated are analysed.

This work is concerned with the investigation of one of these candidate models, called technicolor. This model has been around for a long time, but is still generating significant interest and attention. In the LHC era it remains one of the foremost candidates for the explanation of electroweak symmetry breaking and the continued results of the searches for signals of technicolor at the LHC are eagerly awaited. Here, we focus on numerical simulations investigating a theory which is a candidate for the key sector in a technicolor model. Such simulations aim to detect renormalisation behaviour which is deemed necessary to allow such theories to avoid constraints from existing experimental results.

Because of the strongly coupled nature of these theories, we turn to the non-perturbative power of lattice gauge theory to tackle these questions. This formulation has been heavily developed over a number of years in order to make accurate calculations in the low-energy strongly coupled regime of QCD. Improvements in theoretical understanding, algorithmic efficiency and computational power have led to significant advances in the precision of such studies, crucially with the important inclusion of fully dynamical fermions, resulting in many low energy quantities being calculated with remarkable accuracy. With the majority of the ground-work for the application of these techniques being completed, attention has turned in recent years to other applications of the formulation, of which one of the most fruitful is the investigation of technicolor models.

1.2 Present Work and Thesis Outline

In Chap. 2 we introduce the model involved, building from the Standard Model to electroweak symmetry breaking through to the formulation of technicolor models, in particular introducing the particular model we will study, minimal walking technicolor (MWT). In Chap. 3 we describe numerical studies of MWT and other technicolor models using the formulation of lattice gauge theory, which will also be the method of our study. We outline the goals and the techniques used

to detect the desired signals.

In Chap. 4 we present a comprehensive study of sytematic uncertainties in spectroscopic analyses of MWT, focusing on finite-volume effects present in the results for spectroscopic observables. This study highlights the important nature of competing finite-volume effects in such simulations, while supporting existing conclusions concerning the conformal nature of this theory in the infra-red.

Chap. 5 presents a computation of the leading order QCD vacuum polarisation contribution $a_\mu^{(2)\mathrm{had}}$ to the anomalous magnetic moment of the muon a_μ, through a fully dynamical 2+1 flavour simulation of lattice QCD using domain wall fermions (DWF). This project was chosen for this work because of the similarity of the methods involved to the procedure required for the final project in this work on the S parameter in MWT. Our computation of $a_\mu^{(2)\mathrm{had}}$ discusses some of the systematic uncertainties present in the calculation in detail, and identifies a prescription for bringing them under control. We find a competitive result for $a_\mu^{(2)\mathrm{had}}$ in the limit of physical quark masses

$$a_\mu^{(2)\mathrm{had}} = 641(33)(32) \times 10^{-10} \tag{1.1}$$

Finally Chap. 6 presents preliminary results of a computation of the contribution to the S parameter from MWT, using a mixed-action calculation involving the DWF valence action combined with gauge ensembles generated using the Wilson fermion action. While we are not in a position to present quantitative results for the MWT contribution to S, we have illustrated the feasibility of one of the crucial steps in the computation, the tuning of the DWF action to match the Wilson sea.

Chapter 2

Minimal Walking Technicolor

2.1 Electroweak Symmetry Breaking from an Elementary Higgs

In this section we will describe one candidate description of electroweak symmetry breaking (EWSB), which provides the model to be tested through simulation in this thesis. In order to do this we will first describe in detail the most naive model which could explain electro-weak symmetry breaking (EWSB), which is usually considered as an ingredient of the Standard Model.

2.1.1 Non-Abelian Gauge Theory

The Standard Model is a quantum field theory built by combining a number of different sectors, each of which independently constitutes a non-Abelian gauge theory. Such a theory is defined by considering a theory of matter fields $\chi(x)$ which is symmetric under a local symmetry defined by a representation $\mathcal{D}$ of a Lie group $\mathcal{G}$ on the space of χ fields V

$$\chi(x) \to \mathcal{D}(g(x))\chi(x) \tag{2.1}$$

where $g(x) \in \mathcal{G}$ for each x in Minkowski space-time. In order to define such a theory we must construct the covariant derivative D_μ as

$$D_\mu\chi(x) = \partial_\mu\chi(x) + d(A_\mu(x))\chi(x) \tag{2.2}$$

where $A_\mu(x)$ is a vector field, a spin 1 representation of the Poincare symmetry group. $A_\mu(x)$ are elements of the Lie algebra $\mathcal{L}(\mathcal{G})$, so we can write $A_\mu(x) = A^a_\mu(x)T_a$ in terms of T_a the generators of $\mathcal{L}(\mathcal{G})$, and d is the representation of $\mathcal{L}(\mathcal{G})$ induced by $\mathcal{D}$. For the theory to be symmetric under the action of $\mathcal{G}$, $A_\mu(x)$ must transform as

$$A_\mu(x) \to g(x)A_\mu(x)g^{-1}(x) - (\partial_\mu g)(x)g^{-1}(x) \tag{2.3}$$

so as to ensure that

$$D_\mu\chi(x) \to \mathcal{D}(g(x))D_\mu\chi(x) \tag{2.4}$$

We define the field strength tensor $F_{\mu\nu}$ as

$$\begin{aligned} F_{\mu\nu}(x) = [D_\mu, D_\nu] =& \partial_\mu d(A_\nu(x)) - \partial_\nu d(A_\mu(x)) + [d(A_\mu(x)), d(A_\nu(x))] \\ =& \partial_\mu d(A_\nu(x)) - \partial_\nu d(A_\mu(x)) + d([A_\mu(x), A_\nu(x)]) \\ =& (\partial_\mu A^a_\nu(x) - \partial_\nu A^a_\mu(x) + c_{bc}{}^a A^b_\mu(x)A^c_\nu(x))d(T_a) \\ \equiv& F^a_{\mu\nu}(x)d(T_a) \end{aligned} \tag{2.5}$$

This ensures that

$$F_{\mu\nu} \to \mathcal{D}(g(x))F_{\mu\nu}\mathcal{D}^{-1}(g(x)) \tag{2.6}$$

From this we can see that the coefficients of $F_{\mu\nu}$ are independent of the representation used, and so we can define a kinetic term for the vector fields $A_\mu(x)$ which will appear in the Lagrangian density of the theory in terms of $F^f_{\mu\nu}$, the field strength tensor in the fundamental representation, as

$$\mathcal{L} \supset \frac{1}{4g^2}\kappa(F^f_{\mu\nu}, F^{f\mu\nu}) \tag{2.7}$$

where κ is the Killing form on $\mathcal{G}$ and g is the coupling constant of the theory. In the case of the compact groups we will consider, $\kappa(T_a, T_b) = \kappa_{ab} = -\delta_{ab}$ and this reduces to

$$\mathcal{L} \supset -\frac{1}{4g^2}F^a_{\mu\nu}(x)F^{a\mu\nu}(x) \tag{2.8}$$

If we take $\chi(x)$ to be a scalar field, i.e. a spin zero representation of the

Poincare group, written $\Phi(x)$, the standard kinetic term for $\phi(x)$ is written[1]

$$\mathcal{L} \supset \frac{1}{2}(\partial_\mu \Phi)^\dagger(x)\partial^\mu \Phi(x) \tag{2.9}$$

This term is rendered gauge invariant by making the substitution $\partial_\mu \rightarrow D_\mu$:

$$\mathcal{L} \supset \frac{1}{2}(D_\mu \Phi)^\dagger(x) D^\mu \Phi(x) \tag{2.10}$$

This is called the *principle of minimal coupling*. Similarly for a fermionic field $\psi(x)$, a spin $\frac{1}{2}$ representation of the Poincare group, the Dirac action is also rendered gauge invariant through the principle of minimal coupling, becoming

$$\mathcal{L} \supset \bar{\psi}(x)(i\gamma^\mu D_\mu - m)\psi(x) \tag{2.11}$$

where the γ^μ are the Dirac matrices and $\bar{\psi}(x) = \psi^\dagger(x)\gamma^0$, and m is the mass of the fermion described by $\psi(x)$.

2.1.2 The Standard Model

The Standard Model involves three gauge symmetries, those of *colour*, *weak isospin* and *hypercharge*, with gauge groups, $SU(3)$, $SU(2)$ and $U(1)$ respectively. The action of the theory contains a term of the form (2.7) (or equivalently (2.8)) for each symmetry, involving distinct coupling constants g_s, g and g' respectively. Together, the weak isospin and hypercharge sectors make up the *electro-weak* theory, while the colour sector considered in isolation is referred to as *quantum chromo-dynamics* (QCD).

The fermions coupling to these gauge theories come in two categories. The *leptons* do not transform under the colour gauge symmetry of $SU(3)$, and as a result they do not couple to the gauge bosons of QCD, the *gluons*. The *quarks* however, are charged under colour $SU(3)$, as well as under the weak isospin and hypercharge symmetries. The leptons come in pairs. That is, if we describe the fields representing the two lightest leptons (the electron e^+ and the neutrino ν_e), the rest of the leptons are described by exact copies of the same fields. These copies are called *generations*. The only difference between the generations is the physical mass of the particles, to which we will return shortly. There are three

[1] We allow $\phi(x)$ to be a complex field

generations in the case of the leptons. There are also three generations of quarks, but in this case they must be introduced in a combined fashion. The relationship between the three generations of quarks and leptons remains unexplained, as does the vast hierarchy in their masses.

The leptons are defined as follows. Let us introduce fermion fields $L(x)$ and $R(x)$. As stated the leptons are invariant under the colour $SU(3)$ gauge transformation. $L(x)$ is defined to transform in the fundamental of the weak isospin $SU(2)$ while $R(x)$ is invariant. This means that, $L(x)$ is in fact a doublet of fermion fields. Taking the family involving the electron as an example, $L(x)$ and $R(x)$ would be defined in terms of the physical electron e and neutrino ν_{e} as

$$L(x) = \begin{pmatrix} \nu_{\mathrm{e}}(x) \\ e_{\mathrm{L}}(x) \end{pmatrix} \qquad\qquad R(x) = e_{\mathrm{R}}(x) \tag{2.12}$$

where

$$e_{\mathrm{R/L}}(x) = P_{\mathrm{R/L}} e(x) = \frac{1}{2}(1 \pm \gamma_5) e(x) \tag{2.13}$$

The representations of $U(1)$ are 1-dimensional, and can be written $\mathcal{D}(z) = z^Y$ for some real Y. For our purposes we call Y the *hypercharge* and assign it as $Y = -1$ for $R(x)$ and $Y = -\frac{1}{2}$ for $L(x)$. It is this choice that results in the correct electromagnetic charges of 0 for ν_{e} and -1 for e, along with the correct couplings to the electro-weak gauge bosons.

Kinetic terms for these leptons can be introduced very easily:

$$\mathcal{L} \supset \bar{L}(x) i\gamma^\mu D_\mu L(x) + \bar{R}(x) i\gamma^\mu D_\mu R(x), \tag{2.14}$$

however there is no gauge invariant mass term which can be constructed from the fields L and R. A mass term for these fields will be generated from a Yukawa coupling to an additional $SU(2)$ doublet, called the Higgs field, which will aquire a non-zero *vacuum expectation value* (VEV). The Higgs field,

$$\phi(x) = \begin{pmatrix} \phi_1(x) \\ \phi_2(x) \end{pmatrix}, \tag{2.15}$$

is scalar under Lorentz transformations and carries hypercharge $Y = \frac{1}{2}$. The

Higgs sector of the Lagrangian is

$$\mathcal{L} \supset (D^\mu \phi(x))^\dagger D_\mu \phi(x) - V(\phi(x)) \tag{2.16}$$

The potential $V(\phi(x))$ is assumed to have a minimum at $\phi_0(x)$ with $|\phi_0^\dagger \phi_0| = \frac{1}{2}v^2$, i.e. the field ϕ has a non-zero VEV, in contrast to every other field in the model. It is entirely trivial to construct a functional form for $V(\phi(x))$ with this property, but how such a form involving an elementary Higgs field might arise will not be discussed here. The physical degrees of freedom can be seen by expanding $\phi(x)$ about this minimum ϕ_0, which because of the gauge symmetry can be written without loss of generality as

$$\phi_0 = \frac{1}{\sqrt{2}} \begin{pmatrix} 0 \\ v \end{pmatrix} \qquad \phi(x) = \phi_0 + H \tag{2.17}$$

The electro-weak gauge bosons are coupled to the Higgs field through the covariant derivative D_μ, and when the Higgs field is expanded around its VEV, mass terms for the physical W and Z bosons arise, and thus the electro-weak gauge symmetry is broken [4–6]. The photon remains massless, and so the $U(1)$ of electro-magnetism remains unbroken.

Gauge invariant mass terms for the leptons can be generated by including Yukawa terms of the form

$$\mathcal{L} \supset -\sqrt{2}G[\bar{L}(x)\phi(x)R(x) + \bar{R}(x)\phi^\dagger(x)L(x)]. \tag{2.18}$$

Taking L and R to again relate to the electron family, when expressed in terms of the physical degrees of freedom, this coupling would produce a mass for the electron of the form $m = Gv$. This term does not generate a mass for the related neutrino field, which requires the inclusion of an accompanying right handed neutrino which is invariant under the weak isospin transformation, or alternatively a term which has mass dimension 5 in the Lagrangian, making it non-renormalisable.

The inclusion of the quarks into the theory is very similar to that of the leptons, although in the case of the quarks there are no accompanying neutrinos, the left-handed $SU(2)$ quark doublet comprises the left-handed component of the "up-type" quark with electromagnetic charge $\frac{2}{3}$ in units of the charge on the

electron, and the left-handed component of the "down-type" quark with charge $-\frac{1}{3}$. Both up and down-type quarks have right handed components which are included as singlets under $SU(2)$. The process is further complicated by non-trivial relations between the quark families parameterised by a complex rotation matrix known as the Cabibbo-Kobayashi-Maskawa (CKM) matrix [7, 8].

Despite these intricacies, the couplings of the quarks to the Higgs field are introduced in a very similar manner to those of the leptons, with the conjugate field $\phi^c(x) = i\tau\phi^*(x)$ providing an additional combination of fields which allows for the generation of masses for the up and down-type quarks. As such the non-zero VEV of the Higgs generates the required quark masses in an analogous fashion to the mechanism for the leptons.

This method of coupling the electro-weak gauge bosons and fermion content of the model to an elementary scalar Higgs field which is forced to attain a VEV then exhibits all the required features of EWSB, including fermion masses, in the most simple way possible, and it is this powerful elegance that has led to importance of the Higgs mechanism in the Standard Model.

2.1.3 Problems with the Standard Model

Despite the attractiveness of this simple model, on closer inspection it has some features which commonly lead to the conclusion that this model, while undoubtedly applicable to physics at or below the energy scale of EWSB, is in fact most likely to be an effective description of a more complex theory which provides the true description of nature above the EWSB scale.

Besides the obvious question of how the required potential might be generated correctly, there are two main commonly raised issues which we will describe.

1. Triviality

   The simplest parameterisation of the Higgs potential $V(\phi(x))$ which produces the correct VEV for Higgs field is written

   $$V(\phi) = \lambda(\phi^\dagger(x)\phi(x) - v^2)^2 \tag{2.19}$$

   with $v^2 \geq 0$. However, an analysis of the running of the parameter λ under the renormalisation group indicates that on the removal of the cut-off Λ needed to regularise the theory, i.e. sending $\Lambda \to \infty$, the self-coupling

λ approaches zero. This indicates that a model with the potential (2.19) can only describe physics up to a certain scale above which new physics must be relevant, that is it can only be an effective description of a more complex and more fundamental theory. This is significant because any form of $V(\phi(x))$ which produces the correct VEV will be well approximated by (2.19) near the vacuum state.

2. Naturalness

   If the field responsible for EWSB is determined to be an elementary spin zero scalar, it would be the first such particle observed in nature, all the other fields which are currently believed to be elementary being either spin one-half fermions, or spin one vector bosons. Despite the fact that this would be a novel discovery, it would be surprising because of the symmetry properties of scalar fields.

   One important feature of the fermion and gauge boson fields of the standard model is that in each case there is a symmetry of the theory which prevents the inclusion of explicit mass terms for these fields in the bare Lagrangian of the theory. Gauge symmetries are responsible for this in the case of the vector bosons. This restriction means, in turn, that these mass terms cannot be generated immediately through quantum effects, and as a result, that the gauge bosons and fermions do not receive large additive renormalisation shifts to their masses.

   In the case of a scalar field, there are only two symmetries which could do this job. They are

   (a) a shift symmetry, $\phi(x) \rightarrow \phi(x) + f(x)$, however requiring that the Higgs field respect this symmetry would restrict the Higgs to derivative couplings, making it appear as a Goldstone boson of some other broken symmetry.

   (b) supersymmetry [9–11], which requires that each particle in the theory be accompanied by a *super-partner* field with a spin differing by one-half. The loop corrections to many quantities involving these fields then cancel due to the minus sign associated with a fermionic loop, meaning that the mass of a scalar field will not receive a large additive renormalisation shift. This property was described in the context of

theories with a compactified extra dimension, both in the continuum and on the lattice in [12].

In addition to this attractive feature, supersymmetry is a very appealing theoretical construct with many other beautiful properties. As such it has attracted significant interest, both in efforts to understand how it might be realised as an extension of the Standard Model and the resulting phenomenological implications, and also in independent research involving many different theories not necessarily directly related to the Standard Model.

Given that neither of these symmetries are realised in the Standard Model, there is a significant question as to whether this theory can be viewed as natural. The problem is that without an appropriate symmetry to protect it, the mass of the Higgs boson would receive a large additive shift after renormalisation of the theory. This shift would be of the order of the ultra-violet cut-off of the theory, and so if we expect this theory to be an accurate representation of physics up to energies up to and beyond the TeV-scale, then the bare Higgs mass would require significant fine-tuning in order to produce the expected physical Higgs mass around the 100-200 GeV scale. Called the hierarchy problem, this has been very important in particle physics for many years and has motivated a huge effort to construct a valid, sensible theory as a solution.

2.1.4 Solutions to the hierarchy problem

Numerous extensions of the Standard Model have been invented, designed to alleviate these problems while still representing observed low-energy physics [13]. Invariably these models are motivated by simple attractive concepts, but often result in a large amount of complexity at intermediate and high energies in order to produce a consistent model.

Supersymmetric models for example, while solving the hierarchy problem in a very simple and elegant manner, produce many phenomenological questions. The most obvious of these is the observation that we have not detected any superpartners of Standard Model particles in experiments up to now. This means that supersymmetry must be broken at some energy above the scale of EWSB.

This can be achieved in a number of ways, but after this and other issues have been addressed, the model no longer appears anywhere near as simple or powerful as the initial idea.

In this way, an expansive and diverse collection of models are currenty in circulation and development, vying to be perceived as the most elegant and comprehensive candidate for the mechanism responsible for EWSB, and the most effective solution to the ills of the Standard Model. Proponents of each model also hope that their favourite theory will receive supportive indications from experimental data that continues to emerge from runs at the Tevatron collider at Fermilab in Illinois, US, and the enormous bulk of early data that is beginning to be delivered from the various experiments at the LHC at CERN.

There have been some interesting suggestions from this large volume of LHC data, and while there are indications they may be on the verge of finding the elusive Higgs boson [14, 15], there is, at the moment, what is for many, a surprising absence of new particles being discovered at the record energies which are being probed [16, 17]. The situation is very preliminary, and will no doubt develop very quickly in the months and years ahead.

The model of EWSB which is the focus of this work comes under the broad title of Technicolor, although the class of models to which this title pertains has evolved significantly over the years since the term was coined. This type of model, while addressing the issues with the Standard Model almost immediately, is not at all immune to the feature of expanding complexity required to make it consistent on all levels. In addition, Technicolor models have been received with significant criticism over the lifetime of the concept due to difficulties in constructing a model which avoids existing low-energy experimental constraints. However, in recent years the idea has been viewed with renewed interest due firstly to the development of a number of variants which do better at avoiding experimental constraints, and also because of the difficulties encountered by many models when attempting to resolve them with existing constraints.

2.2 Dynamical symmetry breaking from QCD

Technicolor models achieve EWSB through a mechanism that initially appears quite different to that of the Standard Model Higgs mechanism. In fact the

formulation is analogous, despite the fact that the field playing the role of the Higgs in Technicolor models is not explicitly included in the formulation of the model.

The motivation for the original idea of Technicolor arose from the hope that the process responsible for EWSB could be described without resorting to a model involving parameters which would be required to take values in a certain restricted range in order for the model to work as necessary, i.e. that the model would be free from fine-tuning. This is clearly not the case for the Standard Model Higgs mechanism given that the Higgs potential is required to take on quite a specific form to give the Higgs a VEV and lead to EWSB, and when expanded about its minimum, the parameter v^2 in (2.19) is required to be positive.

This leads to the question of whether a symmetry breaking of the type required for EWSB can exist more naturally, without undesirable tuning of the model being necessary. The answer came from another sector of the Standard Model, where such a process had been observed for many years.

2.2.1 QCD dynamics

The theory of QCD introduced in Sec. 2.1.2 is the only observed case of a non-Abelian gauge theory whose gauge symmetry remains unbroken at low-energies. The Lie group which defines QCD is the special unitary group $SU(3)$, a close relative of the $SU(2)$ and unitary group $U(1)$ which define the electroweak theory. $SU(N_c)$ theories are markedly different from Abelian gauge theories, as was notably described by [18, 19] for which a Nobel prize was awarded.

We can see where this difference arises by analysing a quantity called the β function of the theory. This object defines how the gauge coupling g of the theory will evolve as a function of the renormalisation scale.

$$\beta(\alpha) = \frac{\partial \alpha}{\partial(\log \mu^2)} \tag{2.20}$$

with $\alpha(\mu) \equiv \frac{g(\mu)^2}{4\pi}$. For small couplings, the β function of a gauge theory can be written as a power series in the coupling constant as

$$\beta(\alpha) = -\beta_0\alpha^2 - \beta_1\alpha^3 - \beta_2\alpha^4 + \dots . \tag{2.21}$$

The coefficients β_n are calculated through computing all loop diagrams of the theory up to a certain order. In a non-Abelian gauge theory with gauge group $SU(N_\mathrm{c})$, i.e. having N_c colours, and N_f flavours of quarks in the fundamental representation, the first coefficient in this expression is given by the expression

$$\beta_0 = \frac{1}{4\pi}\left(\frac{11}{3}N_\mathrm{c} - \frac{2}{3}N_\mathrm{f}\right). \tag{2.22}$$

The sign of this term is very important. This expression leads the β function to be negative at weak couplings, in contrast to the result in the Abelian theory. As a result of this the gauge coupling runs in the opposite direction as a function of the energy scale. At high energies, the theory becomes weakly coupled and can be described accurately using perturbation theory, a property known as *asymptotic freedom*, while at low energies the coupling becomes strong.

This behaviour has two important consequences. Firstly it means that the theory is consistent and predictive at arbitrarily high energy-scales, very different from the behaviour of the Abelian theory which encounters a singularity called a *Landau pole*. Secondly, perturbation theory can only be applied to this theory down to a certain energy scale where the coupling becomes $\mathcal{O}(1)$, i.e. perturbation theory breaks down at low energies. Clearly a more powerful description is required to explain the properties of this sector of the theory at low energies. Such a description emerged from observations of the structure of the hadronic matter of the Standard Model.

Another property of QCD at low energies is the breaking of *chiral symmetry*, the symmetry involving rotations between the quark fields and between their left and right handed components. The strong dynamics of the theory produce a vacuum expectation for the quark condensate, and hence a dynamical quark mass which breaks the total chiral symmetry to a vector subgroup. This process arises totally naturally, without any semblance of fine-tuning, and bears some of the properties required of the process responsible for EWSB. We might then ask, if there is a construction which would allow this symmetry breaking to be communicated to the electro-weak sector.

2.2.2 EWSB from chiral symmetry breaking

The answer is suspiciously fortunate. In fact, the QCD and electro-weak sectors, when coupled in the nature of the Standard Model, but omitting the Higgs sector, is perfectly sufficient for this. The dynamical breaking of the chiral symmetry in the QCD sector commmunicates itself to the electroweak theory and breaks the gauge symmetry in precisely the manner required to mimic the Standard Model Higgs mechanism. This is a remarkable feature of this model, and would lead to an extremely satisfying explanation of EWSB.

Unfortunately while the model provides a simple and appealing description of EWSB, it does not, in itself represent a valid model of electro-weak scale physics, as it does not reproduce the correct scale. In addition the model is far from a complete description of all the features of the Standard Model.

In this section we will outline the mechanics of this process, and deduce the disappointing cause for its failure. In order to do this we must discuss chiral symmetry in detail, and from it determine an effective description of QCD dynamics at low energies.

Each generation of quark comprises a pair of quarks, with both composed of a left and right-handed component which are introduced separately. As in the case of the leptons, the left-handed components make up a doublet transforming in the fundamental representation of the local weak isospin $SU(2)$ gauge symmetry, while the right-handed components transform trivially under this symmetry.

The full theory involves three generations, but for now we will introduce only the first generation involving the *up* and *down* quarks. This generation is the most relevant at low energies, due to the relative lightness of the up and down quarks. Being almost degenerate, they are often referred to collectively as the light quarks. In addition, the study of the light quarks alone allows for the simplest analysis of the effects of the QCD dynamics on the electro-weak sector.

We can arrange the left-handed ($u_{\mathrm{L}}(x)$, $d_{\mathrm{L}}(x)$) and right-handed ($u_{\mathrm{R}}(x)$, $d_{\mathrm{R}}(x)$) components of the quarks in doublets $q_{\mathrm{L/R}}(x)$ as

$$q_{\mathrm{L/R}}(x) = \begin{pmatrix} u_{\mathrm{L/R}}(x) \\ d_{\mathrm{L/R}}(x) \end{pmatrix}. \tag{2.23}$$

Quark masses are also found to be a sub-dominant effect in the dynamics of QCD, and so we will first consider the case where the quarks are massless, and

afterwards relax this assumption. The massless theory respects a global $U(2) \times U(2)$ symmetry whereby

$$q_{\mathrm{L}}(x) \to U_{\mathrm{L}} q_{\mathrm{L}}(x) \qquad\qquad q_{\mathrm{R}}(x) \to U_{\mathrm{R}} q_{\mathrm{R}}(x) \tag{2.24}$$

with $U_{\mathrm{L/R}} \in U(2)$. This *chiral* symmetry is commonly labelled $U(2)_{\mathrm{L}} \times U(2)_{\mathrm{R}}$. Clearly if we include further quark generations this chiral symmetry will be extended to involve all the quark fields, replacing $U(2)$ with $U(N_{\mathrm{f}})$ for N_{f} flavours, i.e. $\frac{N_{\mathrm{f}}}{2}$ generations.

The chiral symmetry of the light quarks is often referred to as *isospin*. While the left isospin symmetry is clearly closely related to the weak isospin gauge symmetry, importantly they are distinct.

We can rewrite this symmetry as a vector symmetry $U(2)_{\mathrm{V}}$ where $U_{\mathrm{L}} = U_{\mathrm{R}}$ and an axial symmetry $U(2)_{\mathrm{A}}$ with $U_{\mathrm{L}} = U_{\mathrm{R}}^{\dagger}$. Deconstructing these $U(N)$ symmetries using $U(N) = SU(N) \times U(1)$ we can express the full symmetry of the theory as $SU(2)_{\mathrm{V}} \times SU(2)_{\mathrm{A}} \times U(1)_{\mathrm{V}} \times U(1)_{\mathrm{A}}$. In fact the axial $U(1)$ is broken by a quantum anomaly, and so is not a symmetry of the theory. Further, the vector $U(1)$ symmetry represents the conservation of quark number, and so is relatively uninteresting. It is the $SU(2)_{\mathrm{V}} \times SU(2)_{\mathrm{A}}$ which represents the symmetry of the theory under rotations of the quark fields, and so we will restrict ourselves to this from here on.

In order to have a quantitative tool to describe the low energy dynamics of QCD, we would like to construct an effective field theory of the low-lying hadron spectrum, specifically the light pseudoscalar mesons, and their interactions. This is done by introducing an object Σ which transforms in the adjoint representation of $SU(2)_{\mathrm{V}}$, $\Sigma \to U \Sigma U^{\dagger}$.

Parameterising Σ as $\Sigma = e^{\frac{2i\phi}{f}}$, with ϕ an element of the $SU(2)$ Lie algebra, transforming in the adjoint representation of the algebra $\phi \to [U, \phi]$. The constant f is related to the decay constant of the pion f_{π} and in turn to the scale of the QCD strong dynamics Λ_{QCD}.

Decomposing the Lie algebra in an appropriate basis, we identify the coordinates of ϕ with bosonic fields representing the three pseudoscalar mesons, i.e. $\phi = \pi^a \tau^a$, with $\{\pi^a\} = \{\pi^0, \pi^+, \pi^-\}$ and τ^a the generators of the $SU(2)$ Lie algebra, which can be defined using the three Pauli matrices σ^a. This process defines *chiral perturbation theory*, originally developed in [20, 21] and reviewed in

[22].

We can then write a kinetic term for the meson fields as

$$\mathcal{L}_{\text{eff}} \supset \frac{1}{8} f^2 \text{Tr}[(D_\mu \Sigma)^\dagger D^\mu \Sigma] \tag{2.25}$$

The covariant derivative D_μ includes the couplings to the electroweak gauge fields and is written

$$D_\mu \Sigma = \partial_\mu \Sigma - i\frac{g}{2}\tau^a A^a_\mu \Sigma + i\frac{g'}{2}\Sigma\tau^3 B_\mu \tag{2.26}$$

A^a_μ and B_μ are the weak isospin and hypercharge gauge fields respectively, while g and g' are their respective gauge couplings. After a field redefinition

$$\{A'^a_\mu\} \equiv \{A^1_\mu, A^2_\mu, A^3_\mu - \frac{g'}{g} B_\mu\} \tag{2.27}$$

the argument of the trace in the kinetic term of the effective Lagrangian becomes

$$|D_\mu \Sigma|^2 = \frac{g^2}{4}\left(A'^a_\mu - \frac{4}{fg}\partial_\mu \pi^a\right)^2 \tag{2.28}$$

and a few other terms with zero trace. Clearly this corresponds to a mass term for the gauge field

$$W^a_\mu \equiv A'^a_\mu - \frac{4}{fg}\partial_\mu \pi^a \tag{2.29}$$

and that is all. The π^a fields are completely removed from the Lagrangian by this redefinition. The W^a_μ field encodes the massive W and Z gauge bosons. They are not degenerate due to the definition necessitated to return the kinetic terms to canonical form, and in fact produce the correct ratio observed in the Standard Model.

$$\frac{m^2_{\text{W}}}{m^2_{\text{Z}}} = \frac{g^2}{g^2 + g'^2} = \cos^2\theta_{\text{W}} = 0.77 \tag{2.30}$$

This fact however, is not entirely surprising. It can be shown to be a feature of any model which breaks the symmetry in the correct way.

Clearly this model is highly attractive from an aesthetic point of view. It requires no additional input to the theory other than the two main gauge sectors which we know to exist, requires no tuning to produce the correct features and relies upon dynamics with which we are already very familiar to do the job. This type of model where the EWSB proceeds automatically due to the strong gauge

dynamics of another sector has been termed *dynamical* electro weak symmetry breaking, DEWSB.

Firstly, the masses of the W and Z bosons which would arise from this mechanism can be calculated, from the experimentally observed value of f_π, to be ~ 50 MeV. Comparing this to the observed values of these masses ~ 100 GeV we see that the two scales are utterly incompatible.

In addition, there are a number of features of the Standard Model which this model fails to reproduce. Most importantly, there is no mention of fermion masses in this model. Explicit mass terms remain forbidden by the gauge symmetries, and there is now no additional VEV aquiring field to which we can couple the fermions to produce Yukawa terms which might do the job.

As a result, this simple model can not provide the explanation of EWSB which we seek. However it does indicate that EWSB could be achieved through a dynamical mechanism which would remove the necessity for the inclusion of an elementary scalar field or for the fine-tuning of its potential. The effort to modify this model in order to generate EWSB at the correct scale, while keeping all the desirable features of this model, lead to the development of Technicolor.

2.3 Naive technicolor

Technicolor, as it quickly became to be known, refers to the extension of the concept of DEWSB to construct a model of EWSB which operates at the correct energy scale, producing the physical masses of the W and Z gauge bosons and all other features required of a sensible description of EWSB. Recent reviews of the background to this subject can be found at [23, 24].

2.3.1 Technicolor

The original idea [25–27] involved a straghtforward extension of the Standard Model, with the Higgs sector omitted, to include an additional non-Abelian gauge sector with symmetry group $SU(N_{\mathrm{TC}})$. This new sector would come equipped with corresponding fermionic content, referred to as *techniquarks*, and as is expected for a non-Abelian gauge sector, would become strongly coupled at some low energy scale Λ_{TC}. As long as it is ensured that at least some of this fermion content is coupled to the electro-weak gauge forces, the chiral symmetry breaking

induced by the strong dynamics of this new sector would then be communicated to the electro-weak sector in an analogous fashion to that outlined for QCD in Sec. 2.2.2 producing the desired EWSB.

Given that we have no observational experience of any non-Abelian gauge theory except for QCD, we cannot speculate as to what value the scale Λ_{TC} would likely take. We are free to speculate that there is some value of N_{TC} along with a particular fermion content which would result in a value of Λ_{TC} at the weak scale, generating EWSB in the correct manner. Such a construction defines a technicolor model, providing an attractive solution to the core problem of EWSB. However, this concept does not provide any explanation for the generation of Standard Model fermion masses, and a number of other features that are required. We will discuss how to tackle these issues in Sec 2.3.2.

One feature of such a model which is undesirable is the contribution of the new matter content in the theory to a quantity know as the S-parameter of the theory. This quantity is tightly constrained from experiment, and it is necessary that the contribition from any new physics be small. We will define this quantity and discuss its contribution from technicolor models in Sec. 2.3.3.

2.3.2 Extended technicolor

While this simple model is capable of generating EWSB in the correct manner and thus in turn the correct gauge boson masses, it makes no claim to generate the masses of any fermions in the model. While the techniquarks and quarks would receive dynamical masses through the spontaneous breaking of the technicolor and QCD chiral symmetries respectively, they would have no hard masses, which is impossible to reconcile with the large masses of all but the three lightest quarks. The pseudoscalar mesons of QCD would be almost massless, and the leptons would be necessarily so. In order to begin to generate these masses, it is necessary to augment the theory further.

The symmetry breaking that is responsible for EWSB in this model occurs in the technicolor sector, and is communicated to the electro-weak gauge symmetries via the Nambu-Goldstone bosons of the breaking of the chiral symmetry on the techniquarks, the *technipions*. The Standard Model fermions are oblivious to this process, as they are not coupled to the technicolor sector.

To couple these Standard Model fermions to the technicolor sector, we must

extend the gauge symmetry of the model to involve additional interactions under which the leptons, quarks and techniquarks are charged, and we call such a construction a model of *extended* technicolor (ETC) [28, 29]. This larger group is then hypothesised to be broken by some unspecified mechanism at a scale Λ_{ETC}, to produce the gauge symmetries of the Standard Model plus the technicolor sector at energies below Λ_{ETC}.

The process responsible for this symmetry breaking might be a dynamical process in the vein of technicolor, or possibly a more conventional Higgs mechanism involving an elementary scalar Higgs field contained in a super-multiplet of some supersymmetric model. It is sometimes speculated that there might be a series of such symmetry breakings occuring at different scales, each often connected with a different generation of fermion, possibly providing an explanation for the large flavour hierarchies we see in the spectrum of the Standard Model [30]. However, we will not discuss the nature of this process further here. For our purposes we simply require that it couples to our fermions in the correct way, and is broken down to the required symmetry at Λ_{ETC}.

To analyse the consequences of a generic such model let us consider the effective operators induced in the low-energy theory below the ETC scale. We denote the Standard Model quarks and leptons as belonging to a collective vector ψ, and the techniquarks to a similar object Ψ.

The original ETC gauge interaction must be coupled to currents of the form $\Psi\Gamma T^a\Psi$, $\Psi\Gamma T^a\psi$ and $\psi\Gamma T^a\psi$, where T^a are the generators of the Lie algebra of the ETC gauge group, and the Γ represent some gamma matrix structure which can allow for a chiral theory where the left and right handed fermions couple to the ETC interaction differently.

The coupling to these currents in the high energy theory leads to a number of effective interactions in the low energy theory after integrating out the extra ETC gauge bosons. They can be written

$$\frac{\overline{\Psi}\Gamma T^a\Psi\overline{\Psi}\Gamma T^b\Psi}{\Lambda^2_{ETC}}, \qquad \frac{\overline{\Psi}\Gamma T^a\Psi\overline{\psi}\Gamma T^b\psi}{\Lambda^2_{ETC}}, \qquad \text{and} \qquad \frac{\overline{\psi}\Gamma T^a\psi\overline{\psi}\Gamma T^b\psi}{\Lambda^2_{ETC}}. \tag{2.31}$$

Three of the terms which have the greatest phenomenological consequences are

the interactions of the scalar densities

$$\mathcal{L} \supset \alpha_{ab}\frac{\overline{\Psi}T^a\Psi\overline{\Psi}T^b\Psi}{\Lambda_{\mathrm{ETC}}^2} + \beta_{ab}\frac{\overline{\Psi}T^a\Psi\overline{\psi}T^b\psi}{\Lambda_{\mathrm{ETC}}^2} + \gamma_{ab}\frac{\overline{\psi}T^a\psi\overline{\psi}T^b\psi}{\Lambda_{\mathrm{ETC}}^2} \tag{2.32}$$

where α_{ab}, β_{ab} and γ_{ab} denote the coefficients of these terms appearing in the Lagrangian, and will also be used to label the terms. These quantities will remain unknown, but there is no reason to expect that they would be anything other than $\mathcal{O}(1)$.

These three terms each have different but important implications for the low energy theory:

α terms: Technipion masses

The four-techniquark interaction can produce a contribution to the mass of the Nambu-Goldstone bosons of the techniquark chiral symmetry breaking. While three of these states are eaten by the electro-weak gauge bosons, to become their longitudinal component and provide the boson with a mass, a generic technicolor model may have a chiral symmetry breaking pattern which produces additional such states. These states emerge as massless bosons, and there is nothing in the technicolor model to provide the with a mass, so the generation of this mass in ETC is a welcome effect, as these states are not observed in current experiments.

β terms: Hard fermion masses

The presence of these effective interactions below Λ_{ETC} leads to the generation of masses for the Standard Model fermions below Λ_{TC}. This can be seen as a coupling of the fermions to the techniquark condensate, through the propagation of an ETC gauge boson. We can estimate the VEV of the techniquark condensate by assuming it behaves analogously to the QCD quark condensate, giving $\langle\overline{\Psi}\Psi\rangle \sim N_{\mathrm{TC}}\Lambda_{\mathrm{TC}}^3$. The scale of the generic mass shift generated by this coupling is then given by

$$m \sim \frac{\langle\overline{\Psi}\Psi\rangle}{\Lambda_{\mathrm{ETC}}^2} \sim \frac{N_{\mathrm{TC}}\Lambda_{\mathrm{TC}}^3}{\Lambda_{\mathrm{ETC}}^2} \tag{2.33}$$

γ terms: Flavour interactions

The four-quark interaction generates a more undesirable feature of the theory. These terms leads to flavour changing interactions, called flavour changing neutral currents (FCNCs) which are heavily constrained from existing observational data.

Any model of EWSB resulting in such interactions will also have to provide an explanation for why they appear to be so suppressed in nature.

To estimate the constraints put on the scales of our theory by requiring this suppression, let us consider one of the tightest constraints, arising from the K_{L}-K_{S} mass difference, denoted here by δm. The constraint on this quantity arising from experiment is roughly $\frac{\delta m^2}{m_{\mathrm{K}}^2} \lesssim 10^{-14}$ while an estimate of the contribution to such a quantity arising from the effective interaction in (2.32) would be $\gamma \frac{f_{\mathrm{K}}^2 m_{\mathrm{K}}^2}{\Lambda_{ETC}^2}$, where m_{K} is the kaon mass, f_{K} the kaon decay constant, and γ a representative value of the coefficients γ_{ab}.

Even after taking into account the Cabibbo angle which might produce a coefficient $\gamma \sim 10^{-2}$, this still results in a constraint on the ETC scale of roughly

$$\Lambda_{\mathrm{ETC}} \gtrsim 10^3\,\mathrm{TeV} \tag{2.34}$$

Substituting this value into (2.33), and assuming that the technicolor scale Λ_{TC} lies relatively close to the weak scale, leading to a rough estimate of $\Lambda_{\mathrm{TC}} \sim 1\,\mathrm{TeV}$, indicates that an ETC theory with such a high Λ_{ETC} could only generate hard fermion masses of the order of

$$m \lesssim 100\,\mathrm{MeV} \tag{2.35}$$

even allowing for a coefficient $\beta \sim 10$ and number of technicolours $N_{\mathrm{TC}} \sim 10$. While this might be enough to cater for the light quarks, such a model can clearly not explain the higher mass of the charm, bottom, or top quarks.

2.3.3 Precision electroweak constraints

When we add a new sector to the interactions of the Standard Model, we must be careful to keep track of the effect of this new sector on the familiar processes which at tree-level involve only Standard Model particles, but may receive quantum corrections from any new physics.

The weakly coupled sector of the Standard Model, the electroweak sector, is particularly amenable to a high level of experimental accuracy, because the initial and final states in the relevant processes can be relatively easily identified. The precision involved is more than sufficient to identify and quantify quantum

corrections to the tree-level results for these interactions. In addition, the theoretical values for these corrections can be calculated to a high degree of accuracy, due to the perturbative nature of this sector.

One of the ways to study these corrections is through the accurate investigation of four-fermion interactions, which receive dominant contributions from the propagation of electroweak gauge bosons. Distinctions have been made between various types of contributions to such processes:

Direct corrections: Quantum corrections to four-fermion processes which are dependent on which initial and final states are involved, are termed *direct* corrections. These arise through corrections to interaction vertices, and also through box diagrams which are of a markedly different form to the tree-level interaction.

Oblique corrections: Another set of corrections contributes only by altering the propagation of the intermediate electroweak gauge boson, and are independent of the initial or final states. These are termed *oblique* corrections. They are also known as vacuum polarisation contributions or self-energy corrections to the gauge boson propagator.

When considering constraints on models of DEWSB, the more relevant of these categories are the oblique corrections. Constraints from direct corrections are less strong, because these contributions are typically suppressed by a factor such as $\frac{m_{\mathrm{f}}^2}{m_{\mathrm{Z}}^2}$ where m_{f} is the mass of the external fermion.

The oblique corrections were formulated conveniently in 1991 [31, 32] into three parameters, S, T and U. Most electroweak observables can be described as linear combinations of these quantities. The parameter U is found to play a relatively unimportant role, as most precisely measured observables are insensitive to U. In addition, in most models, U is found to be sub-dominant to S and T, and so electroweak constraints are often visualised in the $S-T$ plane.

The oblique correction parameters are defined in terms of the vacuum polarisation amplitudes $\Pi_{\mathrm{XY}}(q^2)$ where (XY) is one of (11), (22), (33), (3Q), (QQ). These labels refer to the currents involved in the two-point function defining

$\Pi_{\mathrm{XY}}(q^2)$

$$ig_{\mu\nu}\Pi_{XY}(q^2) + \mathcal{O}(q_\mu q_\nu) \equiv \int d^4x\, e^{-iqx}\langle J^\mu_{\mathrm{X}}(x) J^\nu_{\mathrm{Y}}(0)\rangle \tag{2.36}$$

J_{Q} is the electromagnetic fermion bi-linear current, and J_i are the equivalent weak-isospin currents. The S-parameter is defined as

$$S \equiv 16\pi \frac{d}{dq^2}[\Pi_{33}(q^2) - \Pi_{3\mathrm{Q}}(q^2)]|_{q^2=0} \tag{2.37}$$

As they arise from the vacuum polarisation, the dominant contributions of distinct sectors to the S-parameter are additive in nature. For this reason, by convention, experimental results for S and T are quoted after subtraction of the predicted Standard Model results, so that agreement with the Standard Model is indicated by measured values of S and T consistent with zero.

Collating independent measurements of electroweak observables, restricts the allowed values of the oblique correction parameters to an ellipse in the $S - T$ plane. The most up to date measurement of the oblique correction parameters are [2]

$$S = 0.03 \pm 0.09, \qquad T = 0.07 \pm 0.08 \tag{2.38}$$

consistent with $S = T = 0$ and thus consistent with the simple Standard Model prediction.

Any model of new physics must contribute to S and T a value in agreement with these bounds, and this restriction is usually a tight constraint on viable models. While T can receive significant contrbutions from ETC models, the S-parameter is more restrictive as it is sensitive simply to the extra strongly coupled sector involved in technicolor models. As a result, S has become one of the strongest direct constraints on technicolor.

There are a number of sensible ways to compute a contribution to S, however, due to the strongly coupled nature of a proposed technicolor sector, a perturbative calculation in the full high-energy theory is not expected to be reliable. In order to do better, we can resort to a low-energy model of a strongly interacting theory, or attempt to make inference from observation of low-energy QCD.

In [32] the calculation using a dispersion integral over the $e^+e^- \to$ hadrons cross-section assumed to be dominated by vector meson propagation, is in

reasonable agreement with the same integral performed over experimental data for such a cross-section from QCD. For a technisector involving a symmetry group $SU(N_{\mathrm{TC}})$ and N_{D} doublets of Dirac techniquarks in the fundamental representation, the result is roughly

$$S \simeq 0.3 N_{\mathrm{D}} \frac{N_{\mathrm{TC}}}{3} \tag{2.39}$$

Comparing to (2.38), this result is worryingly large. In fact this feature has proven problematic for technicolor models, and has led to significant doubt as to whether they can be made to agree with existing experimental constraints. Restrictions on the value of T have an impact on the design of ETC models, but it is the restrictions on the allowed values of S that are seen as the most significant hurdle for technicolor models to overcome.

In Sec. 2.4 we will describe one powerful alteration to the standard technicolor picture, and how it might alleviate some of the difficulties which have disfavoured technicolor, and in Sec. 2.4.4 how they relate in particular to the S-parameter.

2.4 Near-conformal technicolor

The two main issues raised above;

1. the need to suppress FCNCs leading to a diminished ability to generate significant fermion masses

2. and the problematic contributions to the S-parameter

cause significant problems for ETC models, and for long periods have lead to the impression among a large portion of the particle physics community that technicolor was an invalid model, and had been ruled out as a candidate explanation for EWSB.

However this impression has been weakened over recent years by two main factors:

1. Tight constraints are being encountered by most, if not all candidate models for EWSB, including possibly the most prevalent candidate, supersymmetry [16]. This has led to increased acceptance of problems within candidates,

and more willingness to expend considerable effort to find ways that such models might be altered to reconcile these issues.

2. Against this backdrop, it is also becoming widely understood that the calculations of the constraints on technicolor models derived from current experimental data have, without exception, been performed under the assumption that the dynamics of the technicolor sector, aside from involving a different strong scale $\Lambda_{TC} \neq \Lambda_{QCD}$, are otherwise entirely identical to those of QCD, and this has a large impact on the evaluation of the model.

   The reason for this assumption is clear. QCD is the only non-Abelian gauge theory realised at low energies in nature, and as a result is the only strongly-coupled gauge theory with which we are at all familiar. Restricting ourselves to considering similar theories allows us to avail of observational and theoretical experience gained over decades of trying to understand QCD, to make predictions on the behaviour and features of such technicolor models.

   However, it is a tight constraint on the theory-space that we are willing to consider, and rules out many different classes of theories with dynamics that are significantly different to those of QCD, which can have considerable phenomenological implications.

As we saw in Sec. 2.2.1, the most important property of QCD, asymptotic freedom, can be seen to originate from the properties of the β function of the theory. As a result we may hope that by analysing the possible different behaviours of the β function of a non-Abelian gauge theory, we might deduce some interesting dynamics possible in such theories. By then considering such theories as the technicolor sector in a model of DEWSB, we might determine whether any such theory would allow us to build a complete technicolor model better able to overcome the issues encountered by the original model.

2.4.1 The conformal window

An interesting set of distinct behaviours of these theories can be determined from the first two coefficients of the β function, defined in (2.21). These two coefficients are universal, that is they are independent of the regularisation scheme used to control the divergences of the theory, which cannot be said for the other

coefficients in the expansion of β. In a theory with N_c colours, and N_f flavours of Dirac fermion in the fundamental representation they are

$$\beta_0 = \frac{1}{4\pi}\left(\frac{11}{3}N_c - \frac{2}{3}N_f\right) \tag{2.40}$$

$$\beta_1 = \frac{1}{4\pi^2}\left[\frac{34}{3}N_c^2 + \left(\frac{1}{N_c} - \frac{13}{3}N_c\right)N_f\right] \tag{2.41}$$

The sign of these two terms will determine the low-order behaviour of β. We see that for any value of N_c ($N_c \geq 2$ for $SU(N_c)$), and a low value of N_f, that both of these coefficients are positive. As a result, to $\mathcal{O}(\alpha^3)$, $\beta(\alpha)$ is a monotonically decreasing function of α, ensuring asymptotic freedom at high energies.

If we are to increase the amount of fermion content in the theory, increasing N_f, then to this order, the first significant development encountered would be a change of sign, in the second coefficient β_1. If we choose a N_f such that $\beta_1 < 0$ then the β function looks markedly different. As we increase α, $\beta(\alpha)$ will at some point begin to increase, until it reaches zero, at a value $\alpha^* = -\frac{\beta_0}{\beta_1}$.

A theory with such a β function would appear drastically different to QCD. The ultra-violet properties of asymptotic freedom would not be affected, as $\beta(\alpha) < 0$ for $\alpha \sim 0$. However, in the infra-red, the dynamics would be very different. The zero of the β function at α^* indicates a non-trivial fixed point of the theory, i.e. in the infra-red, the gauge coupling would plateau at α^*, and in the deep infra-red, the theory would become perfectly conformal.

If we take a large enough N_f, then α^* can be driven to a small value, meaning that the perturbative approximation is valid. For small enough α^*, our two-loop, $\mathcal{O}(\alpha^3)$ truncation of the β function, becomes an accurate approximation, and the theory is completely described by this β function. This scenario was first studied in [33], and the fixed point at α^* has been coined a Banks-Zaks fixed point.

If α^* is not small, and the fixed-point is therefore not in the perturbative regime, then the truncated description is not reliable in the infra-red. In order to determine the infra-red dynamics, it would be necessary to perform a non-perturbative analysis of the dynamics.

If we are to consider the implications of further terms in the perturbative expansion of the β function, we must bear in mind that all terms beyond β_1 are renormalisation scheme dependent, and so the detailed profile of the β function is not truly reliable. However, it can be shown that the existence of a non-trivial

zero in the β function is a scheme independent property.

As a result, we can divide the theories with $\beta_1 < 0$ into those which retain the non-trivial infra-red fixed point after taking into account all non-perturbative information, and those which do not. Theories with the fixed point will look very much like the Banks-Zaks theory, except the infra-red theory will not be describable perturbatively. Theories without the fixed point will look more like QCD in the infra-red, with the onset of chiral symmetry breaking, confinement, and the expected strong dynamics.

If we were to increase N_f still further, then we would eventually change the sign of β_0. This would result in the loss of asymptotic freedom, and the theory would more closely resemble the dynamics of QED rather than QCD. We will not consider such theories in any detail.

The range of N_f, between the value resulting in the development of an infra-red fixed point, and the value at the loss of asymptotic freedom, is said to define the *conformal window*, for a certain value of N_c.

2.4.2 Walking coupling

In building a model of DEWSB, we need to choose a technicolor sector with a certain number of properties. As a stand-alone theory, the interaction describing this sector must be asymptotically free, and must also be truly strongly coupled in the infra-red, in order to bring about the chiral symmetry breaking which will be responsible for EWSB.

This rules out the set of theories in the conformal window, as described in Sec. 2.4.1, as they retain their chiral symmetry in the infra-red. It should be noted however, that when such a theory is attached to the theory of the Standard Model interactions, the situation is more complex. The technicolor sector would be conformal assuming the techniquarks obtained no hard mass terms. As we will discuss in Sec. 3.2, any techniquark masses, or a number of other more complicated possible interactions, would drive the theory away from the conformal fixed-point, and towards chiral symmetry breaking.

Restricting to the massless case however, we can assume that there is a range of N_f, for which our theory will not lie in the conformal window, but will lie close to it. Such a theory would not be truly conformal in the infra-red but would display some properties of being near to conformality, i.e. *near-conformal*

behaviour.

While the exact non-perturbative profile of the β function is not thought to be scheme independent (excepting the presence or lack thereof of a zero), we can deduce the expected behaviour of a near-conformal theory from a deformation of a β function which exhibits a zero.

We hypothesise that a near-conformal theory has a β function which decreases from zero as α increases from zero, then at some point begins to increase, but rather than reaching another zero, reaches a local maximum near zero, and then begins to descend as α increases further. Such a theory would be expected to have a coupling with a very particular renormalisation behaviour.

Still being asymptotically free, the theory would have a small coupling at large renormalisation scales. The negative β function near $\alpha \simeq 0$ then determines that the coupling increases as the scale decreases. When the β function begins to increase, this running slows, until the point where the β function nears zero, where the running becomes very slow. Eventually, the β function decreases again, the running accelerates as we move to the infra-red, producing a strong coupling, chiral symmetry breaking, etc.

This behaviour, where the coupling is supposed to run very slowly over an extended range of renormalisation scales, has been termed *walking*. This behaviour is very different to that of QCD, where the coupling runs very quickly over the whole range of scales.

2.4.3 Walking and ETC

The inclusion of a technicolor sector associated with a walking dynamics, into a model of DEWSB, has implications for the tension between the need to suppress FCNC's, and the need to generate significant fermion masses in such a model.

As described in Sec. 2.3.2, the fermion masses generated through ETC interactions are estimated as $m \sim \frac{\langle\overline{\Psi}\Psi\rangle}{\Lambda^2_{ETC}}$, where $\langle\overline{\Psi}\Psi\rangle$ is the techniquark condensate. In fact, more specifically, what is involved here is the techniquark condensate evaluated at the extended technicolor scale Λ_{ETC}: $\langle\overline{\Psi}\Psi\rangle_{ETC}$. This is related to its equivalent at the technicolor scale Λ_{TC} by a renormalisation factor

$$\langle\overline{\Psi}\Psi\rangle_{ETC} = Z(\Lambda_{TC}, \Lambda_{ETC})\langle\overline{\Psi}\Psi\rangle_{TC} \tag{2.42}$$

This factor Z is given by

$$Z(\Lambda_{TC}, \Lambda_{ETC}) = \exp\left(\int_{\Lambda_{TC}}^{\Lambda_{ETC}} \frac{d\mu}{\mu}\gamma(\mu)\right). \tag{2.43}$$

The integral is over the renormalisation scale μ, and $\gamma(\mu)$ is the anomalous dimension of the techni-quark condensate at the scale μ.

In QCD, where asymptotic freedom sets in rapidly above Λ_{QCD}, the anomalous dimension is roughly proportional to the coupling $\gamma(\mu) \sim \alpha(\mu)$ which vanishes rapidly $\alpha(\mu) \to 0$ when $\mu > \Lambda_{QCD}$. As a result, if the dynamics of the technicolor sector in our model were similar, the integral in Z would have very little support, meaning $Z \simeq 1$.

If however, the coupling were expected to run very slowly above the scale of strong dynamics associated with this sector Λ_{TC}, then the anomalous dimension would also be expected to be roughly constant in this range. The result for Z would then be $Z(\Lambda_{TC}, \Lambda_{ETC}) = \left(\frac{\Lambda_{ETC}}{\Lambda_{TC}}\right)^{\gamma}$, giving

$$\langle\overline{\Psi}\Psi\rangle_{ETC} = \left(\frac{\Lambda_{ETC}}{\Lambda_{TC}}\right)^{\gamma} \langle\overline{\Psi}\Psi\rangle_{TC} \tag{2.44}$$

In such a model, γ would be expected to be $\mathcal{O}(1)$, so taking this estimate $\gamma = 1$ we would obtain for the estimate of fermion masses generated through ETC interactions

$$m \sim \left(\frac{\Lambda_{ETC}}{\Lambda_{TC}}\right) \frac{N_{TC}\Lambda_{TC}^3}{\Lambda_{ETC}^2} \tag{2.45}$$

Then, using the same constraints as in our previous estimate, $\Lambda_{TC} \sim 1$ TeV to produce the scale of EWSB, and $\Lambda_{ETC} \gtrsim 10^3$ TeV to satisfactorily suppress FCNC's, we obtain a new estimate

$$m \lesssim 100\,\text{GeV} \tag{2.46}$$

Clearly this enhancement of the techniquark condensate at the ETC scale, has allowed the theory to generate far larger fermion masses while still suppressing FCNC's. The scale of fermion masses generated may not be at a sufficient scale to accommodate the top quark, but it is a significant step in the right direction, and there have been additional proposals of how the top mass might be generated.

It has been observed that a technicolor model with a near-conformal dynamics

will exhibit a spectrum with a number of particles at relatively low mass, and well within reach of the LHC [34], in particular the vector mesons ρ_{TC} and ω_{TC} are particularly interesting discovery candidates. Recent searches based on current data have ruled out these particles below the $400 - 500$ GeV scale [17].

2.4.4 Walking and the S-parameter

As described in Sec. 2.3.3, many models of technicolor encounter difficulties due to their relatively large contribution to the oblique elctroweak correction parameter S. However, the calculations of the S contributions outlined in Sec. 2.3.3 were based on the assumption that the dynamics of the technicolor sector are similar to those of QCD. Under this assumption, many theoretical uncertainties are under control, and we can draw inference from our extensive observations from QCD to draw conclusions about the contribution to S in a technicolor model.

In the case where the technisector exhibits a near-conformal dynamics in the infra-red, there is far less certainty about what the resulting contribution to S might be, in fact arguments have been made to suggest that the contribution to S could be suppressed in this case [35, 36]. There remains no clear way to conduct a theoretical estimate for S in this scenario, in order to study this problem there is a need for fully non-perturbative first-principles calculations.

2.4.5 Higher representations

In Sec. 2.4.1 we described how varying the number of fermion flavours included in a non-Abelian gauge theory can drastically alter its dynamics, by moving the theory closer to, or into the conformal window. We can also alter the fermionic content of our gauge theory by considering some, or all, of the fermions to be in a representation of the gauge group other than the fundamental. The screening effect of a fermion is proportional to the dimension of the representation of the gauge group under which it transforms [37].

Because of this it is possible for a theory to attain a zero of the β function with a lower number of flavours of fermion, if some, or all, of those fermions transform under a representation of the gauge group other than the fundamental. It is expected that the enhanced screening contribution of higher representation fermions dominates the increased contribution of such fermions to

the S parameter.

2.5 Minimal walking technicolor

In Sec. 2.4 we have motivated the concept of near-conformal technicolor, where the difficulties encountered by naive technicolor models, such as the tension between suppressing FCNC's and generating reasonable fermion masses in ETC, and the large contribution to the S-parameter, are alleviated by the proposal of a technicolor model whose technisector has a fermion content such that its renormalisation dynamics contrast strongly with those of QCD, in that they display a slow running of the gauge coupling over a large range of energy scales as we approach the infra-red.

Given that we have no observational experience of any strongly coupled gauge theory other than QCD, verifying near-conformal behaviour in any theory is a difficult proposition. Perturbative and quasi-perturbative arguments have been made for a number of interesting theories to have these properties [37]. Focus has centered on theories with a low number of technicolors N_{TC}, and a low number of flavours of techniquark N_{TF}.

In this regard, one of the most interesting candidates that has emerged is the $SU(2)$ gauge theory with two flavours of Dirac fermion transforming in the adjoint or symmetric representation.

The conformal nature of this theory was first highlighted in the context of *planar* equivalence [38, 39], which establishes the correspondence between the bosonic sector, of the large-N limit, of so called *orientifold* theories, with $\mathcal{N} = 1$ super Yang-Mills theories. This correspondence means that some of the conformal properties of the supersymmetric *parent* theory, should also hold in the non-supersymmetric *daughter* theory. The orientifold theories are vector-like, containing fermions in the rank-two antisymmetric, or symmetric representation.

In the $SU(2)$ theory, the symmetric representation equates to the adjoint, and the possible benefits of the use of this theory in a model of technicolor were illustrated in [40]. The $SU(2)$ theory with two adjoint fermions involves the lowest number of colour and flavours, while believed to lie in, or near to, the conformal window, and has come to be know as *minimal walking technicolor* (MWT) [41].

In a valid MWT model we must [40] include an additional family of heavy

leptons in order to cancel the Witten anomaly [42], but otherwise the construction of such a model is straightforward. The phenomenology of such models has been studied extensively ([43, 44], and more recently [45] and [46]) and it is thought that such models are entirely consistent with current experimental constraints, arising from both flavour changing processes, and electroweak precision tests.

Chapter 3

MWT on the lattice

In Sec. 2.4 we outlined the motivation for, and consequences of, models of technicolor with a new strongly-coupled sector involving near-conformal renormalisation dynamics. Despite the convincing nature of the origins of the concept of near-conformal dynamics, because of the non-perturbative nature of the phenomenon, quantitative conclusions on its existence or consequences are few and far between. To make matters worse, we have no observational experience to guide us, as the only strongly-coupled gauge theory observed so far in nature displays no features of this behaviour.

For these reasons, over the past few years, attention has turned to lattice gauge theory (LGT) in the hope that it could provide answers to some of the many questions surrounding near-conformal gauge theories. LGT is the only formalism allowing a fully non-perturbative, robust, first principles approach to strongly-coupled gauge theories. The formalism of LGT is described in App. A and many of the tools used in common simulations, as well as those used for the studies in this work are introduced.

3.1 Strategies for lattice technicolor

To investigate near-conformal dynamics on the lattice, there have been two major approaches adopted:

3.1.1 Renormalisation studies:

We can seek to identify and explore near-conformal behaviour in a gauge theory by examining the behaviour of the theory under renormalisation flow. There are a number of schemes available within a LGT framework which allow this type of study, and they have been put to good use in recent years in confronting these questions.

Primarily the *Schrödinger functional* has been utilised to investigate the running of the coupling, [47, 48] and the quark mass [48] in a number of theories which are good candidates for posessing near-conformal dynamics. More recently, the Monte-Carlo renormalisation group (MCRG) has been implemented to tackle some of these questions [49].

3.1.2 Spectral studies:

Alternatively, we can attempt to discern near-conformal behaviour by measuring the major phenomenological features of a theory, and detecting properties associated with near-conformality.

In this vein, many studies have measured the low-lying mesonic spectrum of candidate theories, and studied how the spectrum scales as the quark mass (usually taken to be degenerate) is varied [50–54]. In Sec. 3.2 we will describe the scaling expected, and its origin in near-conformal theories.

Another line of investigation under this heading is the investigation of the contribution to electroweak oblique correction parameters from theories which are candidates for near-conformal behaviour. In Sec. 2.4.4 we described the predicted effect of near-conformal behaviour on the S-parameter, and in order to confirm these expectations, results from LGT would be very helpful.

Efforts in this area began with a study of the QCD contribution to S within the Standard Model [55, 56], to avail of existing QCD data, expertise and simulation frameworks, while also verifying the methodology required for similar computations involving interesting technisector candidates. Subsequently, studies involving potential technicolor sectors have emerged [57], and the indications are that the contribution to S from a theory closer to the conformal window is indeed

likely to be reduced.

3.2 Mass-deformed conformal theories

As mentioned in Sec. 3.1.2, many lattice studies of theories thought to exhibit near-conformal behaviour have focused on properties of the low-lying mesonic spectrum of the theory, in an effort to identify scaling associated with near-conformal theories. Here we will describe this scaling, and its origins in near-conformal theories.

Strategies such as those described in Sec. 3.1.2 investigate theories which are believed to lie in or near the conformal window. As we shall see, differentiating between these two scenarios is difficult using only results of lattice simulations. The reasons for this are the limitations on LGT simulations, where a finite volume and non-zero quark mass are necessary for practical purposes.

Either of these restrictions alone means that a theory with a true conformal symmetry can not be simulated on a lattice. By construction, a conformal theory must not involve any scale, like a mass or length. The lattice formalism requires several of these, and so does not allow the study of a true conformal theory.

Thankfully, this does not preclude the type of study necessary. In fact, the departure of the theory from conformality, when described correctly, will encode the main features of the theory which will allow us to identify near-conformal behaviour.

3.2.1 Hyperscaling

These features are discussed in [58–61] in which the renormalisation behaviour of a gauge theory which posesses an infra-red fixed point, perturbed from conformality by the presence of fermion mass m, is studied. Such a model is termed a *mass-deformed infra-red conformal gauge theory.*

From experience of statistical mechanics, critical phenomena and phase transitions, it is known that near the fixed point at $m = 0$, all observables with the same dimension will scale to zero with the same critical exponent, a property known as *hyperscaling.* In order to determine the expected value of this exponent, we consider the theory around the infra-red fixed point $g(\mu) \to g_*$ as $\mu \to 0$. The renormalisation flow of the mass is determined by its anomalous

dimension, which is the negative of that of the quark condensate operator, $\mu\frac{d}{d\mu}m(\mu) = -\gamma(g(\mu))m(\mu)$. At the fixed point, this will take a value $\gamma(\mu) \to \gamma_*$ as $\mu \to 0$.

In [58] it is shown that as we return to the conformal case, by taking the chiral limit $m \to 0$, all physical observables $M_{\rm X}$ with the dimensions of a mass will scale to zero with an exponent determined by the value of the anomalous dimension at the fixed point:

$$M_{\rm X} \propto m(\mu)^{\frac{1}{1+\gamma_*}}. \tag{3.1}$$

As a result, if the chiral theory is indeed conformal, we would expect to observe simultaneous scaling of all mass observables to zero in the chiral limit. The mass-splitting between bound states would be expected to be heavily suppressed.

3.2.2 Deducing conformality

This property is in stark contrast to the expected behaviour in a theory which breaks chiral symmetry in the infra-red. In such a theory all hadronic states of quarks would be expected to have a mass of the order of the scale of strong dynamics of the theory, except that is for the pseudoscalar mesons corresponding to the Goldstone bosons of the chiral symmetry breaking, analogous to the pions of QCD.

The pseudoscalar states can be expected to become massless in the limit of zero quark masses, scaling as the square root of the quark mass, while the remainder of the spectrum retains a mass at the order of the strong scale of the theory, staying roughly constant in the immediate vicinity of the chiral point. This behaviour can be derived from chiral perturbation theory, and is clearly verified in lattice simulations.

The distinction between these behaviours provides a clear candle-stick which should allow us to discriminate between the possible dynamics of a gauge theory which have been discussed. In a lattice simulation this would be studied by measuring the mass, in lattice units, am_Γ of the ground-state mesons in each channel of quantum numbers, and determining their scaling with the quark mass, also in lattice units, am.

If the spectrum develops a large splitting between the pseudoscalar states and others, then this indicates strong chiral symmetry breaking, and the absence

of any near-conformal behaviour. If, on the other hand, this splitting is not observed, and the whole spectrum scales to be simultaneously massless at the chiral point, this illuminates the conformality of the massless theory, within the precision of the study.

If the massless theory were not quite conformal, but in fact near-conformal, in the sense of Sec. 2.4.2 then depending on the proximity to conformality, such a study would observe a hyperscaling behaviour for a range of masses before at some point in approaching the chiral limit, the chiral symmetry breaking in the infra-red would dominate over the near-conformal behaviour, and the mass-splitting between the pseudoscalar states and others would become significant, with the pseudoscalar states scaling to zero in the truly chiral limit and others remaining massive.

In addition to simply identifying the presence of some near-conformal behaviour, this method will also allow us to quantify the impact of the feature on the viability of a technicolor model with this technisector, by providing a simple measure of γ, the anomalous dimension of the quark condensate in the theory concerned. This is of great interest phenomenologically because it determines the level of enhancement of the techniquark condensate, and thus the Standard Model fermion masses, in a model of walking technicolor (2.44).

As discussed in Sec. 2.4.2, the technisector of a technicolor model cannot be truly conformal in the infra-red, and as such, in this limit the mass anomalous dimension cannot be constant. However, the analysis leading to (3.1) shows that, even in a theory perturbed from conformality, the scaling behaviour is determined by properties of the theory at the conformal point. Similarly, the value of the mass anomalous dimension in a near-conformal theory comprising the technisector of a technicolor model can be expected to be well approximated by the value of the anomalous dimension at the fixed point in the chiral theory.

As a result, we can in principle fit the behaviour of the meson masses am_Γ as a function of the quark mass am, according to a fit ansatz of the form (3.1), using γ_* as a free parameter, and hence obtain an estimate of the anomalous dimension.

In a theory which breaks chiral symmetry but in which the coupling runs very slowly over a large range of renormalisation scales, γ is expected to remain roughly fixed over this range of energies, close to its value at the theory's scale of strong dynamics, where it is expected to be $\mathcal{O}(1)$. It is estimated that a value of γ

in this range is required for the enhancement of the condensate which is required to generate sufficiently heavy fermion masses.

3.2.3 Difficulty of the chiral limit

These features indicate some of the difficulty in drawing firm conclusions from these studies. Firstly, the strength of the conclusions we can draw will be governed by how close we can get to the chiral point in our simulations. The difficulty of this approach to the chiral limit is a familiar problem in LGT, where it has been a primary obstacle to the power of lattice QCD throughout the history of its study.

Typically simulations of QCD using LGT have used quark masses which are significantly heavier than those in nature, and by observing the scaling of results with the quark mass, an extrapolation to the physical point can be performed, producing the desired quantity in the fundamentally relevant physical theory. Simulating light quarks on the lattice is difficult because of the increasing difficulty involved in inverting the Dirac matrix as we reduce the quark mass.

Secondly, clearly any computation performed on a computer can only involve pure numbers. In the case of lattice simulations this operates through the rescaling of all fields so that they become dimensionless quantities, reabsorbing the scale emerging from space-time integrals when they are transformed into discrete sums.

This scale is most easily represented by the variable a which represents the physical distance represented by the gap between sites of the lattice. All couplings are also rescaled to have a dimensionless representation on the lattice, e.g. a mass variable m is represented in lattice units am. This means that a lattice simulation cannot by itself provide any information on the scale of the physics being calculated, all quantities emerge in lattice units.

In order to relate results of lattice simulations to physical scales, it is necessary to find a way to determine the lattice scale a in any simulation. In the study of QCD on the lattice, this is achieved by choosing a quantity which is well known experimentally, and which can be expected to be relatively reliably measured in the relevant lattice simulation, albeit in lattice units.

We can then compare these two quantities, and by insisting that the simulation should reproduce the physical parameter, we can deduce the value of a. This process is known as *setting the scale*. Using this we can then convert all

other quantities into physical units, and determine the level of agreement with corresponding experimental values, as well as make predictions concerning quantities which are not otherwise well known.

In contrast to the study of QCD, the scale cannot be set definitively in studies of other gauge theories, because there is no experimental determination of any quantity with which we can compare our results. This leaves us in the difficult position of being unable eventually to physically quantify our results. While in QCD, we can establish how close any simulation is to the physical point, we can only determine the proximity of any simulation to the interesting chiral point in terms of lattice units. This weakens the conclusions that can be drawn from lattice simulations of theories other than QCD, but does not preclude us from drawing inference, so long as we qualify our results with this uncertainty.

3.3 Candidate theories

In this short section we will briefly describe the main results of searches for near-conformal dynamics in theories other than MWT, in order to set the scene and give an indication of the amount of work going on in this field, as well as the interesting results that have emerged, along with some of the more controversial cases which are currently attracting significant debate.

3.3.1 Fundamental fermions

$\mathbf{N_c = 2}$

The $SU(2)$ theory with $N_\mathrm{f} = 6$ fundamental Dirac fermions has been studied in [62] where it is determined that the gauge coupling runs relatively slowly in this theory, when compared to the result from a truncated perturbation theory result. In addition a suggestion of an enhanced anomalous mass dimension in the infra-red is detected.

$\mathbf{N_c = 3}$

Because the $SU(3)$ theory with $N_\mathrm{f} = 6$ fundamental fermions amounts to QCD (although lattice simulations of QCD rarely need consider $N_\mathrm{f} > 3$), a large amount of simulation infrastructure is easily adapted to studying $SU(3)$ with any N_f. For

this reason a large amount of work has been done analysing theories with a value of N_f such that the theory is expected to be in or near the conformal window while retaining asymptotic freedom, which suggests a range of $6 \leq N_\mathrm{f} \leq 12$.

The phase diagram of the $SU(3)$ theory as a function of N_f was first studied on the lattice in [63, 64], where they conclude that the conformal window begins at $N_\mathrm{f} = 7$. Later studies [65, 66] found that the theory with $N_\mathrm{f} = 8$ breaks chiral symmetry in the infra-red. In [67] the $N_\mathrm{f} = 10$ theory was determined to be infra-red conformal. There are a number of independent programs of investigation being conducted into the $N_\mathrm{f} = 12$ theory. The authors of [65, 68–72] have all concluded that the theory is conformal in the infra-red, however separate studies [73, 74] have deduced that this theory is chirally broken in the infra-red. This issue is still being debated and was discussed at length in [75].

3.3.2 Sextet fermions

The symmetric representation of $SU(3)$ is six dimensional and so is also known as the sextet. As described in Sec. 2.5, theories with fermions in the symmetric or anti-symmetric representation are termed orientifold theories, and as such the $SU(3)$ theory with sextet fermions is in the same class as MWT. This has led to the $SU(3)$ theory with $N_\mathrm{f} = 2$ flavours of Dirac fermion in the sextet representation to be termed *next to minimal walking technicolor* (NMWT) [76].

The theory was first studied on the lattice in [77], where evidence was found for conformality. This has been supported by evidence from a diverse selection of studies [78–81], while a separate study has found evidence for the opposite conclusion [82, 83].

3.4 Results from MWT

As discussed in Sec. 3.3, lattice simulations are in heavy use in the effort to determine the limits of the conformal window for different gauge groups and fermion representations, and the impact of near-conformal dynamics on the phenomenology of a theory. There are also clearly some uncertainties in the interpretation of results, as is evidenced by the opposite conclusions reached by different research groups regarding certain theories.

In this section we will attempt to summarise in more detail the results

pertaining to possibly the most interesting candidate theory, MWT. Several studies investigating the renormalisation behaviour of the theory, and also directly analysing the phenomenology of the theory have been performed.

3.4.1 Renormalisation

In [47, 48] analyses of the running coupling in MWT using the Schrodinger functional were carried out. Evidence for the conformality of the theory from the behaviour of the coupling was presented in [47], while in [48] more modest claims on this basis were made, fully taking into account their uncertainties. However evidence was presented for a non-zero mass anomalous dimension in [48], which, while not $\mathcal{O}(1)$ as would be preferred in order to best allow the theory to generate sufficient fermion masses, is an indication of near-conformal behaviour.

A study with equivalent goals, but using an alternative method, the Monte-Carlo renormalisation group (MCRG) was performed in [49]. This detected supporting evidence for near-conformal behaviour, but was qualified with similar uncertainties.

3.4.2 Spectroscopic

Significant attention has been paid to analysing the spectrum of MWT in order to ascertain the presence, or lack thereof, of near-conformal behaviour. This was initially explored in [50] wherein on a number of small lattices they find intriguing if inconclusive suggestions of near-conformal behaviour.

Such studies were expanded into more thorough programs in [51, 54, 58, 59] and also [53]. In these works significant evidence was accumulated that the spectrum of these theories is heavily influenced by an underlying near-conformal dynamics. The most significant conclusions are:

- The phenomenon of hyperscaling is observed with considerable clarity. The ground-state meson masses in the channels analysed are seen to scale together very closely as the quark mass m is varied. This feature is highlighted by considering the ratio between the pseudoscalar (PS) meson mass m_{PS} and that of the vector (V) m_{V}. This quantity is observed, as expected to be > 1 for all quark masses, but appears to be constant as

$m \to 0$, indicating the retention of chiral symmetry, and the hyperscaling feature.

- The scaling of $m_{\rm PS}$ with m also indicates near-conformal behaviour, most clearly seen in the ratio $\frac{m_{\rm PS}^2}{m}$. This quantity would be expected to be constant as $m \to 0$ in a chirally-broken theory, but is seen to scale to zero in the chiral limit.

- The anomalous dimension governing the scaling of the meson masses in the chiral limit is found to be small, certainly not $\mathcal{O}(1)$. This is determined through simple fits to the m dependence and also through finite size scaling (FSS) analyses.

3.4.3 Summary

Combining the evidence from all these studies, the most ready conclusion is that the MWT theory lies within the conformal window, and posesses an infra-red conformal fixed point. In order to increase the certainty of this statement it is necessary to push closer to the chiral limit and to ensure that finite-size effects, lattice artifacts and all other systematic uncertainties are under control.

Chapter 4

Improved Mesonic Spectroscopy of MWT

In this section we will describe the first project comprising this work. The aim of this study is to conduct a robust exploration of systematic effects present in the results of spectroscopic studies of MWT searching for evidence of near-conformal dynamics. We follow on from work conducted over recent years [51, 54, 58, 59].

As described in Sec. 3.4.2, these studies attempt to identify signals of near-conformal dynamics from the properties of the low-lying mesonic and, in the case of [54, 58], gluonic states of the theory. We focus on the ground-state mesons, their masses and decay amplitudes.

4.1 Introduction

As described in Sec. A.6, the standard way to extract masses from lattice simulations is to look at the exponential decay of correlators of operators with the quantum numbers of interest. For infinite separation between the source and sink operator, the exponential decay is governed by the ground state mass in the channel being explored. At finite time extent, this leading behaviour receives corrections that are exponentially suppressed in the mass difference between the ground state and the excitations. Underestimating the importance of these corrections leads to systematic errors in the determination of the ground state mass. In addition to the effects of the finite maximal separation between the source and the sink (often referred to as finite temperature effects), the finite

spatial extension of the lattice can also give sizeable corrections to the spectral masses.

The simplest source and sink observables to study for mesons are fermion bilinears in which the two fermion fields are at the same lattice point (*point sources*). These sources have been widely used in previous investigations of the spectrum of MWT. However, the experience accumulated over 30 years of numerical studies in lattice QCD favours the use of *extended sources*, which are gauge-invariant combinations of two fermion fields at different points, engineered for reducing the contamination from the excited states. In lattice QCD masses extracted from correlators of extended sources prove to be affected by smaller systematic errors. In this study, we investigate whether this proves to be the case also for MWT. Specifically, we perform a study of mesonic observables extracted from extended sources using the configurations presented in [51, 54, 59]. We explore a large set of schemes for building extended operators and we systematically analyse their efficiency for the computation of meson masses and decay constants, comparing the results with results obtained using point sources. With this study, we expect to determine the size of systematic uncertainties in current studies, which have as yet been largely unexplored, and to assess their impact on the physical picture emerging from the previous spectroscopical studies. Some of the results presented here have already appeared in Ref. [84].

The rest of the chapter is organised as follows. In Sec. 4.2 we describe the background to this study and briefly illustrate the effects of the use of different smearings on effective observables. Technical details on the smearing procedures and the resulting observables can be found in Appendices A.5 and A.6 respectively. In Sec. 4.3 we quantify the consequences of the smearing both for autocorrelation times and quality of plateaux. A full set of results obtained using wall smearing are presented in Sec. 4.4, while in Sec. 4.5 we comment on the significant finite-volume effects highlighted by the smeared results. Finally, our conclusions are reported in Sect. 4.6. This work has been presented previously [84] and recently published [85].

4.2 Systematic Spectroscopy

This study builds on the work described in [51, 59] where spectroscopic observables of MWT were measured through lattice simulations. The computation was performed using the *HiRep* code, designed to simulate theories of generic number of colours, and with fermions in a generic representation of the gauge group. The simulations used the Wilson gauge action, and the Wilson fermion formulation along with the RHMC algorithm. A number of lattice volumes have been analysed, from 16×8^3 to 64×24^3 with a range of bare quark masses. The majority of the ensembles have been generated at $\beta = 2.25$, although we do here present the results of some additional runs on the largest lattice at $\beta = 2.1$.

For this study we have performed some alternative analyses to those in [59]. The *Chroma* suite of lattice software [86] has been extended to operate with several fermionic representations other than the fundamental, including the adjoint. This will allow us to utilise the in-built smearing routines of *Chroma* for our spectroscopic study.

In order to test the modified *Chroma*, we measured the local correlators as defined in (A.49), with $\Gamma = \Gamma'$ both with *HiRep* ($f_\Gamma^{(h)}(t)$) and *Chroma* ($f_\Gamma^{(c)}(t)$). We used an ensemble of configurations on a 8×4^3 lattice with $\beta = 2.25$ and fermion bare mass $am_0 = -1$. Fig. 4.1 illustrates the agreement between the two determinations, defined as:

$$D_1 = \sqrt{\sum_t \left(f_\Gamma^{(c)}(t) - f_\Gamma^{(h)}(t) \right)^2} \qquad D_2 = \sqrt{\sum_t \left(\frac{f_\Gamma^{(c)}(t) - f_\Gamma^{(h)}(t)}{f_\Gamma^{(h)}(t)} \right)^2} . \tag{4.1}$$

We proceeded to utilise the in-built smearing routines found in *Chroma* to perform measurements on the gauge configurations generated with *HiRep* using a number of different quark smearings. We have investigated the use of both wall-smearing and a gauge invariant gaussian smearing, as defined in App. A.5.2. Definitions of all observables discussed can be found in App. A.6.

Gaussian smearing involves two parameters, which can be chosen to optimize the technique. They are the width of the smearing function and the number of applications of the smearing operator, which must be large enough to reasonably approximate the gaussian form. These two parameters have been adjusted in

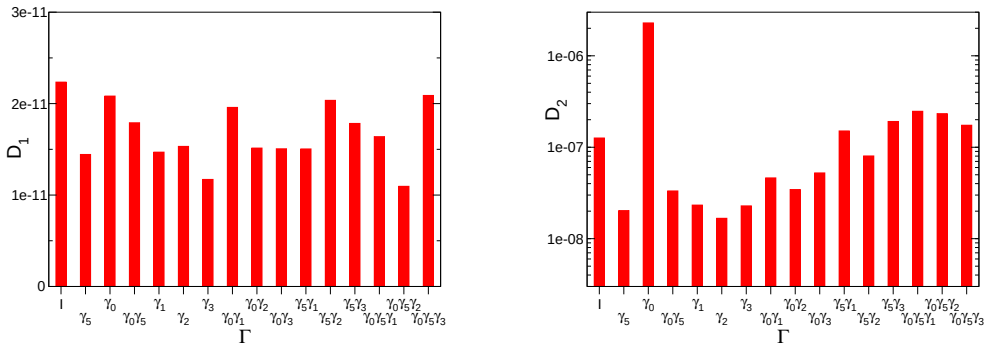

(a) D_1 (b) D_2

Figure 4.1: Discrepancies between local correlators from *HiRep* and *Chroma*, computed to test the extension of *Chroma* (for working with adjoint fermions) against HiRep. The quantities D_1 and D_2 defined in (4.1) are shown in Figs. 4.1(a) and 4.1(b) respectively.

order to maximize the overlap of the smeared operator with the ground state. On the other hand, the wall-smearing is a parameter-free procedure.

We systematically compared local, gaussian (with optimised parameters) and wall-smeared sources on our ensembles. At our lightest masses, the wall-smeared sources have the largest overlap with the ground state, which is reflected in the flattest effective masses. In Figs. 4.2, 4.3, 4.4 we show respectively the PCAC and PS effective masses and the PS effective decay constant computed with the three methods.

Making an initial cursory examination of these graphs we note, firstly, that there is reasonable agreement between the different effective observables at the largest temporal values available, and we will make a detailed analysis of this apparent agreement, and the significance of any discrepancies in Sec. 4.4.

We also note that the temporal dependence of the smeared results is less than that of the local result. This is an indication of the expected reduction in the contamination from excited states in the smeared correlators, and allows the extraction of a more reliable result from the effective observable. We will discuss quantitatively the improvement in the stability of the result over the temporal range in Sec. 4.3.2.

Qualitatively we note that the profile of the effective observables is improved most significantly by the wall smearing on the low mass ensembles. Since we are

mainly interested in the light masses, we will focus on the wall-smeared results in the rest of this work.

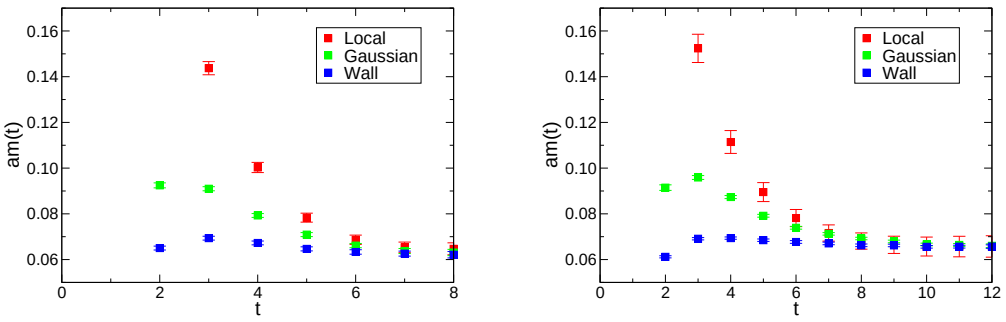

(a) 16×8^3 (b) 24×12^3

Figure 4.2: Comparison of the PCAC mass from different smearings at $am_0 = -1.175$ on a 16×8^3 lattice (Fig. 4.2(a)) and a 24×12^3 lattice (Fig. 4.2(b).

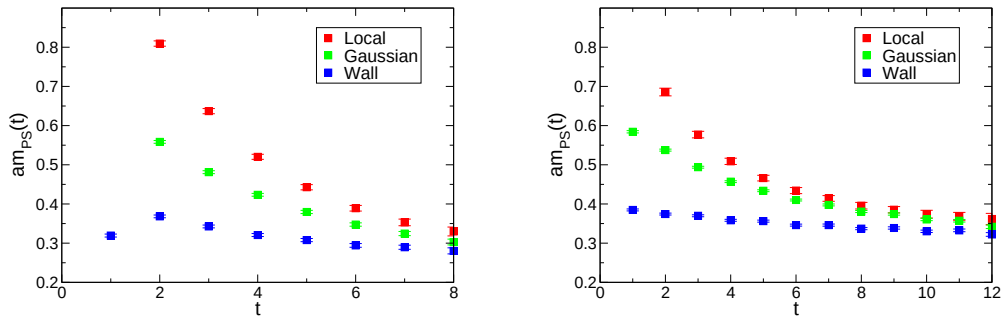

(a) 16×8^3 (b) 24×12^3

Figure 4.3: Comparison of the pseudoscalar mass from different smearings at $am_0 = -1.175$ on a 16×8^3 lattice (Fig. 4.3(a)) and a 24×12^3 lattice (Fig. 4.3(b).

4.3 Effectiveness of the wall-smeared sources

Using smeared sources allows us to choose an operator with a larger projection onto the ground state of a given channel. The wave-function of the ground

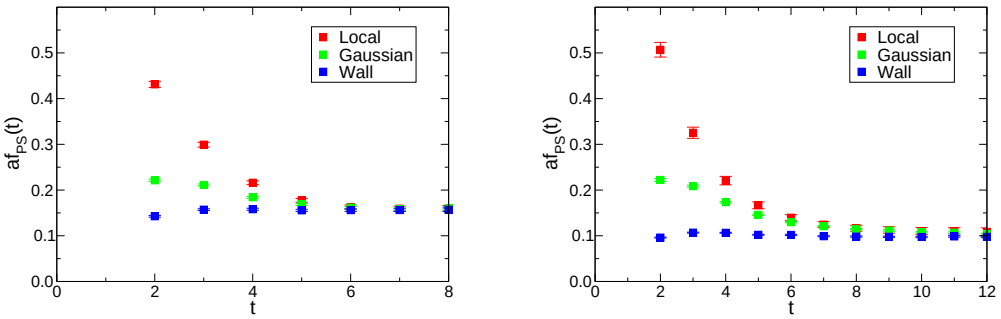

(a) 16×8^3 (b) 24×12^3

Figure 4.4: Comparison of the pseudoscalar decay constant from different smearings at $am_0 = -1.175$.

state is spread over many lattice sites, and we can improve the overlap of the operator with the ground state by giving a spatial size to the source. The smeared correlator will be less contaminated by the excited states, and therefore it will be characterized by a single cosh signal for a larger temporal separation than the one constructed with point operators. This is reflected in a longer plateau in the effective mass. On the contrary one drawback of using smeared sources is that it makes the analysis more sensitive to the algorithm's autocorrelation time. In this section we propose a quantitative study of these two aspects: the behaviour of the size of the plateaux for different kinds of sources, and the autocorrelation time connected with the use of these sources.

4.3.1 Autocorrelations

Correlators generated using sources with an extended spatial profile are expected to be associated with longer autocorrelation times, due to the fact that the low energy modes of the fields need more Monte-Carlo time to propagate. This effect is observed throughout our study, indeed the autocorrelation time associated with the results from smeared correlators is generically at least of the order of twice that of those involved with the local correlators. This is supported both by the direct measurement of the integrated autocorrelation time [87] associated with the observables, and by the analysis of the behaviour of the standard deviation of the observables.

Both the aforementioned studies have been performed by grouping the N data into N/b blocks of a given length b. A reduced dataset of length N/b is created by averaging the required statistic over each block. A bootstrap analysis is then performed on the reduced dataset. By increasing the block size b, we are creating effective estimates less and less autocorrelated, hence when the block size is bigger than the autocorrelation we expect to see a plateau appearing in the standard deviation, signaling that the reduced dataset is decorrelated. We observe that the plateau starts at a block size corresponding to an integrated autocorrelation time of order 1.

Our analysis of the autocorrelation is illustrated in Fig. 4.5, for the PS effective mass obtained with both local (L), and wall-smeared (W) sources, evaluated at two temporal points.

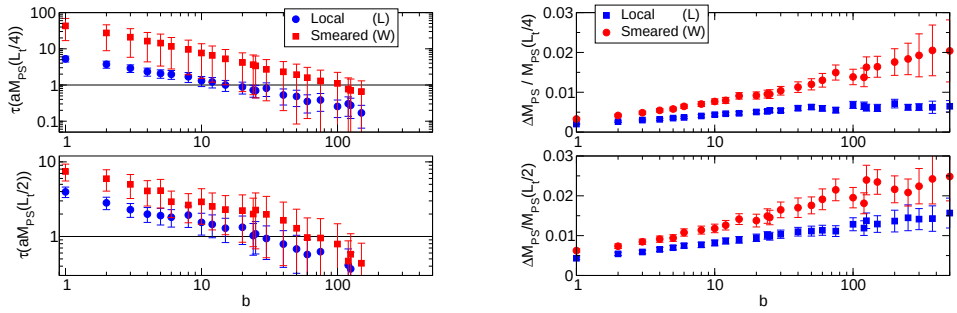

(a) Integrated autocorrelation time.

(b) Relative error.

Figure 4.5: Autocorrelation analysis conducted on a 24×12^3 lattice at $am_0 = -1.175$, for the PS effective mass in two temporal points. In Fig. 4.5(a), integrated autocorrelation time as a function of the block size b. In Fig. 4.5(b), relative error as a function of the block size b. The plateaux in the relative error set in when the integrated autocorrelation time becomes of order 1.

From the left panel of Fig. 4.5 we see that the measured autocorrelation time for the smeared results are generically larger than those for the local results. From the right panel of Fig. 4.5 we see that the standard deviation of our observable increases for both sets of correlators as we increase the block size from zero, up to a point where it appears to reach a plateau for a significant range of b for both cases. The value of b where this plateau sets in is interpreted as the length in simulation time over which the data are uncorrelated. From the right panel of Fig. 4.5 we would conclude that the autocorrelation time of our local result was

~ 30 while that of the smeared result was ~ 80. Indeed returning to the left panel of Fig. 4.5 we see that at this value of b, the corresponding value of the integrated autocorrelation time is close to 1, which supports our conclusion.

This picture is replicated across our ensembles, and we have accounted for this in our results by conducting our bootstrap analysis over appropriately reduced datasets.

4.3.2 Plateaux of the effective masses

If the smearing procedure is effectively suppressing the contribution of the excited states to the correlators, one has to observe the effective masses flattening around the midpoint $t = L_t/2$, and the plateaux becoming longer when visible. We can quantitatively estimate the flatness of the effective mass using the absolute value of the incremental ratio of the effective mass between $t = L_t/2$ and $t = L_t/2 - \Delta t$:

$$\frac{\Delta m_{PS}}{\Delta t} \equiv \left| \frac{m_{PS}(L_t/2 - \Delta t) - m_{PS}(L_t/2)}{\Delta t} \right| . \tag{4.2}$$

A value for $\Delta m_{PS}/\Delta t$ compatible with zero implies that the plateau in the effective mass is at least Δt points long. For very small values of Δt the incremental ratio is dominated by the statistical error. On the other hand the effective masses obtained with smeared sources are sometimes non monotonic. In this case the incremental ratio defined with a too large value for Δt is not a good estimate for the flatness of the plateau. An intermediate range of values for Δt exists, in which our analysis makes sense. We explicitly checked that our conclusions do not change choosing Δt in such a range, and we chose $\Delta t = 4$ for definiteness.

In general the smaller $\Delta m_{PS}/\Delta t$ is, the flatter the plateau. Notice that it is important to take the absolute value in the definition above: while the effective mass defined from local correlators is always decreasing, it is not so for smeared correlators.

In Fig. 4.6, the quantity $\Delta m_{PS}/\Delta t$ is plotted for all our pseudoscalar effective masses on the 16×8^3, 24×12^3 and 32×16^3 lattices, both for local and wall-smeared correlators.

One expects that at small masses the wave function of the pseudoscalar meson is more spread, hence the wall-smeared source should have a larger overlap with

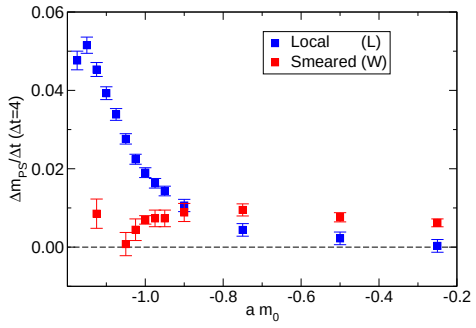

(a) 16×8^3

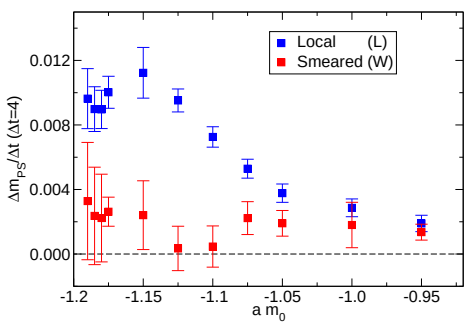

(b) 24×12^3

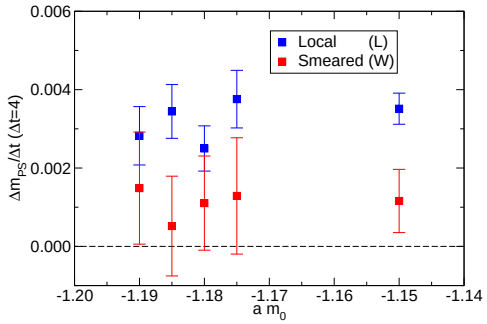

(c) 32×16^3

Figure 4.6: Incremental ratio $\Delta m_{PS}/\Delta t$ as a function of the bare mass. The smaller this quantity, the better the quality of the plateau of the PS effective mass. On the 16×8^3 lattice, the local correlators give flatter plateaux for bare masses larger than -0.8, while the smearing is effective below -0.9. On the 24×12^3 lattice, the local and smeared sources give plateaux of similar quality for the two heaviest masses, while the smearing is effective for all the other masses. Finally the smearing is always effective on the 32×16^3.

the ground state. On the contrary at large masses the wave function is more localised therefore the local sources should work better. Our analysis presented in Fig. 4.6 substantiates this expectation. On the 16×8^3 lattice the wall-smeared sources give better or comparable plateaux than the local sources for masses $am_0 \leq -0.9$. On the 24×12^3 and 32×16^3 lattices the wall-smeared sources are to be (sometimes marginally) preferred to the local ones for all the simulated masses.

In the presentation of the results obtained from wall-smeared sources we will always cut the masses in the 16×8^3 lattice for which the local sources are actually preferable to the wall-smeared ones, unless otherwise stated.

Finally, we point out that the same analyses using the effective V meson mass and the effective PS decay constant produce very similar results.

4.4 Results

In the present section, we will present our results for the mesonic observables from the wall-smeared sources. For the full local results, the reader is referred to [59].

We will consider only those fermionic masses for which the wall-smeared sources give an improvement on the plateaux of the effective masses with respect to the local sources, as discussed in Sec. 4.3.2. For all these masses, the wall-smeared results have to be trusted more than the local ones. The disagreement between the two determinations gives an estimate of the systematic error due to a bad determination of the plateaux, mainly affecting previous results obtained from local sources.

In order to quantify this disagreement we use two different estimators: the *pull* and the *relative discrepancy*. We will denote $O_L \pm \Delta O_L$ and $O_S \pm \Delta O_S$ the determination of the generic observable O using respectively local and smeared sources. The pull estimates the relative size of the systematic and statistical errors and is defined as:

$$P(O) = \frac{|O_L - O_S|}{\sqrt{\Delta O_L^2 + \Delta O_S^2}} \ . \tag{4.3}$$

A small value for the pull is desirable, indicating that the systematic errors are

smaller than the statistical ones. However a small value for the pull can be obtained either with a small systematic error or with a large statistical one. Therefore it is not an absolute estimator of the goodness of a measurement. The relative discrepancy estimates the systematic error, relative to the average of the two determinations:

$$D(O) = \frac{2|O_L - O_S|}{O_L + O_S} \ . \tag{4.4}$$

A small value for the relative discrepancy indicates that the systematic effects contribute to a small fraction of the determination of the observable O.

In what follows, we will consider separately the PCAC quark mass, the PS and V masses and their ratios, the PS and V decay constant. Again, we refer the reader to Appendix A.6 for the definition of these observables. We will present the results for the wall-smearing sources, and we will discuss the differences with the local-source results using the pull and the relative discrepancy.

4.4.1 PCAC mass

In Fig. 4.7 results for the PCAC mass from the wall-smeared correlators on all $\beta = 2.25$ ensembles are presented. The inset illustrates a close up of the approach to the chiral limit, with a linear extrapolation to zero quark mass. Using this we find the critical bare quark mass to be $am_c = -1.2022(14)$, from a fit using the three lightest points on the 24×12^3 lattice, which compares very well to the result obtained from the local data [59].

In Fig. 4.8 we show the stability of this fit against varying the number of points used. We compare this to the result obtained from local correlators, noting the agreement. It is also clear that finite volume effects for this quantity are at most comparable with the statistical uncertainty, which is to be expected as m is a UV quantity.

In Fig. 4.9 we show the pull and the relative discrepancy as defined in Eqs. (4.3) and (4.4) between the local and wall-smeared determinations of the PCAC quark mass. We include all the masses at which the wall-smeared sources give an improvement of the plateaux in the effective masses over the local sources. As shown in the left panel of Fig. 4.9, the pull is always smaller than 1 (or marginally larger than 1 for the smallest volume), indicating that the systematic error due to a short temporal direction is of the order of the statistical uncertainty.

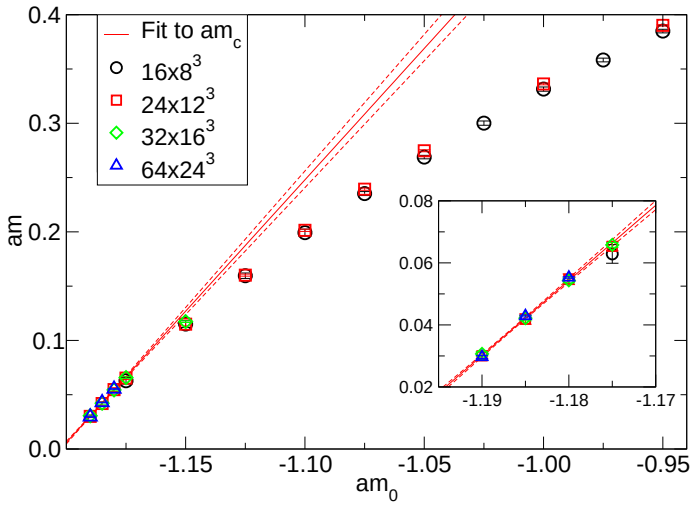

Figure 4.7: PCAC quark mass for ensembles at $\beta = 2.25$, computed with wall-smeared sources, as a function of the quark bare mass. The result of the linear fit for extracting the critical bare mass is also shown. In the inset, the lightest masses are zoomed in.

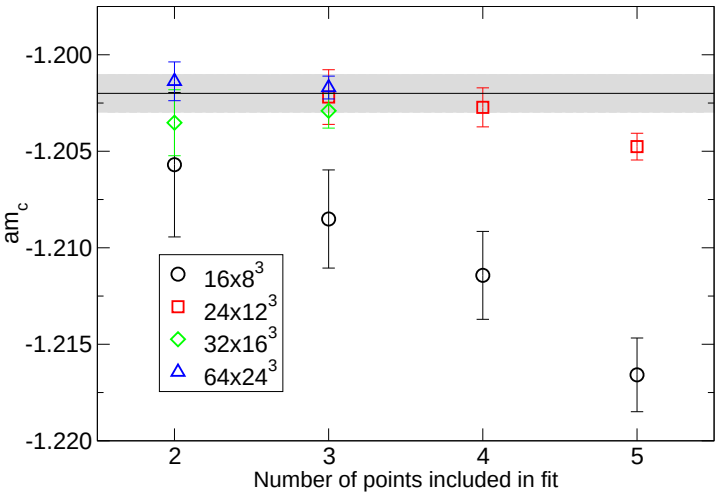

Figure 4.8: Critical quark mass extracted from a linear fit with different fit ranges. The critical mass as obtained from local data is shown as a grey band.

The right panel of Fig. 4.9 shows that the systematic error is of order of a few percents for the PCAC mass.

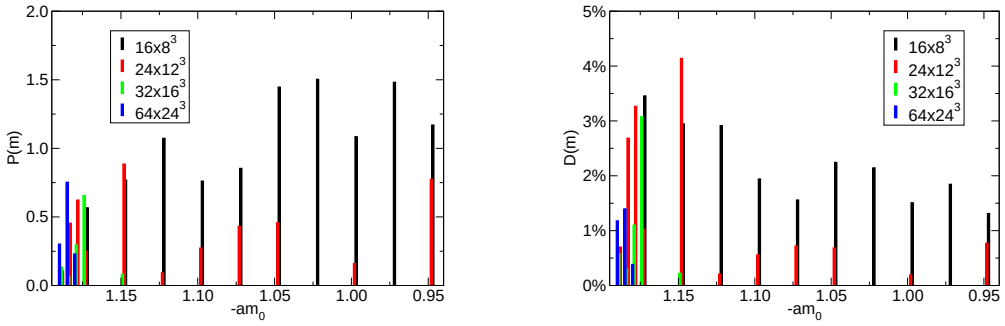

Figure 4.9: Pull and relative discrepancy as defined in Eqs. (4.3) and (4.4) for the PCAC quark mass ($\beta = 2.25$).

4.4.2 Meson masses

Fig. 4.10 shows the results obtained for the pseudoscalar mass M_{PS} as a function of the PCAC quark mass m, from the $\beta = 2.25$ data. Fig. 4.11 shows the ratio M_V/M_{PS}. We recall that the existence of a plateau at small masses of this ratio was one of the main ingredients for arguing in favour of an IR fixed point in [54] and [59]. We notice that the smeared results stabilize the plateaux at very small masses (especially by smoothing the behaviour of the largest volumes), while making more visible some finite-volume effects at intermediate masses. We will discuss the finite-volume effects in Sec. 4.5.

We also report the pull and relative discrepancy as defined in Eqs. (4.3) and (4.4) between the local and wall-smeared determinations of the PS mass in Fig. 4.12. Again, we include all the masses at which the wall-smeared sources give an improvement of the plateaux in the effective masses over the local sources. The local and smeared sources give quite different results at small masses. The relative discrepancy has a very regular behaviour: it is larger for lighter masses or smaller volumes. For bare masses below -1.15 one has to use lattices larger than the 24×12^3 in order to keep the relative discrepancy below the 10% level. Although the relative discrepancy can get fairly large at these masses, the pull is always below 3 which means that the two determinations are compatible within

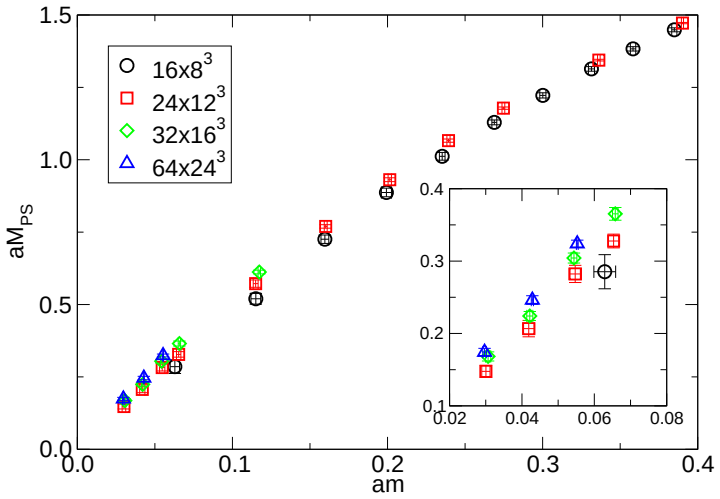

Figure 4.10: Pseudoscalar meson mass for ensembles at $\beta = 2.25$, computed with wall-smeared sources, as a function of the PCAC mass. In the inset, the lightest masses are zoomed in.

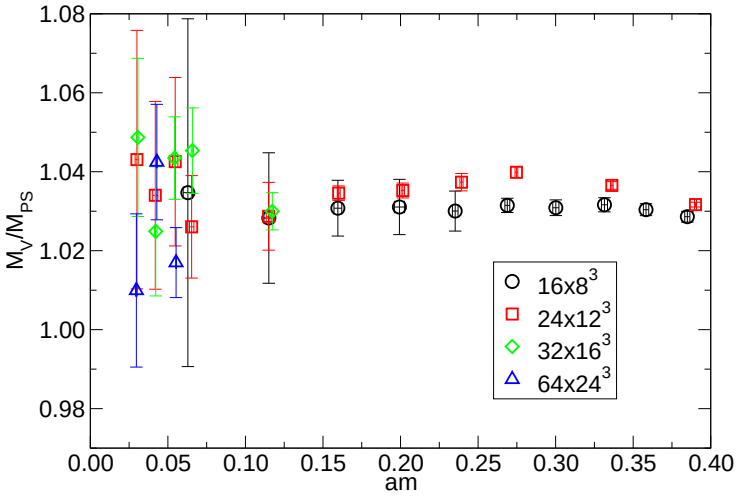

Figure 4.11: Ratio of M_V to M_{PS} for ensembles at $\beta = 2.25$, computed with wall-smeared sources, as a function of the PCAC mass. The plateau in this ratio at small masses has been interpreted in our previous works [54, 59] as a signal for IR-conformality. The smeared sources have amplified the finite volume effects at masses around $am \simeq 0.3$. This effect will be discussed in Sec. 4.5

the 3σ range. This effect is generated by an increase of the relative statistical error at light masses.

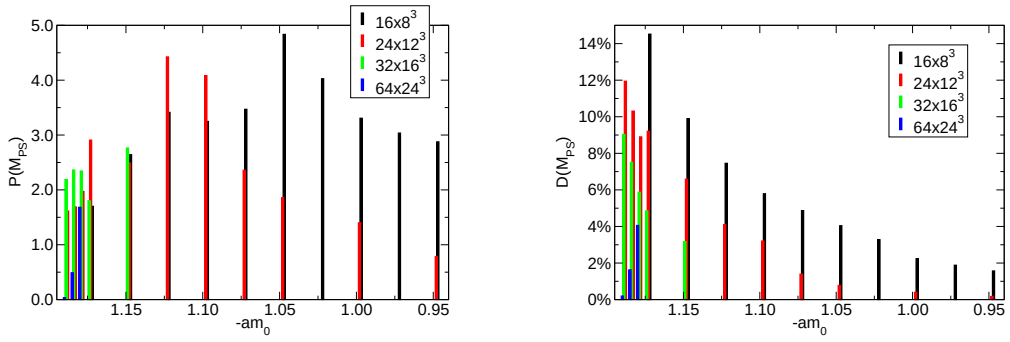

Figure 4.12: Pull and relative discrepancy as defined in Eqs. (4.3) and (4.4) for the PS mass ($\beta = 2.25$).

Fig. 4.13 shows the pull and relative discrepancy between the local and wall-smeared determinations of the M_V/M_{PS} ratio. The situation is better here. The central values of the two determinations never differ by more than 5% (relative discrepancy), and they are generally compatible (except the smallest volume) within the 2σ range (pull).

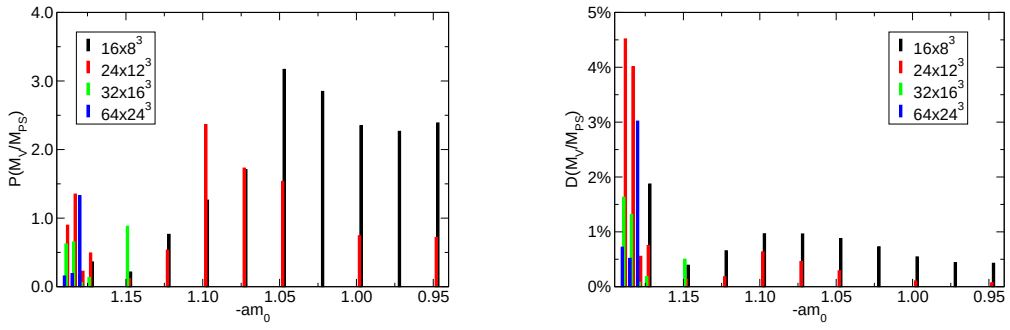

Figure 4.13: Pull and relative discrepancy as defined in Eqs. (4.3) and (4.4) for the ratio of the V mass over the PS mass ($\beta = 2.25$).

4.4.3 Decay constants

Among the observables considered in this study, the PS decay constant is the quantity most affected by systematic errors due to a short temporal dimension. The relative discrepancy between the local and smeared determinations (Fig. 4.14) is almost always very large. On the 24×12^3, 32×16^3 and 64×24^3 lattices, this large relative discrepancy is partly compensated by a large statistical error. In most of the cases the two determinations are compatible (sometimes marginally) within 3σ of the statistical uncertainty (pull). On the 16×8^3 lattice, the difference is more dramatic. However for intermediate masses, the wall-smeared source gives a better defined plateau in the effective PS decay constant as discussed in Sec. 4.3.2, and therefore the smeared results have to be trusted more than the local ones.

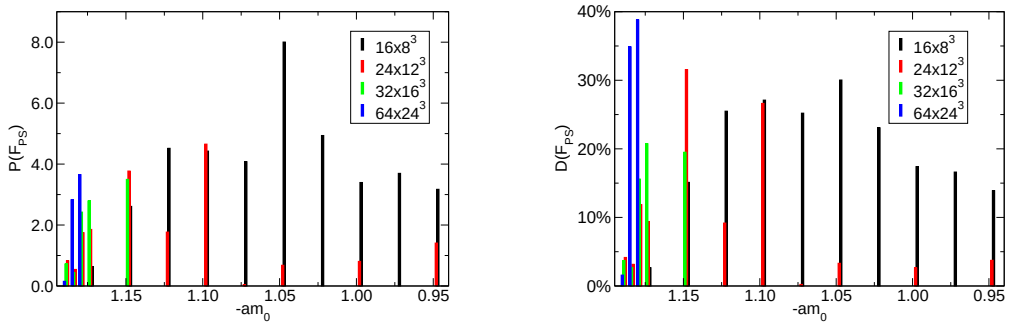

Figure 4.14: Pull and relative discrepancy as defined in Eqs. (4.3) and (4.4) for the PS decay constant ($\beta = 2.25$).

Fig. 4.15 shows the results for the PS decay constant from wall-smeared sources. The difference between the results on the 16×8^3 and 24×12^3 lattices are striking (and was absent in the local determination). This finite-volume effect will be discussed in Sec. 4.5. We also show for completeness the ratio F_V/F_{PS} in Fig. 4.16.

4.5 Comments on finite-volume effects

The wall-smeared results helped us to better understand how finite spatial volume affects the mesonic observables. In Fig. 4.17 we plot the PS and V masses,

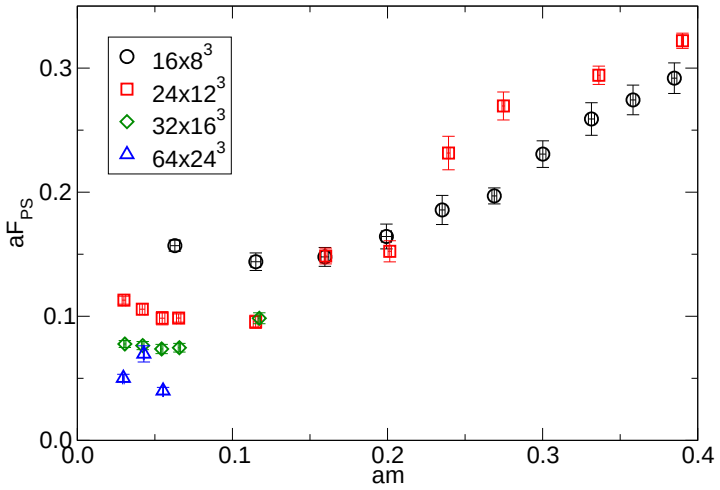

Figure 4.15: Pseudoscalar decay constant for ensembles at $\beta = 2.25$, computed with wall-smeared sources, as a function of the PCAC mass.

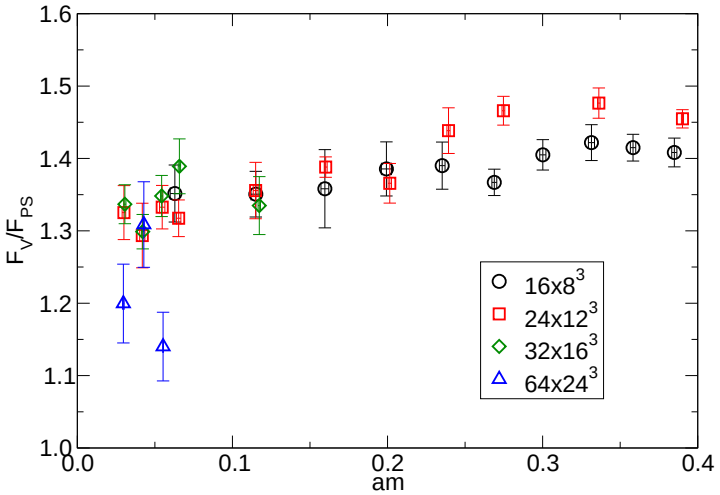

Figure 4.16: Ratio of vector and pseudoscalar decay constants.

their ratio and PS decay constant on the 16×8^3 and 24×12^3 lattices for $am_0 = -1.05$ and $\beta = 2.25$, both from local and wall-smeared sources. For each observable, the gap between the two lattices becomes wider when wall-smeared sources are considered. Having only the data from local sources, there is a risk of underestimating the finite-volume errors. This would be a mistake: the mild dependence on the volume of the local data is actually given by a cancellation of two larger effects: the finite volume and the bad determination of the plateaux in the effective masses.

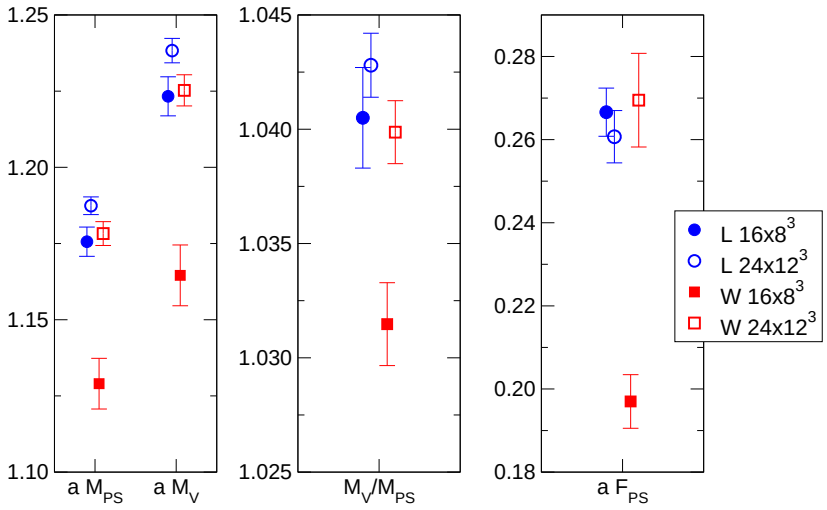

Figure 4.17: PS and V masses, their ratio and PS decay constant on 16×8^3 and 24×12^3 lattices for $am_0 = -1.05$ and $\beta = 2.25$ (L=local, W=wall).

In order to clarify this point, it is useful to look directly at the effective PS mass (Fig. 4.18) and the effective PS decay constant (Fig. 4.19). We will comment on the effective PS mass, but all the observations will be equally valid for the effective PS decay constant.

The first observation is that the effective masses from local sources are always decreasing with the Euclidean time. Therefore, if the temporal size is not large enough to contain the plateau of the effective mass, the estimated mass will be larger than the real one. On the other hand the effective masses from wall-smeared sources on this ensemble are increasing (although this is not true across

all ensembles). Therefore, if the plateau is not reached, the estimated mass will be smaller than the real one.

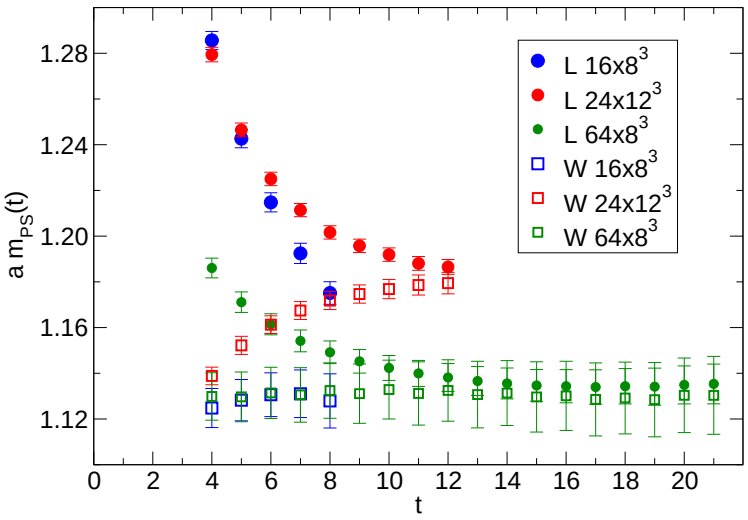

Figure 4.18: Effective PS mass on different volumes for $am_0 = -1.05$ and $\beta = 2.25$ (L=local, W=wall). At t larger than 21, this quantity (on the 64×8^3) becomes much noisier and we cut it for sake of clarity.

Consider now the 24×12^3 effective masses in Fig. 4.18. The local and wall-smeared sources give effective masses whose quality in terms of flatness is similar (compare with Fig. 4.6(b)), and the plateau is not clearly visible in any of the effective masses. However since the gap between the local and wall-smeared effective masses closes down in the midpoint $t = 12$, one can argue that the plateau is effectively reached there.

The situation is completely different for the 16×8^3. The gap between the local and wall-smeared effective masses is always quite big. The wall-smeared source gives a much flatter effective mass than the local source (compare with Fig. 4.6(a)). In order to obtain a more precise estimate for the pseudoscalar mass on the spatial volume 8^3, we simulated on a 64×8^3 lattice. In this case the temporal extent is large enough to obtain very good plateaux for both the local and wall-smeared effective masses.

By comparing the effective masses on the 24×12^3 and 64×8^3 lattices it is clear that the finite volume has the effect of making the pseudoscalar meson lighter.

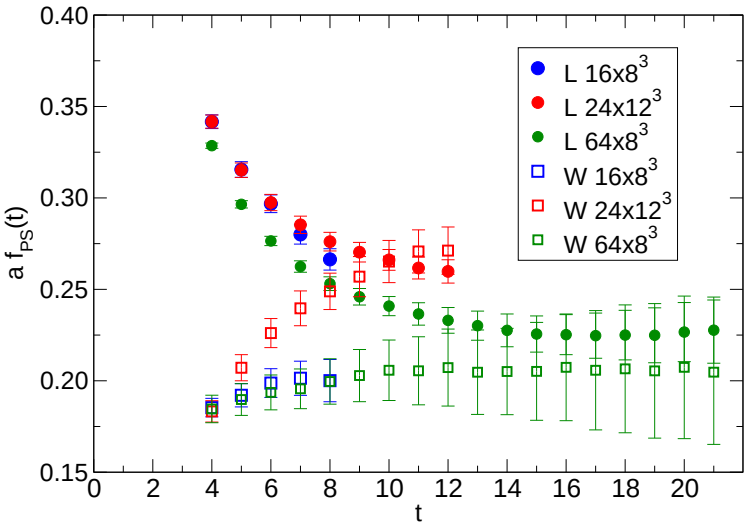

Figure 4.19: Effective PS decay constant on different volumes for $am_0 = -1.05$ and $\beta = 2.25$ (L=local, W=wall). At t larger than 21, this quantity (on the 64×8^3) becomes much noisier and we cut it for the sake of clarity.

What is happening then with the 16×8^3 lattice? The mass estimated with the local sources is affected by two relatively large effects: the finite volume, which decreases the mass and the bad determination of the plateaux, which increases the mass. Having opposite sign and accidentally the same magnitude, these two effects cancel each other. Therefore the finite volume effects are actually larger than what we estimated on the basis of the local sources, and they are better estimated using the wall-smeared source at light enough masses.

The conclusions above are valid also for the vector meson mass and for the ratio $M_{\rm V}/M_{\rm PS}$. In particular from Fig. 4.11 it is clear that on increasing the spatial volume, the ratio $M_{\rm V}/M_{\rm PS}$ slightly increases, and this effect was completely hidden in the local-source determination.

4.6 Conclusions

In this project we have studied systematic effects on the PCAC mass, the mesonic masses and decay constants due to a short temporal size on the SU(2) gauge

theory with two Dirac fermions in the adjoint representation. In order to isolate the ground state in correlators one should take the source and sink infinitely distant. In practice one defines effective quantities (masses and decay constants) which depend on the time separation between source and sink, and which show a plateau at large distances. The value of the plateau gives an estimate for the corresponding mass or decay constant. At fixed temporal extent one can increase the relative amplitude of the ground state in correlators, using smeared sources and/or sinks. This translates into flatter and longer plateaux in the effective quantities.

We have extended the *Chroma* suite of software in order to operate with fermions in the adjoint representation of the gauge group, and we have used the *Chroma* built-in routines for measuring mesonic correlators with both Gaussian and wall-smeared sources. We observe that at our lightest masses the wall-smearing gives always the best overlap with the ground state. At heavy masses the mesonic wave functions are more localized and the local sources give a better overlap with the ground state. There is an intermediate regime of masses in which the local and wall-smearing sources yield plateaux of similar quality. In this case a Gaussian smearing with properly chosen width might be desirable. If one wants a procedure that enhance the overlap with the ground state at any mass, one should use a variational method with a large set of smeared sources. However, since the interesting physical region is close to the chiral limit, we chose simplicity against generality and we focused our detailed analysis on the wall-smearing only.

The enhancement of the plateaux with smeared sources does not come for free. Observables obtained with smeared sources have longer autocorrelation times. For a fixed set of configurations, a better control on the systematic error with respect to local sources is generally obtained at the cost of a larger statistical uncertainty.

Among the observables that we have considered, the PCAC mass is the least affected by the systematics, as expected since this is a UV quantity, while the decay constants are the most affected. In the region $aM_{\rm PS} < 0.5$, the 16×8^3 lattice yields relative systematic errors for the PS mass larger than 10%. At least the 24×12^3 lattice is needed in order to stay below 10%.

We also investigated how the finite temporal extent can conspire to partially mask effects due to finite spatial volume, and discovered that finite-volume effects

were underestimated in our analysis with local sources. The relative difference between the determinations of the PS mass on the 16×8^3 and 24×12^3 lattices is of order 5% at $aM_{\rm PS} \simeq 1$ and it goes up to 14% at about $aM_{\rm PS} \simeq 0.3$. Again, in the interesting region of masses, the 16×8^3 lattice appears to be way too far from the infinite volume limit. A detailed study of finite-volume effects is extremely important in order to address issues like IR-conformality, and represents one of our major research lines.

Finally we notice that our conclusions regarding the near-conformal dynamics of this theory are robust, since the main qualitative features already presented in Refs. [54, 59] are confirmed by the present analysis.

Chapter 5

The Vacuum Polarisation Contribution to the Muon Anomalous Magnetic Moment from DWF

The second project contained in this work departs somewhat from the main theme. It was chosen, in addition to the reasons of the topical and interesting nature of the project, because it formed a natural connection with previous work on the S parameter in QCD [56] which was intended to lay the foundations for a calculation of the S parameter in MWT, which itself comprises the latter project in this thesis.

In this chapter, we present a calculation of the leading order hadronic contribution to the anomalous magnetic moment of the muon for a dynamical simulation of 2+1 flavour QCD using domain wall fermions. The electromagnetic 2-point function is evaluated on the lattice gauge configurations and this is fitted to a continuous form motivated by models of vector dominance. We find broad agreement with previous lattice results for this quantity, while improvements in simulation and theory are clearly needed in order to produce satisfactorily precise results.

5.1 Introduction

The anomalous magnetic moment a of a lepton, is half the discrepancy from 2 ($a = \frac{g-2}{2}$) of g, the gyromagnetic ratio or Landé g-factor, which relates the spin $\vec{S}$ of the lepton to its magnetic moment $\vec{\mu}$ as

$$\vec{\mu} = g\frac{e}{2m}\vec{S}. \tag{5.1}$$

It is given the name "anomalous" because it is a purely quantum effect and so is zero in a classical theory.

The one-loop computation of the electron anomalous magnetic moment a_e by Schwinger [88] was one of the first such calculations, and provided strong evidence in support of the young theory of quantum electrodynamics (QED) by explaining observed hyper-fine phenomena which were not well understood. Since then a_e has become possibly the most accurately determined quantity in science, being known to a precision better than one part per billion [89]. The corresponding theoretical calculation has achieved similar accuracy [90]. Because of the relatively light mass of the electron, the calculation is strongly dominated by QED contributions with virtual electrons, which are known to a good accuracy to four-loops. Using an independent determination of the fine-structure constant α from atomic interferometry results in a value of a_e which agrees with the experimental result, with an uncertainty over 30 times greater. Combining the experimental and theoretical results for a_e in terms of the fine structure constant α provides the most accurate available determination of α [89].

Because of its heavier mass, $\frac{m_\mu^2}{m_e^2} \simeq 40000$, the muon anomalous magnetic moment a_μ is far more sensitive to contributions from other sectors of the standard model, as well as to any potential new-physics contributions. This makes it a far more robust test of the standard model, and a much more interesting searching-ground for signals of new physics. The current experimental result, while not nearly as accurate as that for a_e is still remarkably precise [91]:

$$a_\mu = 11659208.0(6.3) \times 10^{-10}, \tag{5.2}$$

which remains a precision of better than one part per million.

Obtaining a theoretical result for a_μ of comparable precision has proved a

more difficult task than in the case of a_e [92]. This is because, as stated above, the contributions from other sectors of the standard model are more significant. However the calculation has been brought to a point where the uncertainty is of the same order as the experimental uncertainty. Interestingly however, there is a discrepancy between the two values which exceeds the current uncertainty. This has attracted a huge amount of interest to a_μ and led to significant efforts to calculate contributions from potential new-physics sectors.

The current uncertainty in a_μ is strongly dominated by hadronic contributions, specifically the leading order hadronic, and hadronic light-by-light contributions. The light-by-light contribution has attracted significant theoretical interest, and has recently become the focus of considerable work using lattice simulations [93, 94].

This work involves the leading order hadronic contribution, which we denote as $a_\mu^{(2)\mathrm{had}}$, the best estimate of which is currently obtained by relating the hadronic vacuum polarisation of the photon to the cross section for e^+e^- decay into hadrons, allowing a dispersive integral over experimental data for the cross section [95].

Despite the apparent accuracy of the results obtained from this procedure, there remain discrepancies between results from different data sets. As a result, it is not clear if this method of obtaining the vacuum polarisation is under good control [92, 95]. Attempts have also been made to estimate this quantity using models of low energy QCD [96]. It would, however, be preferable to obtain the hadronic contribution to a_μ from a first principles approach. For this the only valid candidate is lattice QCD which alone is capable of producing quantitative results from fully non-perturbative QCD.

This quantity was first tackled through lattice computation in quenched simulations with domain wall fermions [97] , followed by a calculation with improved Wilson fermions [98]. The first dynamical simulation followed [99, 100] using 2+1 flavour staggered quarks, and several studies of this quantity are ongoing, using 2 flavours of improved Wilson fermions [101] and twisted mass fermions [102]. We present a calculation of $a_\mu^{(2)\mathrm{had}}$ from a dynamical simulation of 2+1 flavour QCD with domain wall fermions. This work has been previously released as an eprint [103].

5.2 Background

The Landé g-factor of a fermion can be expressed in terms of the electromagnetic form factors F_1 and F_2 as

$$g = 2\left[F_1(0) + F_2(0)\right]. \tag{5.3}$$

These form factors are defined in the effective electromagnetic scattering vertex whereby the expression for the tree-level graph

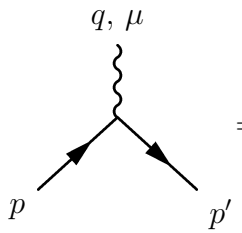

$$= -ie\gamma_\mu \tag{5.4}$$

is replaced by its equivalent including all quantum corrections

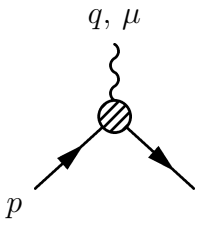

$$= -ie\Gamma_\mu(p', p) \equiv -ie\left[\gamma_\mu F_1(q^2) + \frac{i\sigma^{\mu\nu}q_\nu}{2m}F_2(q^2)\right]. \tag{5.5}$$

From the Born approximation it can be seen that $F_1(0) = 1$ to all orders, and so

$$a = \frac{g-2}{2} = F_2(0). \tag{5.6}$$

We seek to compute the effect of hadronic vacuum polarisation contributions to a_μ which are obtained by calculating contributions to the graph in (5.5) of the form

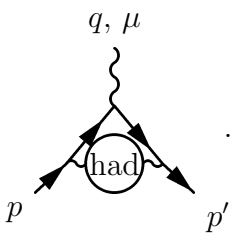

. (5.7)

As described in [97] the contribution to a_μ from the one-loop diagram equivalent to the graph (5.7) with the hadronic blob removed can be expressed as

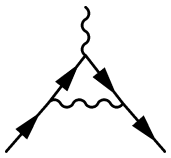

$$\longrightarrow a_\mu^{(1)} = \frac{\alpha}{\pi}\int_0^\infty dQ^2\, f(Q^2) \tag{5.8}$$

where the kernel function $f(Q^2)$ is divergent as $Q^2 \to 0$ and can be expressed

$$f(Q^2) = \frac{m_\mu^2 Q^2 Z(Q^2)^3(1 - Q^2 Z(Q^2))}{1 + m_\mu^2 Q^2 Z(Q^2)^2} \qquad Z(Q^2) = -\frac{Q^2 - \sqrt{Q^4 + 4m_\mu^2 Q^2}}{2m_\mu^2 Q^2} \tag{5.9}$$

From this, the expression for the hadronic vacuum polarisation contribution can be obtained with the insertions:

$$\longrightarrow a_\mu^{(2)\mathrm{had}} = \left(\frac{\alpha}{\pi}\right)^2 \int_0^\infty dQ^2\, f(Q^2) \times \hat{\Pi}(Q^2) \tag{5.10}$$

where $\hat{\Pi}(Q^2)$ is the infra-red subtracted transverse part of the hadronic vacuum polarisation

$$\hat{\Pi}(Q^2) = \Pi(Q^2) - \Pi(0) \qquad \Pi_{\mu\nu}(q) = (q^2 g_{\mu\nu} - q_\mu q_\nu)\Pi(q^2) \tag{5.11}$$

$$\equiv i\Pi_{\mu\nu}(q) \tag{5.12}$$

at Euclidean momentum $Q^2 = -q^2$. The hadronic vacuum polarisation function $\Pi_{\mu\nu}(q)$ can be computed as the Fourier-transformed two-point correlator

$$\Pi_{\mu\nu}(q) = \int d^4x\, e^{iq\cdot(x-y)} \langle J_\mu(x) J_\nu(y)\rangle \tag{5.13}$$

involving the electromagnetic current

$$J_\mu(x) = \sum_i Q_i \bar{\psi}^i \gamma_\mu \psi^i \tag{5.14}$$

where ψ^i is the quark field of flavour i and Q^i is its charge. The path-integral used in the expectation value in (5.13) will involve only hadronic fields, i.e. quarks and gluons.

5.2.1 Simulation

Our computation is performed using configurations generated by the RBC & UKQCD collaborations as part of their program of investigation using 2+1 flavours of domain-wall fermions (DWF). The definition of the DWF fermion action is presented in A.4.3.

We investigate three lattice volumes, each with several ensembles at different values of the light quark mass m_u. The parameters of these ensembles are given in Table 5.1. The ensembles at $\beta = 1.75$ have been generated using a dislocation suppressing determinant ratio (DSDR) in conjunction with the Iwasaki gauge action, with a fifth dimension whose extent is L_5=32 [104, 105]. The lighter of these ensembles is very near to the physical point with a pion mass of $m_\pi \simeq 180$ MeV. The other ensembles used only the Iwasaki action and $L_5 = 16$ [106, 107].

V	β	a^{-1} GeV	$\hat{q}^2_{min}$ GeV^2	am_h	am_u
$24^3 \times 64$	2.13	1.73(2)	0.028	0.04	0.02
$24^3 \times 64$	2.13	1.73(2)	0.028	0.04	0.01
$24^3 \times 64$	2.13	1.73(2)	0.028	0.04	0.005
$32^3 \times 64$	2.25	2.28(3)	0.05	0.03	0.008
$32^3 \times 64$	2.25	2.28(3)	0.05	0.03	0.006
$32^3 \times 64$	2.25	2.28(3)	0.05	0.03	0.004
$32^3 \times 64$	1.75	1.375(9)	0.018	0.045	0.0042
$32^3 \times 64$	1.75	1.375(9)	0.018	0.045	0.001

Table 5.1: Parameters of the lattice ensembles used in our study.

β	am_u	Z_V	am_{V}	am_{PS}	af_{V}
2.13	0.02	0.696(2)	0.579(6)	0.3227(7)	
2.13	0.01	0.700(2)	0.529(5)	0.2422(5)	
2.13	0.005	0.699(2)	0.505(6)	0.1904(6)	
2.25	0.008	0.7380(5)	0.388(6)	0.1727(4)	0.078(6)
2.25	0.006	0.7385(6)	0.366(5)	0.1512(3)	0.076(5)
2.25	0.004	0.7387(7)	0.356(6)	0.1269(4)	0.070(11)
1.75	0.0042	0.664(5)	0.570(25)	0.1809(3)	0.102(6)
1.75	0.001	0.669(8)	0.558(44)	0.1249(3)	0.105(15)

Table 5.2: Relevant observables measured on our lattices. Results on the $\beta = 1.75$ lattices are preliminary and will be outlined in a forthcoming publication [105], results for f_{V} on the 64×24^3 lattices are currently unavailable.

5.2.2 Vacuum polarisation

We compute the lattice vacuum polarisation as

$$\widetilde{\Pi}_{\mu\nu}(x) = Z_V \sum_i Q_i^2 a^6 \langle \mathcal{V}_\mu^i(x) V_\nu^i(0) \rangle, \tag{5.15}$$

where we have omitted the flavour-nondiagonal terms as they contain only "disconnected" contributions which are expected to be sub-dominant, as will be discussed further below. At the sink we use the DWF conserved vector current [108]

$$\mathcal{V}_\mu^i(x) = \sum_{s=1}^{L_5} \frac{1}{2} \left[\bar{\psi}^i(x+\hat{\mu}, s)(1+\gamma_\mu) U_\mu^\dagger(x) \psi^i(x,s) - \bar{\psi}^i(x,s)(1-\gamma_\mu) U_\mu(x) \psi^i(x+\hat{\mu}, s) \right] \tag{5.16}$$

while at the source we have the local vector current $V_\nu^i(x) = \bar{q}^i(x)\gamma_\nu q^i(x)$ where $q^i(x) = P_+\psi^i(x, L_5 - 1) + P_-\psi^i(x, 0)$, and $P_\pm = \frac{1}{2}(1 \pm \gamma_5)$. Because of the use of the local vector current, a factor of the vector current renormalisation constant, Z_V, is included in our definition of the vacuum polarisation. The values of Z_V used on each ensemble are given in Table 5.2, as measured in [107].

These correlators were generated for, and used in, the measurement of the QCD contribution to the electro-weak S-parameter [56]. However, they will prove perfectly sufficient for our purposes, as long as we are mindful of Ward Identity violations, which will be discussed in Sec. 5.2.3.

There are two possible ways to perform a Wick contraction of the fermionic

fields in the correlator (5.15). In order to estimate the correlator, we will compute only the connected contraction. We will make an estimate of the corresponding systematic uncertainty in our results. By calculating the relevant correlation functions to NLO in chiral perturbation theory, it has been shown [109] that, in the $N_{\mathrm{f}} = 2$ theory, the disconnected contribution is suppressed relative to its connected counterpart by a factor of 10.

We Fourier transform into momentum space:

$$\widetilde{\Pi}_{\mu\nu}(\hat{q}) \equiv Z_V \sum_i Q_i^2 \sum_x e^{iqx} a^6 \langle \mathcal{V}_\mu^i(x) V_\nu^i(0) \rangle \tag{5.17}$$

using the discrete momenta $q_\mu = \frac{2\pi n_\mu}{L_\mu}$ where n_μ is a 4-tuple of integers, and L_μ is the length of the lattice in the μ direction. From here, we will use the lattice momentum

$$\hat{q}_\mu = \frac{2}{a} \sin\left(\frac{\pi n_\mu}{L_\mu}\right). \tag{5.18}$$

We associate the quantity $\hat{q}^2 = \sum_\mu \hat{q}_\mu^2$ with the continuum momentum Q^2.

5.2.3 Ward identities

In order to ensure that this reproduces a vacuum polarisation of the form (5.11) we must verify that this lattice correlator satisfies the Ward identity $q_\mu \Pi_{\mu\nu} = 0$ which in general is not the case, as although both operators $\mathcal{V}^i$ and V^i have the correct continuum limit

$$\mathcal{V}_\mu^i, V_\mu^i \xrightarrow{a \to 0} J^i = \bar{\psi}^i \gamma_\mu \psi^i \tag{5.19}$$

the additional irrelevant operators introduced into the lattice action modify the Ward identity for $\widetilde{\Pi}_{\mu\nu}$. In coordinate space, the Schwinger Dyson equation for $\widetilde{\Pi}_{\mu\nu}$ reads

$$\langle (\Delta_\mu \mathcal{V}_\mu^i(x)) V_\nu^i(0) \rangle + \left\langle \left(\frac{V_\nu^i(0) \overleftarrow{\partial}}{\partial \psi^i(x)} \psi^i(x) \right) - \left(\bar{\psi}^i(x) \frac{\vec{\partial} V_\nu^i(0)}{\partial \bar{\psi}^i(x)} \right) \right\rangle = 0 \tag{5.20}$$

where Δ_μ is the backward lattice derivative. Because the local current used is not point-split, the second term in (5.20) vanishes and we have as a result that $e^{\frac{iaq_\mu}{2}} \hat{q}_\mu \widetilde{\Pi}_{\mu\nu} = 0$.

This is illustrated in Fig. 5.1 where we see that it is necessary to include

the factor $e^{i\frac{aq_\mu}{2}}$ in the Ward identity for the first index of $\widetilde{\Pi}_{\mu\nu}$, while there is no fulfilled Ward identity for the second index.

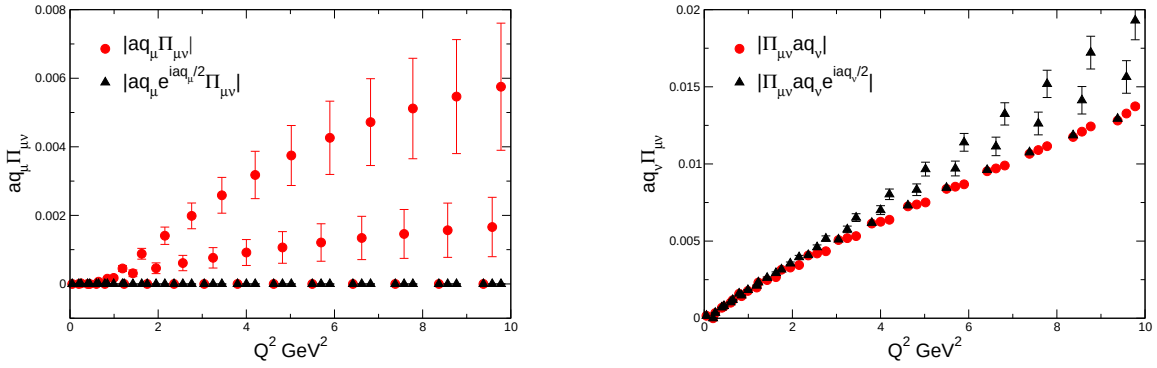

(a) $a\hat{q}_\mu\widetilde{\Pi}_{\mu\nu}$ (b) $\widetilde{\Pi}_{\mu\nu}a\hat{q}_\nu$

Figure 5.1: Illustration of Ward identity violations in $\Pi_{\mu\nu}$ on $32^3\times64$ lattice at $\beta = 2.25$ and $am_u = 0.004$.

5.2.4 Decomposing the vacuum polarisation

We must extract from $\widetilde{\Pi}_{\mu\nu}(\hat{q})$ the scalar vacuum polarisation $\widetilde{\Pi}(\hat{q}^2)$ which, corresponding to the continuum (5.11), are related by

$$\widetilde{\Pi}_{\mu\nu}(\hat{q}) = (\hat{q}^2\delta_{\mu\nu} - \hat{q}_\mu\hat{q}_\nu)\widetilde{\Pi}(\hat{q}^2) \tag{5.21}$$

In practice, in order to avoid any longitudinal contribution which might arise due to the non-conservation of Ward identities, for each momentum orientation we choose directions μ such that $\hat{q}_\mu = 0$ and compute

$$\widetilde{\Pi}(\hat{q}^2) = \frac{\widetilde{\Pi}_{\mu\mu}(\hat{q})}{\hat{q}^2} \tag{5.22}$$

where in the above there is no sum over μ.

In Fig. 5.2 we show an example of the resulting vacuum polarisation function, and compare this to the three-loop continuum perturbation theory result from [110], using two massless flavours of quarks and one massive flavour which we associate with the strange quark. This result is quoted in the $\overline{\text{MS}}$ scheme and as such we require the strange quark mass in our simulations expressed in $\overline{\text{MS}}$.

The non-perturbative renormalization factor $Z_{mh}^{\overline{\mathrm{MS}}}$ relating the bare strange quark mass in physical units $\tilde{m}_\mathrm{h}$ and the renormalised mass in the $\overline{\mathrm{MS}}$ scheme $\overline{m}_\mathrm{h}$,

$$\overline{m}_\mathrm{s} = Z_\mathrm{mh}^{\overline{\mathrm{MS}}} \tilde{m}_\mathrm{s} \tag{5.23}$$

is determined in [107] by first calculating the renormalisation factor in a non-perturbative lattice scheme before converting to $\overline{\mathrm{MS}}$ using perturbative results. The result is extrapolated to the chiral limit, with a very slight chiral dependence, and then further extrapolated to the continuum limit. They obtain

$$Z_{mh}^{\overline{\mathrm{MS}}} = 0.1533(6)(33) \tag{5.24}$$

and using this we calculate the renormalised strange quark mass in the $\overline{\mathrm{MS}}$ scheme in lattice units from the bare strange quark mass in lattice units on each of our ensembles

$$a\overline{m}_\mathrm{s} = Z_\mathrm{mh}^{\overline{\mathrm{MS}}} a m_\mathrm{s}. \tag{5.25}$$

5.3 Deducing $a_\mu^{(2)\mathrm{had}}$

In order to infer the value of $a_\mu^{(2)\mathrm{had}}$ from our data we must carry out the integral (5.10) which we split into high and low momentum regions at some momentum cut Q_C^2

$$a_\mu^{(2)\mathrm{had}} = 4\alpha^2 \left[\int_0^{Q_C^2} dQ^2 f(Q^2) \times \hat{\Pi}(Q^2) + \int_{Q_C^2}^{\infty} dQ^2 f(Q^2) \times \hat{\Pi}(Q^2) \right]. \tag{5.26}$$

A continuous description of $\Pi(Q^2)$ at low momenta is obtained by performing a fit to our lattice data, which allows us to perform the low Q^2 integral. The value of $\Pi(0)$ from this fit combined with a high-momentum description of $\Pi(Q^2)$ from perturbation theory allows us to perform the high momentum integral. As we shall see, the integral is strongly dominated by the low momentum contribution.

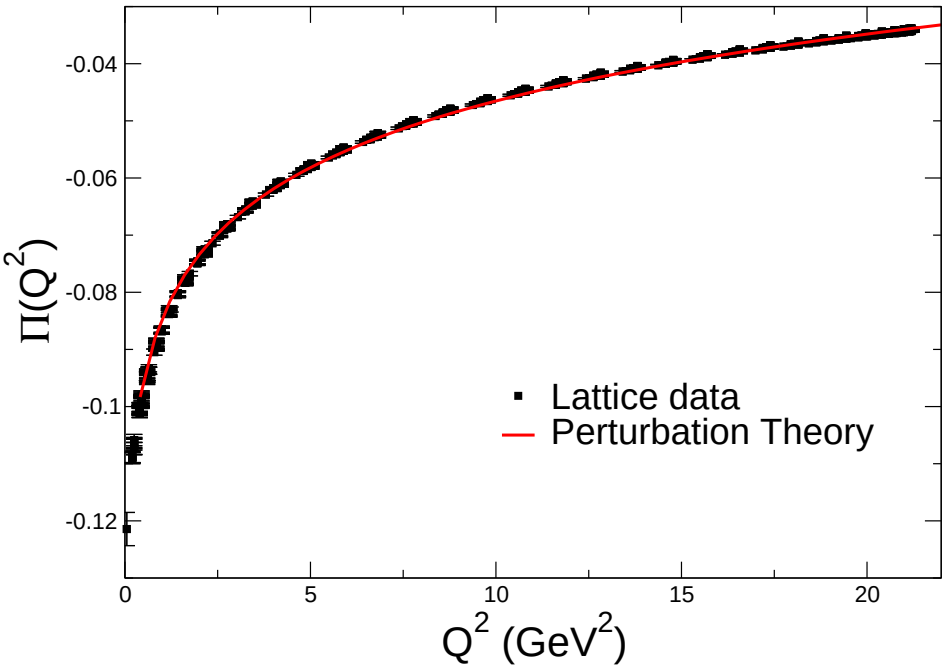

Figure 5.2: Vacuum polarisation function $\Pi(Q^2)$ as measured on 64×32^3 lattice at $\beta = 2.25$ and $am_u = 0.004$.

5.3.1 Fitting the low Q^2 region

We have attempted to fit a continuous form to our lattice data for the vacuum polarisation using a number of different fit forms. The effect that the choice of fit function can have on the result for $a_\mu^{(2)\mathrm{had}}$ has been highlighted in previous studies [100], and this behoves us to ensure that the systematics with regard to this choice are under control.

The suitability of a given fit-form should be judged on two main criteria:

- Firstly, the chosen expression must describe the data closely, and must do so regardless of the range of data included in the fit. As such we require the reduced χ^2 of the fit to be consistently low as a function of Q_C^2 which defines the range of data in the fit.

- Secondly, in order to deduce that the fit-form results in an integral over momentum which is relatively stable, we desire that the result for $a_\mu^{(2)\mathrm{had}}$ is

again relatively stable as a function of Q_C^2.

Ref. [100] also illustrated the use of a fit form originating in the expression for the vacuum polarisation calculated in chiral perturbation theory. The dominant component of this expression is due to the vector meson contribution, which at tree-level is

$$\Pi_V^{tree}(Q^2) = \frac{2}{3}\frac{f_V^2}{Q^2 + m_{\mathrm{V}}^2} \tag{5.27}$$

where the vector decay constant f_V is defined

$$\langle \Omega | J_\mu | V, p, \epsilon \rangle = m_{\mathrm{V}} f_V \epsilon_\mu(p). \tag{5.28}$$

Motivated by this expression the fit-form we use is closely related, differing only in the inclusion of the contribution of an additional vector resonance,

$$\Pi(Q^2) = A - \frac{F_1^2}{Q^2 + m_1^2} - \frac{F_2^2}{Q^2 + m_2^2}. \tag{5.29}$$

The one-loop contribution from the pseudoscalar sector, shown in [100] to have small momentum dependence, will not strongly affect our results and so, in our effort to make a continuous description of the lattice data, it will be omitted from our fit ansatz.

We fit the lattice vacuum-polarisation data in two ways:

- Firstly using A, $F_{1,2}$ and $m_{1,2}$ as free parameters.
- Also, fixing the parameter m_1 to the mass of the vector meson m_{V} as measured in [107]. This we do by constraining m_1 to lie in the one-sigma band defined by the estimate of m_{V} and its variance. This method was found to maintain the stability of the fit routine, while incorporating the extra information provided by m_{V}. In this fit A, $F_{1,2}$ and m_2 remain as true free parameters.

The behaviour of such fits are shown in Fig. 5.3. Clearly such a form is a very good representation of the data, over practically the whole range of Q_C^2. In addition the results for $a_\mu^{(2)\mathrm{had}}$ using such fits are very stable as the fit range is varied, allowing far greater confidence in the reliability of the result. In particular we conclude that using a fit form (5.29) with the mass of the first pole fixed to

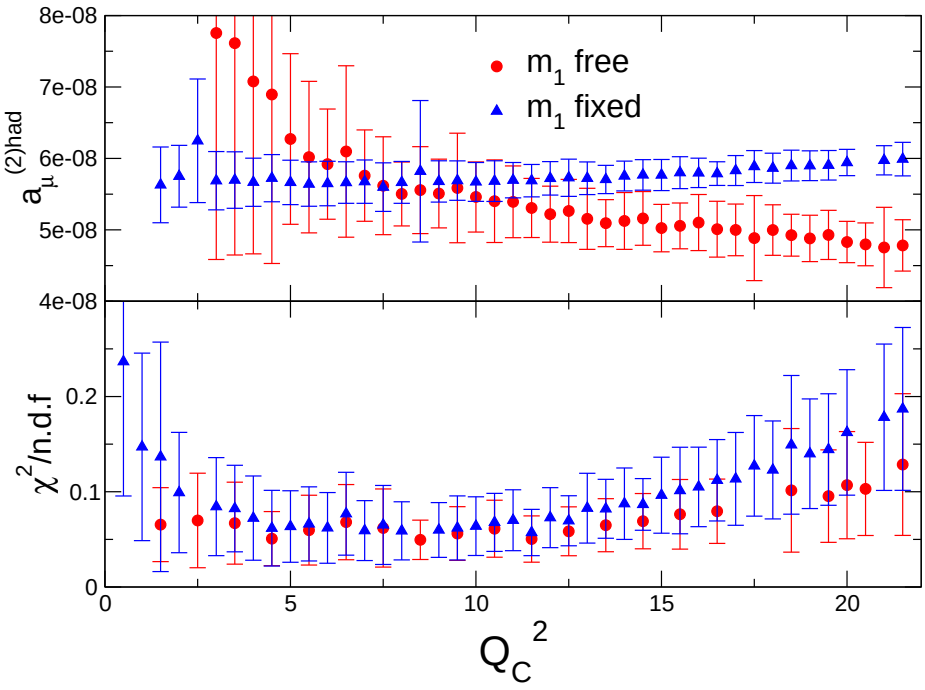

Figure 5.3: Properties of fits to the lattice vacuum polarisation using the ansatz (5.29) on the $\beta = 2.25$ lattice at $am_u = 0.004$. Only points for which the fitting procedure was reasonably stable are shown.

the ground-state vector meson mass to be the optimal method of describing the lattice data for the hadronic vacuum polarisation.

In Fig. 5.4 we see the value of the fit parameter m_1 from (5.29) as determined from fits to the lattice vacuum polarisation. The value of m_V obtained in [107] is shown in green, and this defines the band in which m_1 was constrained to reside in the fixed version of this fit. We have not attempted to model $O(4)$ breaking effects present in our data. Though such effects do appear to be present to a moderate degree on certain ensembles, they do not prevent the extraction of a reasonable signal from our data at this point. These effects could also be alleviated by the use of twisted boundary conditions [111].

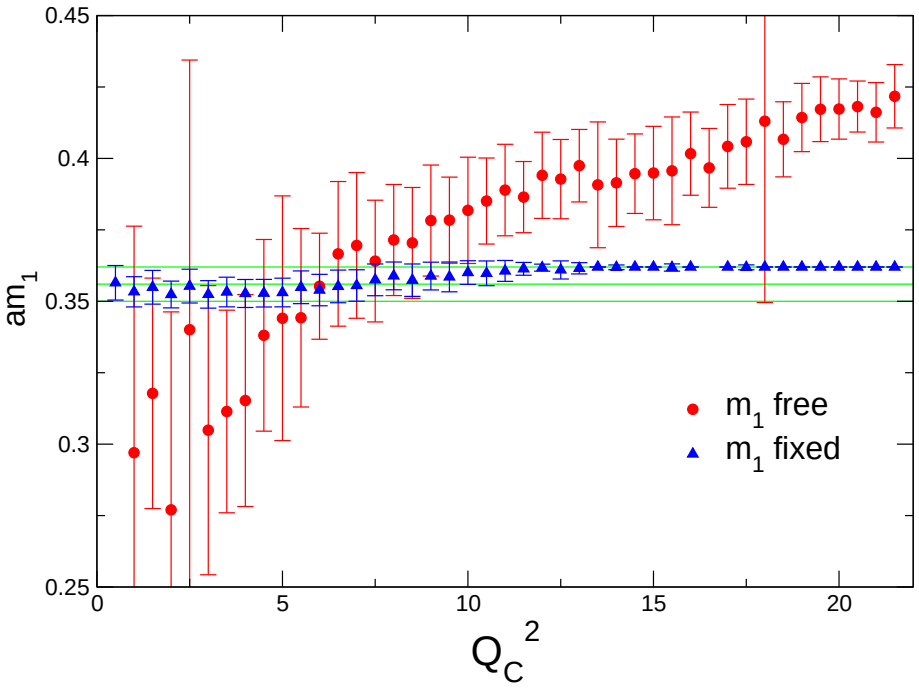

Figure 5.4: Value of the fit parameter am_1 in fits using the ansatz (5.29) on the $\beta = 2.25$ lattice at $am_u = 0.004$. The vector mass am_V as determined on this lattice is shown in green. Note in the fit where m_1 was fixed, it was only constrained to lie within the green band. It is clear that for a high Q_C^2, m_1 will emerge at the upper limit of the band, indicating some tension between the fit-form and the data, but as can be seen in Fig. 5.3, this has very little impact on the goodness of the fit.

5.3.2 Evaluation of (5.26)

Illustrations of the integrand can be seen in Fig. 5.5. Because the integrand is dominated by contributions in the low momentum region, we change our integration measure to better sample the region of interest. To do this, we make the change of variables

$$t = \frac{1}{1 + \log \frac{Q_C^2}{Q^2}} \tag{5.30}$$

and so the integral over the low-momentum region becomes

$$\int_0^{Q_C^2} dQ^2 f(Q^2) \times \hat{\Pi}(Q^2) \longrightarrow \int_0^1 dt\, f(Q^2) \times \hat{\Pi}(Q^2) \times \frac{Q^2}{t^2}. \tag{5.31}$$

Overlaid on the depiction of the integrand in Fig. 5.5 is the appropriately subtracted and rescaled vacuum polarisation data. We see from this that, while a large portion of the constraint on the fit is consistently derived from data at higher momentum, the fit is always consistent with the data at low momentum, the region where the integral receives the dominant contribution.

In particular in Fig. 5.5(b) we see that on the larger lattices at $\beta = 1.75$ using the Iwasaki+DSDR action, the data point at the lowest momentum sits exactly where the integrand reaches a maximum, and there are numerous data points in the dominant region, constraining the fit. Clearly using lattices of such size will help in obtaining a precise result for this quantity, and this must be combined with the use of twisted boundary conditions [101] in order to access data at lower values of the lattice momentum.

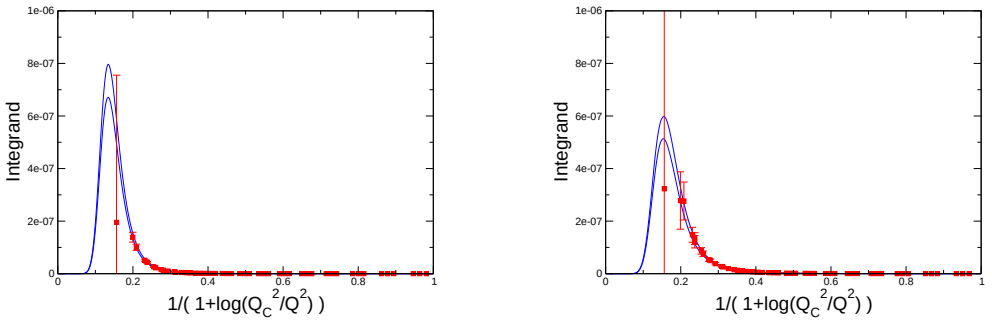

(a) $\beta = 2.25$ $\quad am_u = 0.004 Q_C^2 = 11$ GeV^2 $\quad$ (b) $\beta = 1.75$ $\quad am_u = 0.0042 Q_C^2 = 4$ GeV^2

Figure 5.5: Examples of the integrand in the rescaled integral (5.31).

5.4 Results

We extract our final results from the fit using (5.29) with the first mass fixed to that of the vector meson as measured on each ensemble. Observing the behaviour of the reduced χ^2 as the fit range is varied, we choose a suitable value for Q_C^2 for each ensemble which provides the most reliable result. We attempt to choose a cut which provides a low reduced χ^2 preferably where the parameter m_1 agrees without tension with m_{V}. This produces the results shown in Table 5.3, where we also quote the reduced χ^2 of the fit, and the resulting values of the remaining associated free parameters.

These results are also shown as a function of m_π^2 in Fig. 5.6, where we compare them to previous 2+1 flavour results from [100]. Also shown is an extrapolation to the physical point, using a quadratic chiral ansatz. This produces a final result for the leading order hadronic vacuum polarisation contribution the anomalous magnetic moment of the muon

$$a_\mu^{(2)\mathrm{had}} = 641(33) \times 10^{-10}. \tag{5.32}$$

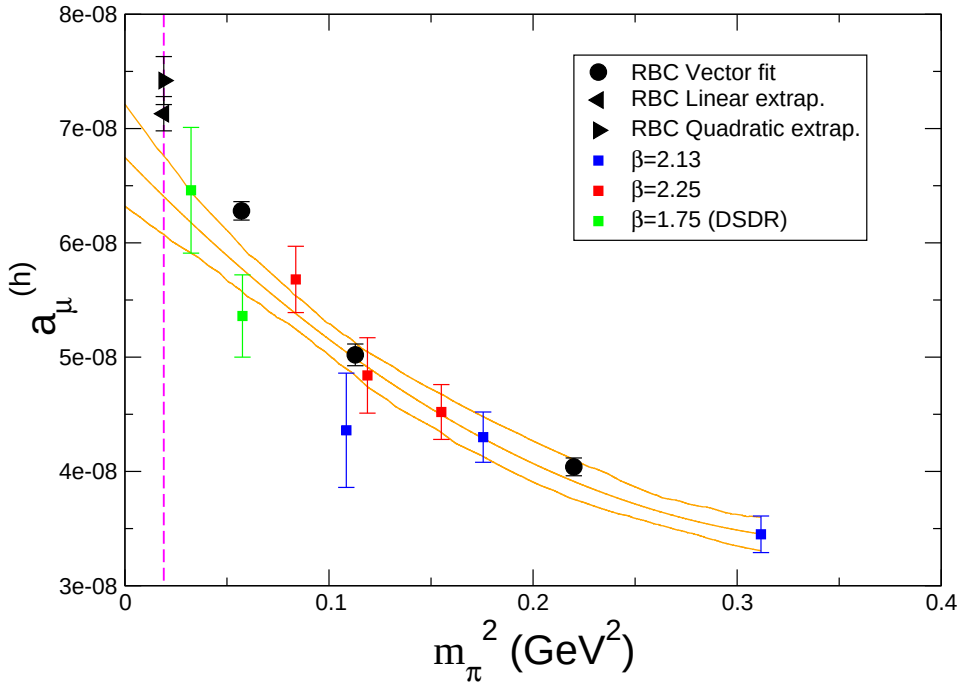

Figure 5.6: Integrated result for $a_\mu^{(2)\mathrm{had}}$ as a function of the pseudoscalar mass squared.

We have also investigated the effect of modifying the kernel function in the integrand (5.10) in the manner outlined in [102], where in an effort to moderate the variation of the outcome of the integral as a function of the quark mass, the momentum argument of the kernel function is rescaled by a factor of the ratio of the value of a relevant observable H (the mass of the vector meson appears to be an optimal choice) measured at the simulated quark mass to its physical value. This effectively defines the calculation of a new quantity which approaches the desired $a_\mu^{(2)\mathrm{had}}$ in the physical limit. We show the results of such a calculation

in Fig. 5.7(a), along with an accompanying chiral extrapolation. The chiral variation in this redefined quantity is 5.3 since for this ensemble the measured vector mass $m_{\rm V}$ is consistent with the physical value. This method does indeed moderate the chiral behaviour of the result, however it has little effect on our data at light quark masses, primarily because the lattice vector meson masses are very near that of the physical ρ meson, and, as of now, are not determined to any great precision on these lattices. As such this technique does not improve our chiral fit at this time, producing a compatible result with a similar uncertainty:

$$a_\mu^{(2)\rm had} = 605(24) \times 10^{-10} \tag{5.33}$$

In Fig. 5.7(b) we compare both chiral extrapolations, with $H = 1$ denoting the standard method, and $H = m_{\rm V}$ indicating the modified prescription of [102] using the vector mass $m_{\rm V}$.

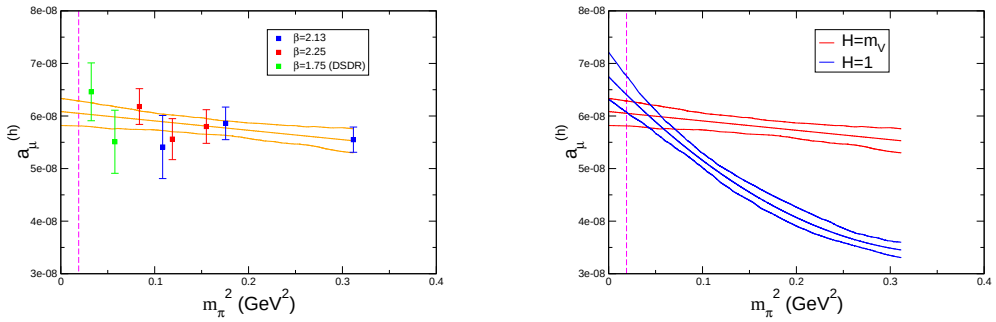

(a) Results using prescription $H = m_{\rm V}$. (b) Comparison of results from both methods.

Figure 5.7: Analysis of results for modified prescription using $H = m_{\rm V}$.

In Fig. 5.8, our result (5.32) is compared to recent 2+1 flavour lattice results [100] along with a recent result arising from a dispersion integral over experimental data from e^+e^- scattering data. We note that our result appears to be slightly lower than expected, however this could be explained by our omission of the disconnected contribution.

In Table 5.4 we attempt a comparison of the value of F_1 (defined in (5.29)) resulting from our fit, to the vector decay constant as measured on each lattice, according to the relation expressed in (5.27). Note, we do not have a result for f_V on the 64×24^3 lattices at this time, although the ratio of the vector coupling to

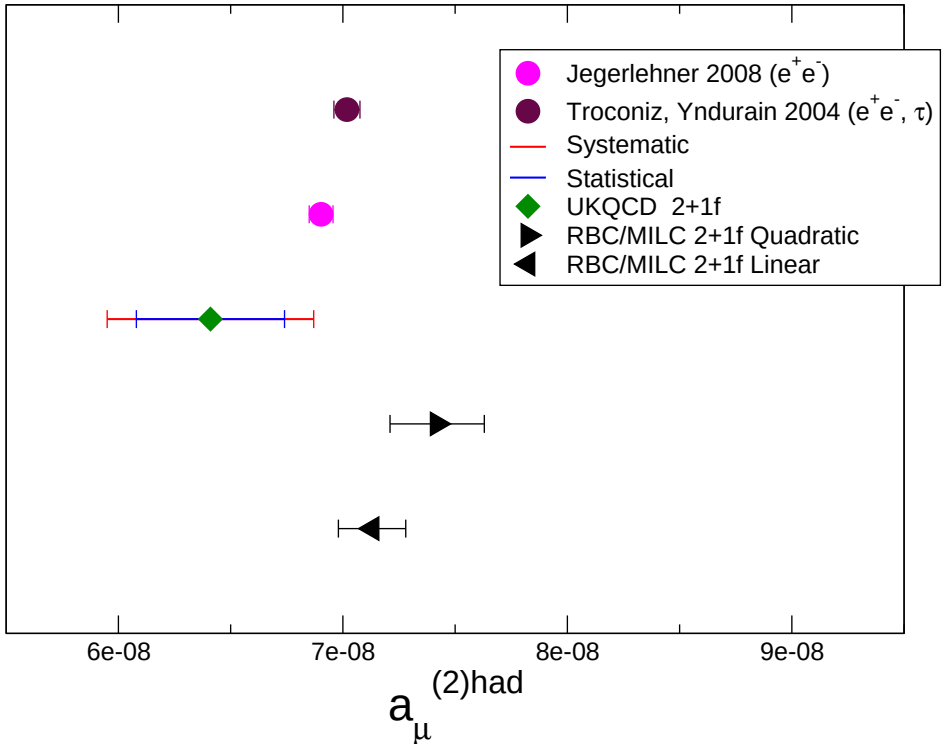

Figure 5.8: Comparison of recent results for $a_\mu^{(h)}$

the vector and tensor currents was studied in [112]. We also make the comparison suggested by the one-loop correction to (5.27) as computed in [100] whereby the relation $F_1^2 \sim \frac{2}{3} f_V^2$ is replaced by $F_1^2 \sim \frac{2}{3} f_V^2 \times C^2$ where

$$C^2 = 1 - \frac{6}{(4\pi f_\pi)^2}\left[m_\pi^2 \log\left(\frac{m_\pi^2}{\mu^2}\right) + m_K^2 \log\left(\frac{m_K^2}{\mu^2}\right)\right] \tag{5.34}$$

with m_π and m_K the pion and kaon meson masses, f_π the pion decay constant, and μ the chiral scale, taken as 1 GeV. In this comparison, we are neglecting the one-loop contribution from the pseudoscalar sector, and so, while neither of these comparisons emerges particularly convincingly, this indicates that the vacuum polarisation is reflective of the analytic approximation.

5.5 Conclusions

We present a fully dynamical calculation of the leading-order hadronic vacuum polarisation contribution to the anomalous magnetic moment of the muon, using a 2+1 flavour simulation lattice QCD using domain wall fermions. Although we have an expensive fermion discretisation, we improve the accuracy of our result by convolving an accurate determination of the ground-state vector meson mass with our determination of the lattice hadronic vacuum polarisation in order to suppress the systematic uncertainty associated with the choice of fit ansatz. Our chiral extrapolation involves lattices at different bare couplings, and thus different lattice spacings, however at this level of precision we do not detect any significant discretisation, or finite volume errors in our result. Our final result we take to be

$$a_\mu^{(2)\mathrm{had}} = 641(33)(32) \times 10^{-10} \tag{5.35}$$

where the first error is statistical and the second is an estimate of the systematic error arising from the extrapolation to the chiral limit, taken as 5%, motivated by the variation between the results (5.32) and (5.33). Our largest systematic uncertainty arises from the omission of the disconnected contributions and is of the order of 10% [113]. In order to obtain a more comprehensive and accurate result, we must include the disconnected contributions in our calculation. Furthermore, this being a first effort at deducing this quantity from our lattices, we have plans to improve it in a number of ways. In addition to the enhancement of our statistics, we would like to obtain a higher momentum resolution through the use of twisted boundary conditions, and also to explore the use of stochastic sources to further enhance our signal.

β	am_u	Q_C^2 GeV^2	$\frac{\chi^2}{n.d.f}$	$a_\mu^{(h)} \times 10^{10}$	aF_1	am_2	aF_2
2.13	0.02	4	0.38(17)	345(16)	0.114(4)	1.48(19)	0.31(5)
2.13	0.01	3.5	0.07(6)	430(22)	0.110(4)	1.50(23)	0.32(7)
2.13	0.005	3.5	0.14(5)	436(50)	0.097(14)	1.16(18)	0.24(3)
2.25	0.008	6	0.18(11)	452(23)	0.079(2)	1.14(4)	0.26(1)
2.25	0.006	6	0.10(6)	484(33)	0.075(3)	1.07(7)	0.24(2)
2.25	0.004	9	0.06(3)	568(29)	0.079(2)	1.23(3)	0.28(6)
1.75	0.0042	2.5	0.16(9)	536(36)	0.108(20)	1.27(20)	0.26(3)
1.75	0.001	2.5	0.27(13)	646(55)	1.06(11)	1.58(61)	0.37(27)

Table 5.3: Results for the hadronic contribution to the muon anomalous magnetic moment.

β	am_u	f_V MeV	$\sqrt{\frac{3}{2}}F_1$ MeV	$\sqrt{\frac{3}{2}}\frac{F_1}{C}$ MeV
2.13	0.02		242(10)	179(7)
2.13	0.01		234(8)	166(6)
2.13	0.005		205(30)	144(20)
2.25	0.008	178(13)	221(6)	155(5)
2.25	0.006	174(11)	211(10)	147(7)
2.25	0.004	160(26)	222(5)	155(4)
1.75	0.0042	140(9)	192(27)	129(19)
1.75	0.001	144(20)	179(18)	127(12)

Table 5.4: Comparison of the vector decay constant as measured on our lattices, to the amplitude of the lowest resonance contribution emerging from our fit to the lattice vacuum polarisation.

Chapter 6

A Mixed Action Determination of the MWT contribution to the S Parameter

6.1 Introduction

In Sec. 2.3.3 we outlined the importance of the S parameter (2.37) in constraining technicolor models, while in Sec. 2.4.4 we described how the contribution to S from a technisector which is near-conformal in the infra-red would be expected to be suppressed. However, there remains to evaluate S quantitatively in a such a theory through analytic methods.

As such, it is possible that LGT calculations may contribute significantly to this area. The S parameter contribution from QCD was calculated recently on the lattice [55, 56], while the first calculation in a candidate theory for near-conformal technicolor [57] showed some evidence that the contribution to S becomes suppressed in a theory closer to the conformal window.

Being calculated from the low-momentum behaviour of the difference of the vector and axial two-point functions, the contribution to the S-parameter is very sensitive to the breaking of chiral symmetry. As such it is necessary to use a fermion formulation which preserves chiral symmetry in the correct way. The best such formulation is that of Domain Wall Fermions (DWF), however performing a simulation with this formulation is for our purposes prohibitively expensive, due to the involvement of an extensive fifth-dimension in the Domain

Wall formulation.

However it may be possible to achieve the necessary chiral symmetry by performing a mixed-action simulation using DWF for the valence action, and a cheaper but chirally less well behaved action for the sea-quarks. This method is widely used for this purpose of restoring chiral symmetry, for example [114, 115], and the details involved in the practice of this method are given in [116]. In our case it is attractive due to the availability of a suite of ensembles of MWT gauge configurations generated using the Wilson fermion action.

Aside from the necessary tuning involved in this project due to mixed-action nature of the study, the procedure required is directly analogous to that used in the lattice determination of the hadronic vacuum polarisation contribution to the anomalous magnetic moment of the muon as described in Chap. 5.

A set of vacuum polarisation functions is calculated from lattice correlation functions over the maximum possible range of momenta. These functions are then fitted with a continuous form using a suitable ansatz, and the result is extracted from the properties of this continuous vacuum polarisation function. In the case of the S parameter, the relevant property is the slope of the function at zero momentum, as opposed to a re-weighted integral over the whole range of momenta as is the case for the contribution to a_μ.

We emphasise that presently this is not a complete, finalised project. Indeed as the progress stands we are not in a position to present quantitative results for the S parameter in MWT. However, we outline the steps required in this project, and present the data as obtained up to now. As such this represents a preliminary investigation of this topic, which it is intended, by the author, to pursue strongly in the near future.

6.2 The DWF Dirac operator inverted on MWT Wilson configurations

The Dirac operator of the Domain Wall Fermion formulation (D_{F}) has three input parameters. They are denoted L_5, M_5 and m_{f}, corresponding to the L_5, M_5 and m_{f} of, for example [117]. In this section I will describe attempts to choose suitable values of L_5 and M_5 for use in our study. In Sec. 6.3 I will outline how we choose the appropriate value of m_{f}.

Data presented in this section always involve a value of m_{f} reasonably close to (within $\sim 10-20\%$ of) the appropriate value as outlined in Sec. 6.3. Furthermore, data presented in this and later sections are extracted simply from the largest time value of the relevant effective operator. An accurate study would require the performance of a fit of the effective observable over some large-time region for each observable considered here, but for the moment this is not carried out.

In the absence of this procedure, we are unable to draw accurate conclusions from our data as they must be qualified with this systematic uncertainty. However, at this point we do not attempt to draw significantly precise quantitative conclusions from our data, and so at this time we do not see this omission as a hindrance.

6.2.1 L_5 and m_{res}

L_5 defines the extent of the fifth dimension involved in the formulation. As such, L_5 has a large impact on the cost of working with this formulation, but it also regulates the extent of unwanted chiral symmetry breaking present, and so we must choose a value of L_5 which provides an acceptable compromise between these two effects.

We monitor the level of unwanted chiral symmetry breaking in our measurements through the residual mass parameter m_{res} defined as

$$m_{\mathrm{res}} = \frac{\langle J^a_{5q}(x) J^a_5(y)\rangle}{2\langle J^a_5(x) J^a_5(y)\rangle} \tag{6.1}$$

where $J^a_{5q}(x)$ and $J^a_5(x)$ are the pseudoscalar correlator defined at the mid-point, and across both extremes of the fifth-dimension respectively, a is a flavour index.

m_{res} is expected to depend strongly on the value of L_5 implemented. In a unitary DWF simulation, we expect [117]

$$m_{\mathrm{res}} \sim A\frac{e^{-\lambda L_5}}{L_5} + B\frac{1}{L_5} \tag{6.2}$$

It will be necessary to study in detail the expected behaviour of m_{res} in our mixed-action simulation, but for the moment we will compare to this behaviour.

In Fig. 6.1 we show the behaviour of the m_{res} as obtained from inversions of the DWF operator on one ensemble of our MWT Wilson gauge configurations.

From the data in Fig. 6.1(a) we can see that m_{res} is a rapidly decreasing function of L_5.

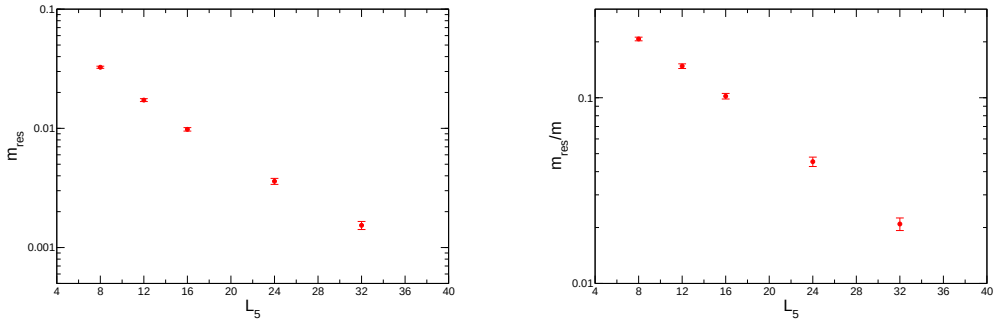

(a) m_{res} (b) $\frac{m_{\text{res}}}{m}$

Figure 6.1: Behaviour of residual mass m_{res} as we vary the extent of the fifth dimension L_5, resulting from inversions of the DWF operator on MWT Wilson gauge configurations on a 24×12^3 lattice at $\beta = 2.25$ and $am_0 = -1.180$.

From this behaviour we must deduce a value of L_5 with which to generate data for our study which will provide an adequate suppression of chiral symmetry breaking. This choice was discussed in [114] where the initial criterion used to decide on a value of L_5 was that the residual mass would be less than 10% of the quark mass on each lattice, i.e. $\frac{m_{\text{res}}}{m} \lesssim 0.1$. From Fig. 6.1(b) we can see that on this particular ensemble, using the unsmeared data, we would require a value of $L_5 > 16$ in order to attain this suppression.

The smeared data in Fig. 6.2 are obtained by performing one HYP smearing [118] step on the $SU(2)$ gauge field before performing the inversion of the DWF Dirac operator. The parameters used in this smearing were the same as those found to be optimal for use when smearing with $SU(3)$ gauge fields. From Fig. 6.2 we see clearly that this smearing produces a huge suppression of m_{res} which would allow the use of a reasonable value of L_5.

The desire to obtain some alternative control over the chiral symmetry breaking in our study apart from the brute force handle of increasing L_5 is made even more accute after observing Fig. 6.3.

Here we illustrate the behaviour of the residual mass on ensembles with different quark masses. In Fig. 6.3(a) we see that m_{res} does not appear to vanish in the chiral limit, and so the ratio $\frac{m_{\text{res}}}{m}$ will diverge as we approach zero

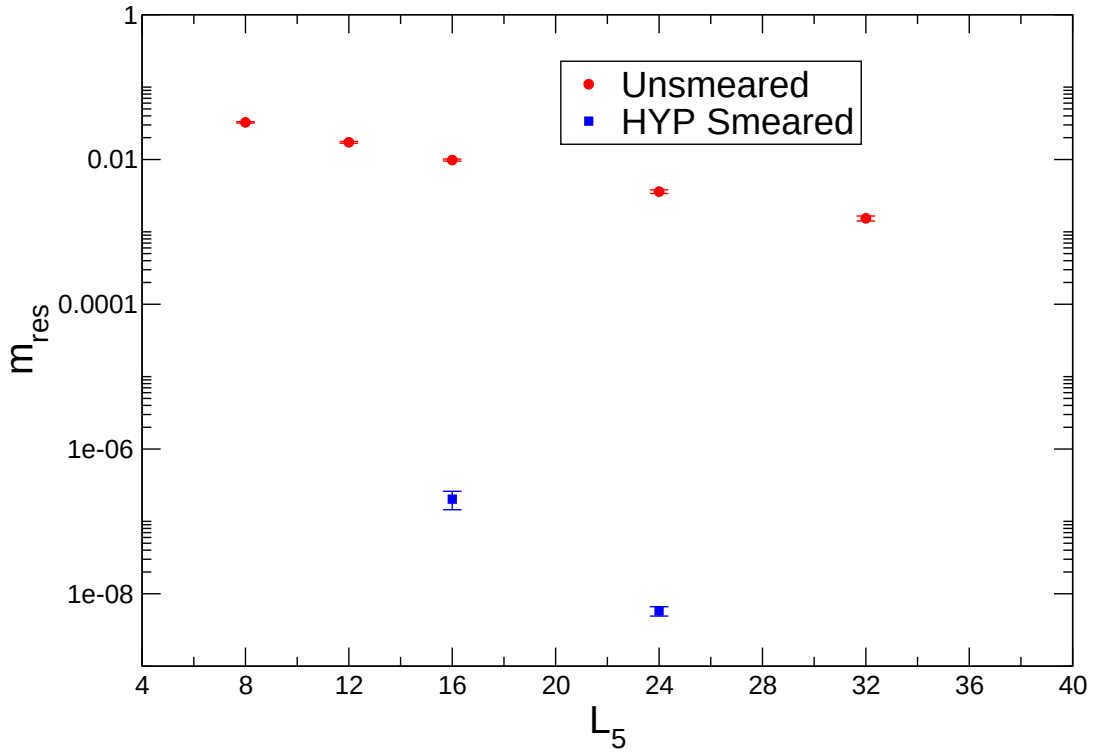

Figure 6.2: Behaviour of residual mass m_{res} as we vary the extent of the fifth dimension L_5 from inversions on smeared and unsmeared gauge fields.

quark mass, as show in Fig. 6.3(b). This will make it significantly more difficult to achieve a factor of 10 in this ratio when working with data at lighter quark masses.

6.2.2 M_5 and the spectral flow

M_5 must be chosen to lie in the "eye" defined by the spectral flow of the Hermitised DWF Dirac operator $H_W = \gamma_5 D_W$. The spectral flow involves the behaviour of the lowest eigenvalues of H_W as a function of M_5. This was analysed in the case of QCD in [117]. In Fig. 6.4 we show the spectral flow of our DWF operator both with and without HYP smearing. Clearly the implementation of a HYP smearing procedure greatly opens up the "eye" of the spectral flow, and

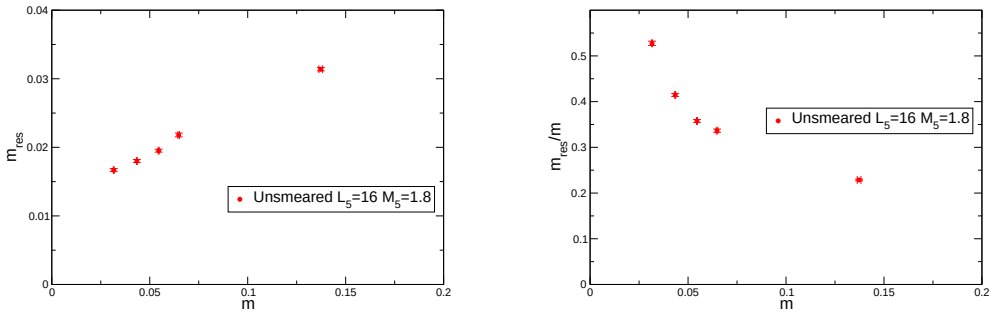

(a) m_{res} (b) $\frac{m_{\text{res}}}{m}$

Figure 6.3: Behaviour of residual mass m_{res} as a function of the quark mass m, resulting from inversions of the DWF operator on MWT Wilson gauge configurations on a 32×16^3 lattice at $\beta = 2.25$.

this is related to the suppression of chiral symmetry breaking discussed in Sec. 6.2.

6.3 Tuning the DWF fermion mass

Assuming we have determined appropriate values of the parameters L_5 and M_5 to use in our study, it remains to ensure that our inversions of the DWF Dirac operator on the MWT Wilson configurations produce data that encode the desired physics. We do this by ensuring that the masses of the lightest mesons in the theory as measured using the mixed-action DWF-Wilson inversions, match up with the same quantities measured in the unitary Wilson simulation.

The remaining handle on the DWF Dirac operator that we will use to ensure this matching is the quark mass parameter m_{f}. In a unitary DWF simulation this parameter would determine the quark mass of the simulation.

In a unitary Wilson simulation, one measures the actual quark mass m through the partially conserved axial current. When using the DWF Dirac operator, we will do the same, ensuring to use the conserved DWF axial current, denoting the result as m'. The bare result from this procedure will also contain contribution from the residual chiral symmetry breaking of the DWF operator, in the form of m_{res}. We expect that the measured quantity $m' - m_{\text{res}}$ will equal the input fermion mass m_{f}.

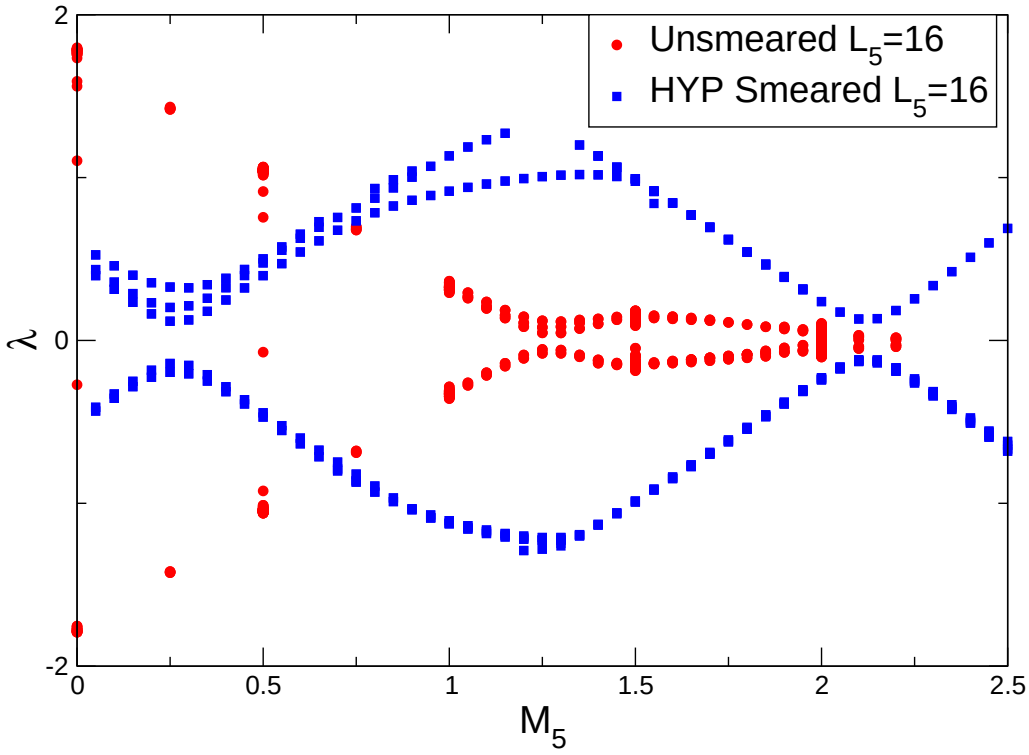

Figure 6.4: Spectral flow of the DWF Dirac operator computed on a single MWT Wilson configuration with a 24×12^3 lattice, at $am_0 = -1.180$.

We test this hypothesis in Fig. 6.5 where we see broad agreement with this assertion. The saturation is more pronounced on the lighter ensemble. In what follows we will work with the subtracted quark mass $m = m' - m_{\rm res}$.

We will attempt to match the meson masses determined from the mixed-action DWF inversions to those determined from the unitary Wilson simulation by varying the quark mass parameter to the DWF operator $m_{\rm f}$. What is important is that the meson masses are simultaneously tunable, but we will also keep track of the tuning of the quark mass m.

In Fig. 6.6 we show the tuning of the quark mass parameter $m_{\rm f}$ on two ensembles. In Figs. 6.6(a) and 6.6(c) it can be seen that the mass of the ground state pseudoscalar meson, $m_{\rm PS}$, and that of the ground state vector meson, $m_{\rm V}$, are simultaneously tunable, while in Figs. 6.6(b) and 6.6(d) we see that the

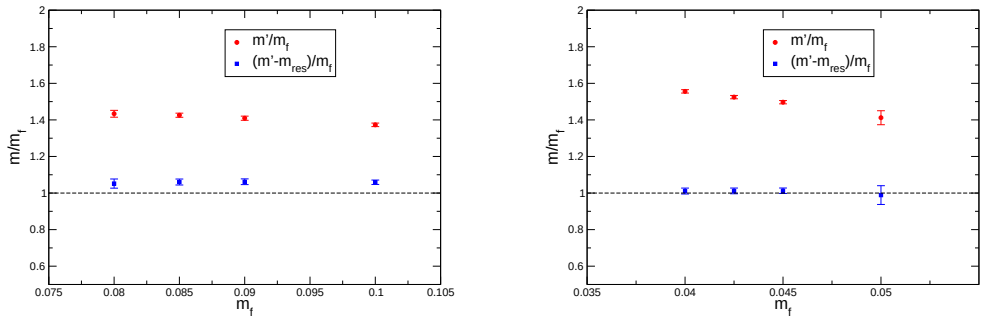

(a) $am_0 = -1.150$ (b) $am_0 = -1.175$

Figure 6.5: Reproduction of the fermion mass m_{f} in two ensembles, one heavier 6.5(a), and one lighter 6.5(b) resulting from inversions of the DWF operator on MWT Wilson gauge configurations on a 32×16^3 lattice at $\beta = 2.25$.

quark mass $m = m' - m_{\mathrm{res}}$ is not simultaneously tunable with m_{PS}. This could be explained by differing values of the renormalisation constant Z_{m} in the unitary Wilson theory, and the mixed-action theory.

Then in Fig. 6.7 we show the analogous tuning of the data obtained from the inversions on gauge fields which had undergone one step of HYP smearing. We see from Fig. 6.7(a) that the pseudoscalar and vector meson masses are simultaneously tunable in the same way as in the unsmeared case, but the quark mass is not tunable in the same way.

6.4 Ward identities of Conserved-Local correlators

The correlators we require for the computation of the S-parameter are the "conserved-local" vector and axial two-point functions. They are defined as

$$\begin{aligned} \Pi^{aV}_{\mu\nu}(q) &= \sum_x e^{iq\cdot x} \langle 0 | \mathcal{V}^a_\mu(x) V^a_\nu(0) | 0 \rangle \\ \Pi^{aA}_{\mu\nu}(q) &= \sum_x e^{iq\cdot x} \langle 0 | \mathcal{A}^a_\mu(x) A^a_\nu(0) | 0 \rangle \end{aligned} \tag{6.3}$$

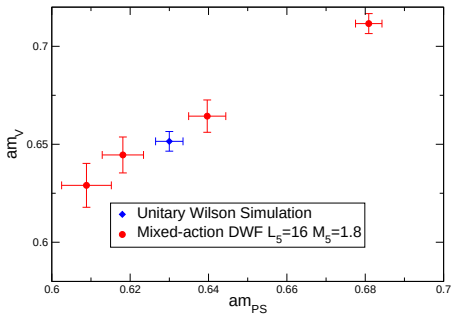

(a) m_{V} vs. m_{PS}, $am_0 = -1.150$

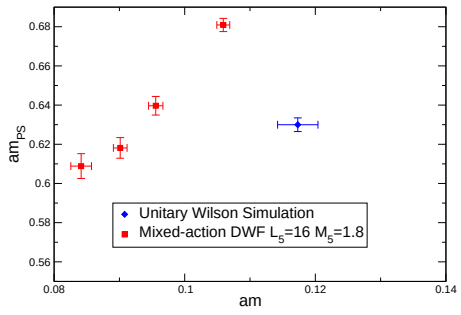

(b) m_{PS} vs. m, $am_0 = -1.150$

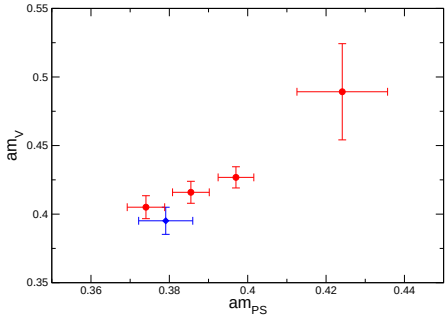

(c) m_{V} vs. m_{PS}, $am_0 = -1.175$

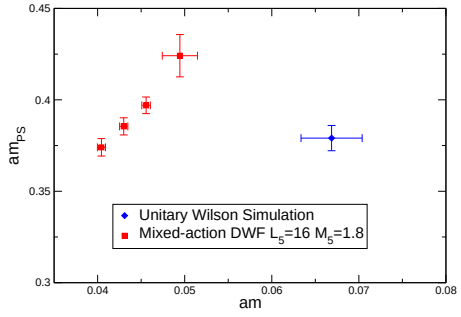

(d) m_{PS} vs. m, $am_0 = -1.175$

Figure 6.6: Tuning of the meson masses by varying the parameter m_{f} in a mixed-action DWF inversion on two 32×16^3 lattices at $\beta = 2.25$.

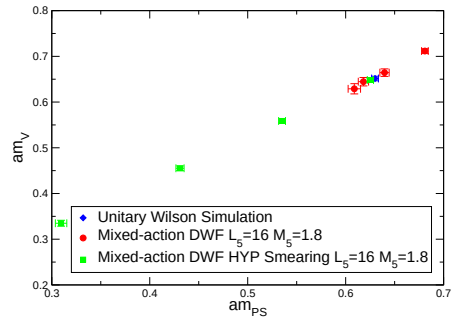

(a) m_{V} vs. m_{PS}, $am_0 = -1.150$

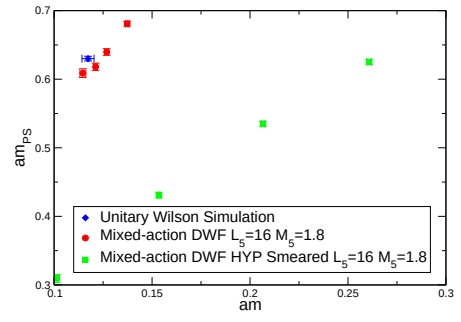

(b) m_{PS} vs. m, $am_0 = -1.150$

Figure 6.7: Tuning of meson masses by varying the parameter m_{f} in a HYP smeared mixed-action DWF inversion on a 32×16^3 lattice at $\beta = 2.25$.

where $V^a_\mu(x) = \bar{q}(x)\gamma_\mu\lambda^a q(x)$ and $A_\mu(x) = \bar{q}(x)\gamma_5\gamma_\mu\lambda^a q(x)$, where $q(x) = P_+\psi(x, L_5 - 1) + P_-\psi(x, 0)$, and $P_\pm = \frac{1}{2}(1 \pm \gamma_5)$, are the local vector and axial currents and $\mathcal{V}(x)$ and $\mathcal{A}(x)$ are their conserved counterparts, defined

$$\mathcal{V}^i_\mu(x) = \sum_{s=1}^{L_5} j^a_\mu(x, s)$$
$$\mathcal{A}^i_\mu(x) = -\sum_{s=1}^{L_5} \text{sign}\left(\frac{L_5 + 1 - s}{2}\right) j^a_\mu(x, s) \tag{6.4}$$

$$j^a_\mu(x, s)\frac{1}{2}\left[\bar{\psi}(x + \hat{\mu}, s)(1 + \gamma_\mu)U^\dagger_\mu(x)\lambda^a\psi(x, s) - \bar{\psi}(x, s)(1 - \gamma_\mu)U_\mu(x)\lambda^a\psi(x + \hat{\mu}, s)\right] \tag{6.5}$$

6.4.1 Exact VV WI

In a full, unitary DWF simulation, the invariance of the lattice action under a chiral symmetry results in the Ward Identity $\sum_\mu e^{\frac{iaq_\mu}{2}}\hat{q}_\mu\Pi^{aV}_{\mu\nu}(q) = 0$. This identity was exhibited in the QCD data presented in Sec. 5.2.3, and we will represent some of those data here for the purpose of comparison.

Note that in the following graphs, data for each momentum configuration is averaged over available statistics and presented independently, as such there is some residual momentum structure present which we do not always attempt to explain.

In Fig. 6.8(a) we illustrate the expression of this Ward Identity in data arising from a full DWF simulation of 2+1 flavour QCD, on a 64×32^3 lattice at $\beta = 2.25$ with a light quark mass $am_u = 0.006$ and heavy quark mass $am_s = 0.03$. In Fig. 6.8(b) we can see that the WI is expressed equally as well in correlators arising from a mixed-action study on the MWT configurations, specifically in this case from a 32×16^3 lattice at $\beta = 2.25$ and $am_0 = -1.150$. In fact, it appears that the expression of this identity is significantly stronger in the MWT data.

6.4.2 Cancellation of divergence under VV-AA

Due to the asymmetry of the conserved-local correlators (6.3) there is no simple Ward Identity for the second index of the individual correlators $\Pi^V_{\mu\nu}(q)$ and $\Pi^A_{\mu\nu}(q)$, as was discussed in relation to the QCD data in Sec. 5.2.3. However,

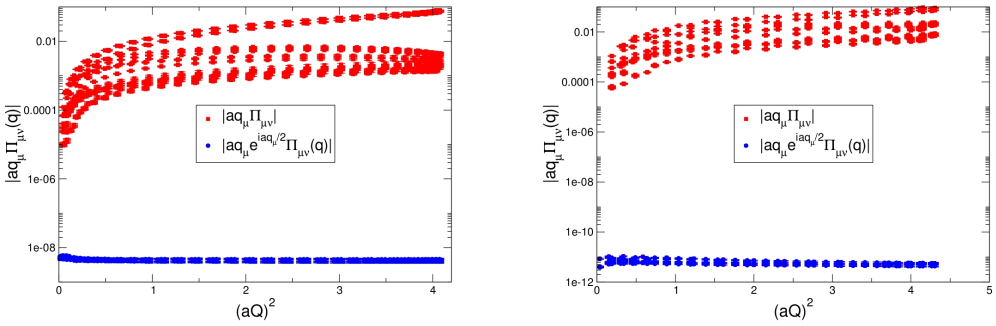

(a) Unitary DWF simulation of 2+1 flavour QCD.

(b) Mixed action MWT simulation.

Figure 6.8: An illustration of the expression of the WI $e^{\frac{iaq_\mu}{2}}\hat{q}_\mu\Pi^V_{\mu\nu}(x) = 0$ in both a unitary DWF simulation of 2+1 flavour QCD and a mixed-action simulation of MWT.

it can be shown that in a chirally symmetric theory, the subtracted correlator, $\Pi^{V-A}(q) = \Pi^V(q) - \Pi^A(q)$ is expected to obey $\hat{q}_\nu\Pi^{V-A}_{\mu\nu}(q) = 0$.

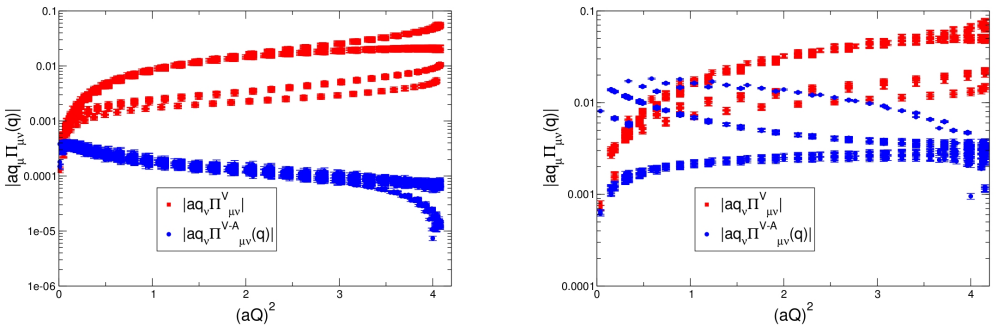

(a) Unitary DWF simulation of 2+1 flavour QCD.

(b) Mixed action MWT simulation.

Figure 6.9: An illustration of the expression of the WI $\hat{q}_\nu\Pi^{V-A}_{\mu\nu}(x) = 0$ in both a unitary DWF simulation of 2+1 flavour QCD and a mixed-action simulation of MWT.

In Fig. 6.9 we show the expression of this identity in the data from both a full DWF simulation of QCD, and a mixed-action simulation of MWT, on the same ensembles as Fig. 6.8. The identity is clearly satisfied on the QCD data, but the cancellation is not so satisfactory on the MWT data.

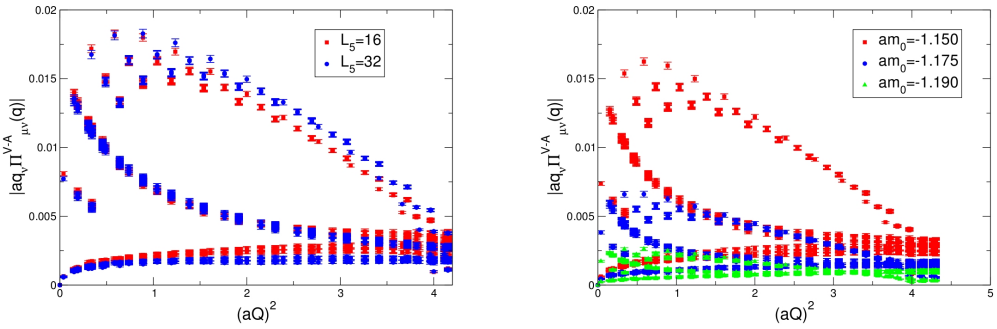

(a) Not a result of residual chiral symmetry breaking.

(b) But appears to resulting from explicit chiral symmetry breaking.

Figure 6.10: An illustration of the dependence of the expression of the WI $\hat{q}_\nu \Pi^{V-A}_{\mu\nu}(x) = 0$ on both L_5 and m.

In Fig. 6.10 we show that the violation of this identity does not appear to be resolved by suppressing the residual chiral symmetry breaking by increasing L_5 (Fig. 6.10(a)), but does appear to be reduced on lighter ensembles (Fig. 6.10(b)).

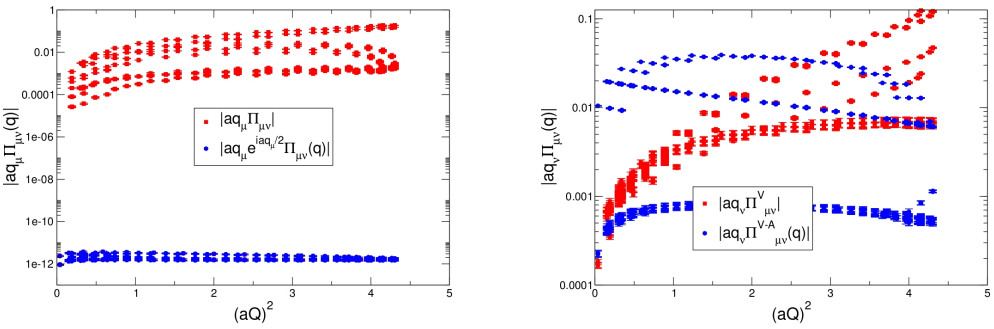

(a) The Vector WI on the smeared data.

(b) The V-A cancellation on the smeared data.

Figure 6.11: The expression of the Ward Identities on the HYP smeared data.

In Fig. 6.11 we show the expression of both of these Ward Identities in the HYP smeared data. Fig. 6.11(a) is the equivalent of Fig. 6.8(b), and shows a comparable, satisfactory agreement. Fig. 6.11(b), the equivalent of Fig. 6.9(b) shows that this cancellation is even less apparent in the smeared data.

6.5 The V-A correlator

In order to determine the MWT contribution to the S-parameter we need to analyse the low momentum behaviour of the subtracted correlator $\Pi^{V-A}(Q^2)$, which is the transverse component of $\Pi^{V-A}_{\mu\nu}(q)$. In Fig. 6.12 we show a comparison of $\Pi^{V}(Q^2)$ and $\Pi^{A}(Q^2)$ from both a full DWF QCD simulation, and our mixed action MWT study. The separation between vector and axial channels appears to be enhanced in the latter case Fig. 6.12(b) over the former Fig. 6.12(a). This is contrary to our expectation based on the near-conformality of MWT, and would result in an enhanced result for the S-parameter.

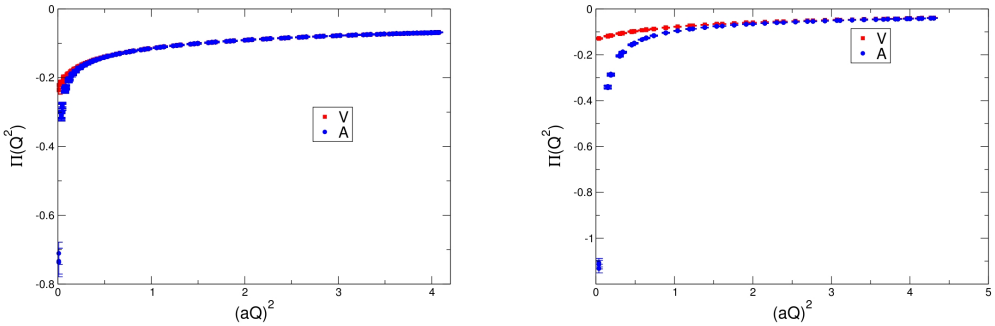

(a) Unitary simulation of 2+1 flavour QCD. (b) Mixed-action MWT simulation.

Figure 6.12: The vector and axial correlators from a full DWF QCD simulation and mixed-action MWT.

In Fig. 6.13 we show several examples of $\Pi^{V-A}(Q^2)$. In Fig. 6.13(a) we show that this enhanced separation between vector and axial channels does not appear to be related to the residual chiral symmetry breaking, and is not reduced through the use of a HYP gauge smearing. In Fig. 6.13(b) we show that the low momentum behaviour of $\Pi^{V-A}(Q^2)$ does moderate to some extent on lighter ensembles, but the function remains quite steep at low momenta.

As described in Sec. 6.1 the next step necessary to extract quantitative results for the S parameter from these data is to fit the discrete lattice data for the function $\Pi^{V-A}(Q^2)$ with a continuous form. Due to the considerable slope of the lattice data at low momentum, it does not seem feasible to carry out this process on the current data. The choice of fit ansatz used to perform the fit would have a large bearing on the result, due to the large slope, and at the moment we see

no way to control this uncertainty.

As such, it is clear that what is necessary for the immediate progression of this project is a more careful analysis of the quantities required for the computation of the S parameter in this mixed-action study. We can only deduce from the observed behaviour of $\Pi^{V-A}(Q^2)$ that there is an undesired contribution to our data which must be subtracted in order to allow the extraction of the desired result. However, the opportunity to progress this project further from its current status for presentation in this work is not available.

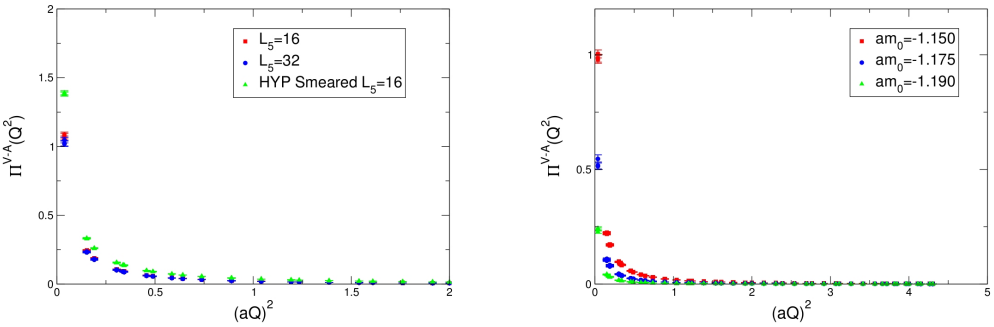

(a) Not a result of residual chiral symmetry breaking.

(b) But appears to resulting from explicit chiral symmetry breaking.

Figure 6.13: An illustration of the dependence of $\Pi^{V-A}_{\mu\nu}(x)$ on both L_5 and m.

Chapter 7

Conclusions

After introducing and explaining the concept of near-conformal technicolor in Chap. 2, and describing the ongoing efforts of the LGT community to evaluate the feasibility of such scenarios through simulations, Chap. 3, we presented in Chap. 4 the results of a comprehensive investigation of systematic uncertainties in recent spectroscopic studies of MWT searching for near-conformal dynamics, focusing on finite-volume effects.

This study illuminated the combination of spatial and temporal finite-volume effects present in such studies, and how in some cases these two effects can have opposite signs, leading to at least a partial cancellation, which can lead to significant underestimation of the finite-volume effects present in the final results for some observables.

We have quantified these effects as they pertain to the results of our simulation, and concluded that while indicating in general larger finite-volume effects, they do not alter the overall conclusion relating to the apparent conformality of MWT in the infra-red, as determined through a scaling analysis of the spectrum.

Though it remains difficult to extract results for the anomalous dimension governing the chiral scaling of the spectral observables, we find no evidence supporting large values of the mass anomalous dimension in MWT.

We have also presented in Chap. 5 the results of a calculation of the leading order vacuum polarisation contribution $a_\mu^{(2)\mathrm{had}}$ to the anomalous magnetic moment of the muon a_μ from a dynamical simulation of 2+1 flavour QCD using domain wall fermions. We find an effective prescription for bringing one of the

dominant systematic uncertainties involved in this calculation under control, and determine a competitive result for $a_\mu^{(2)\mathrm{had}}$ in the limit of physical quark masses

$$a_\mu^{(2)\mathrm{had}} = 641(33)(32) \times 10^{-10} \tag{7.1}$$

Finally in Chap. 6 we present a preliminary report on an ongoing project to compute the MWT contribution to the S parameter through a mixed action simulation involving the DWF valence operator combined with gauge ensembles generated using the Wilson fermion action. Although final results for this quantity are not available to us at the moment, we have illustrated the steps involved in this calculation, including a difficult tuning of the DWF action, and determined the course of action necessary to lead us to a successful computation of this quantity.

Appendix A

Lattice Gauge Theory

Lattice QCD is a non-perturbative technique for performing calculations in Quantum Chromodynamics. It was first proposed by Wilson in 1974 [119]. It corresponds to a momentum cut-off regularisation technique, removing the ultraviolet infinities present in quantum field theory. To begin with we will describe the lattice version of a pure gauge theory containing no matter fields.

A.1 Pure gauge theory

In order to ensure that the action is real, we move to Euclidean space by performing a Wick rotation $t \rightarrow \tau = it$. In this metric the gauge action is written

$$S_{\mathrm{G}} = \frac{1}{2} \int d^4x \mathrm{Tr} \left[\sum_{\mu,\nu} F_{\mu\nu}^2 \right] \tag{A.1}$$

where

$$F_{\mu\nu} = \partial_\mu A_\nu - \partial_\nu A_\mu + g[A_\mu, A_\nu] \tag{A.2}$$

and the gauge field A_μ is given in terms of the generators of the algebra of the gauge group T^a by $A_\mu \equiv A_\mu^a T^a$. We construct the lattice theory by moving from a theory with fields defined as functions continuous space-time variables $x^\mu \in \mathbb{R}^4$ to one where the space-time variables take only discrete values $x^\mu = an^\mu$ where n is a four-vector with integer components. We then confine our theory to a finite volume $V = (aN)^4$ by restricting n^μ to the range $-\frac{N}{2} < n^\mu < \frac{N}{2}$, so we have a simple hypercubic lattice with N^4 sites, and lattice spacing a.

The action now becomes a sum over lattice points

$$S_{\mathrm{G}} = \frac{1}{2}a^4 \sum_{x,\mu,\nu} \mathrm{Tr}[F_{\mu\nu}^2(x)] \tag{A.3}$$

It can be shown that after discretisation, the field strength tensor $F_{\mu\nu}$ can be expressed in terms of elements of the Lie group U which are associated with links between lattice sites. This is related to the interpretation of a gauge field as a path-dependent phase factor, whereby the wave function of any particle with gauge charge g propagating in a gauge field A_μ picks up a path-dependent phase factor given by

$$\psi \to \exp\left(ig \int_{\mathrm{P}} A_\mu \, dx_\mu\right) \psi = U_{\mathrm{P}} \psi \tag{A.4}$$

If we consider such a particle propagating from lattice site x^λ to its neighbour in the μ direction $x^\lambda + e_\mu$, we can aproximate this phase factor taking the value of the field at the midpoint of the path $x^\lambda + \frac{e_\mu}{2}$. We then have

$$U_\mu \equiv \exp\left[igaA_\mu\left(x + \frac{ae_\mu}{2}\right)\right] \tag{A.5}$$

The full action can then be written as

$$S_{\mathrm{G}} = \sum_{\square} \frac{2N_{\mathrm{c}}}{g^2}\left(1 - \frac{1}{N_{\mathrm{c}}} \Re \, \mathrm{Tr}[U_\square]\right) \tag{A.6}$$

where the sum is over all plaquettes, defined by

$$U_\mu U_\nu U_\mu^{-1} U_\nu^{-1} \equiv U_\square \tag{A.7}$$

Note we get a factor of 2 from the equivalence of (μ, ν) and (ν, μ) planes. This convenient form is known as the Wilson action and is often written as $S_{\mathrm{G}} = \sum_\square S_\square$ where

$$S_\square \equiv \frac{\beta}{N_{\mathrm{c}}}(1 - \Re \, \mathrm{Tr}[U_\square]) \tag{A.8}$$

where $\beta = \frac{2N_{\mathrm{c}}}{g^2}$. The constant term is discarded as it has no effect on the dynamics. If we now consider the expectation value of an observable O in the path integral formalism of this pure gauge theory, we see it becomes a path integral over the

gauge group

$$\langle O \rangle = \frac{1}{Z} \int \mathcal{D}U \, O \, e^{-S_{\mathrm{G}}}. \tag{A.9}$$

Z, which in continuum QFT is called the generating functional, becomes a partition function

$$Z = \int \mathcal{D}U \, e^{-S_{\mathrm{G}}} \tag{A.10}$$

The measure $\mathcal{D}U$ is a product over all the link elements

$$\mathcal{D}U = \Pi_{n,\mu} dU_n^{\mu} \tag{A.11}$$

We have reduced the expectation value to a finite dimensional integral, which could in theory be calculated explicitly. However, the dimensionality of the integral, though finite, is still prohibitively high. We can proceed by noting that the exponential factor ensures that the integral is dominated by configurations of the gauge fields for which the action is small. If we evaluate the integrand on a set of configurations with distribution $e^{-S_{\mathrm{G}}}$ we can then approximate the whole integral. First proposed by Metropolis in 1953 [120], this is called a Monte Carlo technique and is used widely in statistical physics. In order to generate gauge field configurations, we begin with some initial configuration and generate a series of others by making consecutive pseudo-random alterations such that the resulting series has the appropriate probability distribution. The simplest algorithm to implement this procedure is the one originally suggested in 1953 [120], the Metropolis algorithm. It proceeds from the initial configuration by successively modifying each link variable U. The algorithm randomly selects a trial replacement U' and calculates the action of the configuration with U replaced with U', $S(U')$. If the action of theory involves only local interactions, then the deviation of $S(U')$ from the original action $S(U)$ will depend only on the nearest neghbours of U. If $S(U') - S(U) < 0$ then the change is accepted. If not, the change is accepted with probability $e^{-[S(U')-S(U)]}$. This operation is performed on each link to produce the next configuration in the series.

A.2 Introducing fermions

We now turn to the quark fields which will be present in full QCD.We will firstly examine the action for a single free fermion on the lattice. Working in a Euclidean representation of the Dirac matrices such that $\gamma_\mu, \gamma_\nu = 2\delta_{\mu\nu}$, explicitly

$$\gamma_0 = \begin{pmatrix} I_2 & 0 \\ 0 & I_2 \end{pmatrix} \quad \gamma_i = \begin{pmatrix} 0 & \sigma_i \\ \sigma_i & 0 \end{pmatrix} \quad \gamma_5 = \gamma_1\gamma_2\gamma_3\gamma_0 = \begin{pmatrix} 0 & iI_2 \\ iI_2 & 0 \end{pmatrix} \tag{A.12}$$

the action for the fermion is given by the Dirac action

$$S_{\mathrm{F}} = \int d^4x \bar{\psi}(\not{\partial} + m)\psi \tag{A.13}$$

where $\not{\partial} = \gamma_\mu\partial_\mu$. Note the action is symmetric under the transformation $\psi \to e^{i\theta}\psi$. In the massless or chiral limit $m \to 0$, there is another symmetry under $\psi \to e^{i\theta\gamma_5}\psi$ called *chiral symmetry*. If we use the finite difference relation $f'(x) \simeq \frac{1}{2a}[f(x+a) - f(x-a)]$ for the derivative, when we move to the lattice this becomes

$$S_{\mathrm{F}} = a^4 \sum_n \left(\bar{\psi}_n \sum_\mu \gamma_\mu \frac{1}{2a}(\psi_{n+e_\mu} - \psi_{n-e_\mu}) + m\bar{\psi}_n\psi_n + \mathcal{O}(a^2) \right) \tag{A.14}$$

This can be written in terms of an $N \times N$ matrix M as

$$S_{\mathrm{F}} \equiv \bar{\psi}_m M_{mn} \psi_n \tag{A.15}$$

where

$$M_{mn} = \frac{1}{2}a^3 \sum_\mu \gamma_\mu(\delta_{m+e_\mu,n} - \delta_{m-e_\mu,n}) + a^4 m\delta_{m,n} \tag{A.16}$$

It is the inverse of this matrix that will make up the lattice propagator for our theory. In order to find an expression for it we move to momentum space.

We write the Dirac spinors in terms of their lattice Fourier transform as

$$\psi_n = N^{-4} \sum_k \widetilde{\psi}_k e^{-2\pi i k\cdot n/N} \qquad \bar{\psi}_m = N^{-4} \sum_l \widetilde{\bar{\psi}}_l e^{2\pi i l\cdot m/N} \tag{A.17}$$

Inserting these into (A.14) and using the orthogonality identity

$$\sum_k e^{-2\pi i k\cdot n/N} = N^4 \delta_{n,0} \tag{A.18}$$

we obtain

$$S_{\mathrm{F}} = a^4 N^{-4} \sum_k \sum_k \bar{\widetilde{\psi}}_k \widetilde{M}_k \widetilde{\psi}_k \tag{A.19}$$

with

$$\widetilde{M}_k = m + \frac{i}{a} \sum_\mu \gamma_\mu \sin\left(\frac{2\pi k_\mu}{N}\right) \tag{A.20}$$

From the expression for M in terms of M we can construct M^{-1}

$$M_{mn} = a^4 N^{-4} \sum_k \widetilde{M}_k e^{2\pi i k\cdot(n-m)/N} \tag{A.21}$$

$$\Rightarrow M^{-1}_{mn} = a^{-4} N^{-4} \sum_k \widetilde{M}_k e^{2\pi i k\cdot(m-n)/N} \tag{A.22}$$

$$= a^{-4} N^{-4} \sum_k \frac{e^{2\pi i k\cdot(m-n)/N}}{m + \frac{i}{a}\sum_\mu \gamma_\mu \sin\left(\frac{2\pi k_\mu}{N}\right)} \tag{A.23}$$

Because of the commutation properties of the γ_μ we have that

$$\left(\sum_\mu \gamma_\mu \sin\left(\frac{2\pi k_\mu}{N}\right)\right)^2 = \sum_\mu \sin^2\left(\frac{2\pi k_\mu}{N}\right) \tag{A.24}$$

and so we can manipulate (A.23) to

$$M^{-1}_{mn} = a^{-4} N^{-4} \sum_k \frac{\left(m - \frac{i}{a}\sum_\mu \gamma_\mu \sin\left(\frac{2\pi k_\mu}{N}\right)\right) e^{2\pi i k\cdot(m-n)/N}}{m^2 + \frac{1}{a^2}\sum_\mu \sin^2\left(\frac{2\pi k_\mu}{N}\right)} \tag{A.25}$$

This can be shown to reduce to the usual fermion propagator in the continuum limit $a \to 0$ by introducing the continuous momentum variable $p_\mu = \frac{2\pi k_\mu}{Na}$ and replacing the sum with an integral as

$$a^{-4} N^{-4} \sum_k \to \int \frac{d^4 p}{(2\pi)^4} \tag{A.26}$$

Poles in (A.25) will correspond to particles. We have proceeded from the action

for a single fermion on the continuum and thus expect to recover a single pole. Unfortunately this is not the case, the discretisation of the theory introduces a degeneracy in the spectrum. This is easiest to see in the chiral limit $m \to 0$. Let k_ν be the only non-zero component of k. We get a pole where the sin function vanishes. This occurs at $k = 0$ which corresponds to the original fermion, but also on the boundary of the first Brillouin zone at $k_\nu = \frac{N}{2}$. We have additional fermions in the theory. This occurs for each direction ν and so we have a total of $2^4 = 16$ different fermion species called tastes. This problem is known as fermion doubling. There are a number of ways of getting around this problem, and in Sec. A.4 I will outline the most important and frequently used of these.

A.3 Single flavour QCD

We are now in a position to examine the lattice scheme for QCD with one quark flavour. This theory can be constructed by combining the pure gauge and free fermion theories and including the interaction between them. This is done according to the principle of minimal coupling, by replacing the derivative in (A.13) with a covariant derivative

$$\partial_\mu \to D_\mu = \partial_\mu + igA_\mu \tag{A.27}$$

The leading order correction to M (A.16) due to this alteration is the insertion of phase-factors U_μ in the kinetic term

$$M_{mn} = \frac{1}{2}a^3 \sum_\mu \gamma_\mu (U_\mu \delta_{m+e_\mu,n} - U_\mu^{-1}\delta_{m-e_\mu,n}) + a^4 m \delta_{mn} \tag{A.28}$$

The action of the theory is then

$$S = S_{\mathrm{G}} + S_{\mathrm{F}} \qquad S_{\mathrm{F}} = \bar{\psi}_m M_{mn} \psi_n \qquad S_{\mathrm{G}} = \sum_\Box S_\Box \tag{A.29}$$

The expectation value of an observable O is given by

$$\langle O \rangle = \frac{1}{Z} \int \mathcal{D}U \mathcal{D}\psi \mathcal{D}\bar{\psi}\, O\, e^{-S} \tag{A.30}$$

where now Z, is written

$$Z = \int \mathcal{D}U\mathcal{D}\psi\mathcal{D}\bar{\psi}\, e^{-S} \tag{A.31}$$

and

$$\mathcal{D}\psi = \Pi_n\, d\psi_n \qquad\qquad \mathcal{D}\bar{\psi}\Pi_n\, d\bar{\psi}_n \tag{A.32}$$

Writing the Dirac action as in (A.29) the fermionic integrals in (A.31) can be performed to give

$$Z = \int \mathcal{D}U\ \det(M) e^{-S_{\mathrm{G}}} \tag{A.33}$$

Comparing (A.33) to (A.10) we see that they differ only in the presence of the determinant $\det(M)$. This factor leads to considerable difficulties when it comes to performing calculations. In order to generate our gauge field configurations we will have to alter our Monte Carlo algorithm to include the determinant in the measure. Unfortunately, using the Metropolis algorithm, every time we update one of our link variables, we must recalculate the determinant. In contrast with calculating the new action, this is a global rather than local operation. As such, computing the determinant is a very time consuming process, even on powerful computers using the most advanced algorithms. This issue led many practitioners to perform simulations in the *quenched approximation*, that is, setting $\det(M) \equiv 1$. This corresponds to neglecting the contributions of closed quark loops in the path integral. However, this procedure leads to uncontrollable errors, typically of the order of 10-20%, depending on the quantity involved.

We can avoid this assumption if we first note that the time needed to compute the determinant is heavily dependent on the value of the quark mass m, in fact it goes like $\mathcal{O}(\frac{1}{m})$. As a result, if we perform our simulations at unphysically high quark masses the operation is no longer prohibitively time consuming. It is then possible to extrapolate to the observed value of the quark mass and recover the physical result. This is usually done through reference to an effective field theory which can yield the behaviour of the parameter as a function of the mass scale.

A.4 Solutions to fermion doubling

A.4.1 Wilson fermions

The first solution to the issue of fermion doubling was put forward by Wilson himself [121]. He suggested adding another term to the fermion action which would vanish in the continuum limit. Explicitly

$$S_{\mathrm{F}} \to \int d^4x\, \bar{\psi} \left(\not{\partial} + m - \frac{ar\partial^2}{2} \right) \psi \tag{A.34}$$

In order to ensure that we have nearest-neighbour interaction only, to convert to the lattice, we use the approximation $f'(x) \simeq \frac{1}{a}[f(x+\frac{a}{2}) - f(x-\frac{a}{2})]$ in decomposing the ∂^2 term so that

$$\begin{aligned} S_{\mathrm{F}} =& a^4 \sum_n \bar{\psi}_n \left[m\psi_n + \sum_\mu \left(\gamma_\mu \frac{1}{2a} \left(\psi_{n+e_\mu} - \psi_{n-e_\mu} \right) - \frac{r}{2a} \left(\psi_{n+e_\mu} - 2\psi_n + \psi_{n-e_\mu} \right) \right) \right] \\ =& a^4 \sum_n \bar{\psi}_n \left[\left(m + \frac{r}{a} \right) \psi_n + \sum_\mu \frac{1}{2a} \left((\gamma_\mu - r)\, \psi_{n+e_\mu} - (\gamma_\mu + r)\, \psi_{n-e_\mu} \right) \right] \end{aligned} \tag{A.35}$$

Following the same procedure as in Sec. A.2 we see that there is another term in the denominator of the lattice propagator

$$\widetilde{M_k} = (m + \frac{r}{a}) + \frac{i}{a} \sum_\mu \left[\gamma_\mu \sin\left(\frac{2\pi k_\mu}{N} \right) + \frac{r}{a} \left(1 - \cos\left(\frac{2\pi k_\mu}{N} \right) \right) \right] \tag{A.36}$$

Note that when $a \to 0$ the additional term is $\mathcal{O}(a)$ and so drops out. However, near the Brillouin zone boundary, when $k_\mu = \frac{N}{2}$ the mass of the unwanted doublers is raised by $\frac{2r}{a}$. Thus in the continuum limit all the unwanted states go to infinte mass and only one, the desired fermion remains. This method of overcoming fermion doubling is attractive because of its simplicity, making it easy to implement. However it has its disadvantages. Most worrying is that the procedure violates the chiral symmetry of the theory. This is a problem because it is chiral symmetry which protects the mass from an additive renormalisation. For this reason people have sought other methods of getting around the issue of fermion doubling. Also, from (A.34) we see that we have added $\mathcal{O}(a)$

discretisation errors to the action, whereas previously they were $\mathcal{O}(a^2)$ (A.14).

A.4.2 "No-go" theorem and the Ginsparg-Wilson relation

We have seen that it is possible to remove the unwanted doubler fermions from the theory through the Wilson prescription, if we sacrifice chiral symmetry. Through the staggering process we can partially remove the taste degeneracy while retaining the chiral symmetry. Is it possible to construct an acceptable technique which does both? Such a prescription must result in an action with the following properties:

1. We must have a real bi-linear action, i.e. S_{F} must be expressable in the form (A.15) with M hermitian. For simplicity we work in the chiral limit, $m = 0$.

2. The theory must be translation invariant, requiring $M_{mn} = D(x_n - x_m)$.

3. It must be local, requiring that the Fourier transform $\widetilde{D}(p)$ of $D(xy)$ must be analytic throughout the Brillouin zone.

4. Far below the cut-off (away from the zone boundary) it must approach the continuum expression in a certain way, i.e. $\widetilde{D}(p) \overset{|p|\to 0}{\simeq} i/p + \mathcal{O}(p^2)$

5. The theory must be free of doubler fermions, equivalent to requiring $\widetilde{D}(p)$ to be invertible for all non-zero momenta.

6. We must have chiral symmetry which can be expressed in the form $\{\gamma_5, D\} = 0$.

Unfortunately however, an action with all of these properties does not exist This result is the Nielsen-Ninomiya "no-go" theorem of 1981 [122]. We are thus required to relax at least one of the above requirements. In 1982 [123] it was suggested that we relax our chiral symmetry requirement from that in 6 to

$$\{\gamma_5, D\} = 2aD\gamma_5 D \tag{A.37}$$

called the Ginsparg-Wilson relation. It emerged in a theory constructed from a chirally symmetric continuum fermion action through a spin-blocking operation.

For the propagator $S = D^{-1}$ it implies

$$\{\gamma_5, S(xy)\} = 2a\gamma_5\delta(xy) \tag{A.38}$$

i.e. the propagator is chirally invariant at all non-zero distances. In 1998 Lüscher [124] found that the remnant chiral symmetry has the infinitesimal form

$$\psi \to \psi + \epsilon\gamma_5(1 - aD)\psi \tag{A.39}$$

Under this transformation however, the fermion measure transforms anomalously. It can be shown that this produces the exact chiral anomaly expected from perturbation theory. The result of these discoveries is that we can simulate a single taste of fermion with the correct chiral physics using the Ginsparg-Wilson relation. A number of methods for doing just this have been devised but we shall describe only one.

A.4.3 Domain wall fermions

It is possible to describe chiral fermions in 4 dimensions by writing a theory of fermions in 5 dimensions in such a way that there are excitations bound to a 4 dimensional cross section of the space. If we use the 5 dimensional Dirac operator

$$D = (\not{\partial} + \gamma_5\partial_s - m(s)) \tag{A.40}$$

where $m(s)$ is a mass term varying with s. The exact form of $m(s)$ is not important, only that it be monotonic with the asymptotic form

$$m(s) \overset{s\to\pm\infty}{\longrightarrow} \pm 1 \tag{A.41}$$

Therefore $m(s) = 0$ at $s = 0$ and so we expect solutions which are massless states on the 4 dimensional $s = 0$ cross-section. This subspace is a domain wall between regions with $m > 0$ and $m < 0$. In order to describe massless propagation on the domain wall these solutions must obey $D\Psi = \not{\partial}\Psi$. As such, they must be of the form

$$\Psi_\pm = e^{ip\cdot x}\phi_\pm(s)u_\pm \tag{A.42}$$

$u_\pm$ are constant 4 component chiral spinors with $\gamma_5 u_\pm = \pm u_\pm$ satisfying

$$(\pm\partial_s m(s))\phi_\pm(s) = 0 \tag{A.43}$$

with solution

$$\phi_\pm = \exp\left(\pm\int_0^s m(s')ds'\right) \tag{A.44}$$

i.e. the massless states decay exponentially in the s direction, and as such are bound to the domain wall. Additionally, only the ϕ_- solution is normalizable and so we are left with one massless state propagating on the domain wall.

In 1992 Kaplan [125] showed that this scenario is reproduced on an infinite lattice, with some differences. In this case both solutions $\phi_\pm$ become normalisable. This amounts to a doubler fermion in the s direction. Additionally we still have doublers in the space-time directions at the boundary of the Brillouin zone. It turns out, however, that with this prescription we are free to add a Wilson term to the full action to remove these doublers, without mutilating the chiral symmetry. So we return to one species of fermion on the domain wall. When we move to the finite lattice we induce another domain wall in the s direction. This is the feature which allows us to evade the Nielsen-Ninomiya theorem. Fermions simulated with this prescription are called domain wall fermions (DWF). It can be shown that the action on the domain wall obeys the Ginsparg-Wilson relation (A.37).

Modern applications of DWF use a formulation developed in [108, 126]. The definition used in this and related works is outlined in [127]. The prescription is defined by the action

$$S_{\mathrm{F}}(\bar{\psi},\psi,U) = -\sum_{x,y,s,s'} D_{\mathrm{F}}(M_5,m_{\mathrm{f}})_{x,s;y,s'}\psi_{y,s'}, \qquad D_{\mathrm{F}x,s;y,s'} = \delta_{s,s'}D^{\parallel}_{x,y}(M_5) + \delta_{x,y}D^{\perp}_{s,s'}(m_{\mathrm{f}}). \tag{A.45}$$

The Dirac matrix $D_{\mathrm{F}}(M_5,m_{\mathrm{f}})$ is defined

$$\begin{aligned} D^{\parallel}_{x,y}(M_5) =& \frac{1}{2}\sum_\mu \left[(1-\gamma_\mu)U_{x,\mu}\delta_{x+\hat{\mu},y} + (1+\gamma_\mu)U^\dagger_{y,\mu}\delta_{x-\hat{\mu},y}\right] + (M_5-4)\delta_{x,y} \\ D^{\perp}_{s,s'}(m_{\mathrm{f}}) =& \frac{1}{2}\left[(1-\gamma_5)\delta_{s+1,s'} + (1+\gamma_5)\delta_{s-1,s'} - 2\delta_{s,s'}\right] \\ & -\frac{m_{\mathrm{f}}}{2}\left[(1-\gamma_5)\delta_{s,L_5-1}\delta_{0,s'} + (1+\gamma_5)\delta_{s,0}\delta_{L_5-1,s'}\right]. \end{aligned} \tag{A.46}$$

The quantity M_5 is reminiscent of the negative of the usual fermion mass in the Wilson fermion prescription, however it is m_{f} that denotes the quark mass in this description. L_5 denotes the extent of the fifth dimension. The formulation also involves a set of scalar fields necessary to cancel some lattice artifacts of the five dimensional fermions, but we will not discuss them further here.

A.5 Correlators and smearings

We have illustrated the basics of the Lattice scheme for QCD and described some of the difficulties that must be overcome in order to make calculations feasible. We will now briefly describe some of the details involved in calculating physical quantities on the lattice.

A.5.1 Local correlators

In order to measure mesonic observables on the lattice we measure zero-momentum correlators of the form

$$f_{\Gamma\Gamma'}(t) = \sum_{\vec{x}} \langle \mathcal{O}_{\Gamma}^{\mathrm{SINK}\dagger}(\vec{x},t)\mathcal{O}_{\Gamma'}^{\mathrm{SRCE}}(\vec{0},0)\rangle, \tag{A.47}$$

where $\mathcal{O}_{\Gamma}^{\mathrm{SRCE,SINK}}$ are interpolating quark bilinear operators with the correct symmetries under spin and parity. We require the isospin non-singlet correlators and so, for example, we could construct a *local* correlator with the most immediate choice

$$\mathcal{O}_{\Gamma}^{\mathrm{SRCE}}(\vec{x},t) = \mathcal{O}_{\Gamma}^{\mathrm{SINK}}(\vec{x},t) = \bar{\psi}_1(\vec{x},t)\Gamma\psi_2(\vec{x},t), \tag{A.48}$$

where the labels i on the quark fields ψ_i denotes the fermion flavour. Here Γ is a matrix in the Dirac algebra, which determines the symmetries of the operator. This choice reproduces the correlators considered in [59]:

$$f^{L}_{\Gamma\Gamma'}(t) = \sum_{\vec{x}} \langle \left(\bar{\psi}_1(\vec{x},t)\Gamma\psi_2(\vec{x},t) \right)^{\dagger} \bar{\psi}_1(\vec{0},0)\Gamma'\psi_2(\vec{0},0)\rangle, \tag{A.49}$$

where here the superscript on $f_{\Gamma\Gamma'}$ indicates the local choice. This correlator is measured by computing the quark propagator $S(\vec{x}, t; \vec{x}', t')$, in terms of which

$$f^L_{\Gamma\Gamma'}(t) = -\frac{a^3}{V_s} \sum_{\vec{x}} \mathrm{Tr}[\gamma_0 \Gamma^\dagger \gamma_0 S(\vec{x}, t; \vec{0}, 0) \Gamma' \gamma_5 S(\vec{x}, t; \vec{0}, 0)^\dagger \gamma_5]. \tag{A.50}$$

The propagator is computed by solving the equation

$$a^4 \sum_{\mathbf{y}} D(\mathbf{x}; \mathbf{y}) S(\mathbf{y}, \mathbf{z}) = I \delta_{\mathbf{x};\mathbf{z}}, \tag{A.51}$$

where the boldface variables denote the full space-time coordinate, I denotes the identity matrix in spin and colour space, and $D(\mathbf{x}; \mathbf{y})$ is the Dirac matrix.

A.5.2 Extended quark fields

In order to obtain an optimum signal for the masses we aim to extract from these correlators, we should construct interpolating operators with a maximised overlap with the desired ground state. The local operators (A.48) are not expected to satisfy this requirement well, as the mesons typically have an extension of many times the lattice spacing in a typical simulation. We can improve the situation by considering an operator which is extended spatially over the lattice:

$$\mathcal{O}_\Gamma(\vec{x}, t) = \sum_{\vec{y}_1, \vec{y}_2} \Psi(\vec{x}, \vec{y}_1, \vec{y}_2) \bar{\psi}_1(\vec{y}_1, t) \Gamma \psi_2(\vec{y}_2, t). \tag{A.52}$$

Usually shell-model wave functions are used [128], meaning the positions of the quark and antiquark are decoupled:

$$\Psi(\vec{x}, \vec{y}_1, \vec{y}_2) = \phi(\vec{x}, \vec{y}_1) \phi(\vec{x}, \vec{y}_2). \tag{A.53}$$

The choice $\phi(\vec{x}, \vec{y}) = \delta_{\vec{x},\vec{y}}$ reproduces the point-point case (A.48).

In general, such wave functions are not gauge invariant, and as such any expectation value over an ensemble of gauge configurations, in which they are used, must vanish, according to Elitzur's theorem [129]. To avoid this we can fix the gauge on each configuration, being careful to check for errors introduced by the issue of Gribov copies.

Using $\phi^{\mathrm{SRCE/SINK}}$ to define $\mathcal{O}^{\mathrm{SRCE/SINK}}$ we see that our correlation function

can be computed as

$$f_{\Gamma\Gamma'}(t) = -\sum_{\vec{x}} \mathrm{Tr}[\gamma_0\Gamma^\dagger\gamma_0\widehat{S}(\vec{x},t;\vec{0},0)\Gamma'\gamma_5\widehat{S}(\vec{x},t;\vec{0},0)^\dagger\gamma_5], \tag{A.54}$$

where $\widehat{S}(\vec{x},t;\vec{x}',t')$ is defined as

$$\widehat{S}(\vec{x},t;\vec{x}',t') = \sum_{\vec{y},\vec{y}'} S(\vec{y},t;\vec{y}',t')\phi^{\mathrm{SINK}}(\vec{x},\vec{y})\phi^{\mathrm{SRCE}}(\vec{x}',\vec{y}'). \tag{A.55}$$

It can be easily seen that if we solve for S', the system

$$a^4\sum_{\mathbf{y}} D(\mathbf{x},\mathbf{y})S'(\mathbf{y},\mathbf{z}) = \phi^{\mathrm{SRCE}}(\vec{z},\vec{x})\delta_{x_0,z_0}, \tag{A.56}$$

we can compute $\widehat{S}$ as

$$\widehat{S}(\vec{x},t;\vec{x}',t') = \sum_{\vec{y}} S'(\vec{y},t;\vec{x}',t')\phi^{\mathrm{SINK}}(\vec{x},\vec{y}). \tag{A.57}$$

In fact it is the choice of a shell-model type wave-function (A.53) that allows us to calculate the correlation function using only one inversion of the Dirac matrix (per colour and spin index).

A.5.3 Smearing examples

A simple guess for an effective form of $\phi(\vec{x})$ is in the form of a Gaussian

$$\phi(\vec{x},\vec{y}) = e^{-\left(\frac{|\vec{x}-\vec{y}|}{R}\right)^2}, \tag{A.58}$$

where $R > 0$ is some effective radius chosen to represent the wave function of the meson of interest. The choice $\frac{1}{R} \to 0$ results in $\phi(\vec{x},\vec{y})$ having equal weight over the whole lattice, and is termed a *wall smearing*.

On a lattice we can approximate the Gaussian as the limit of the iterative form

$$\phi(\vec{x},\vec{y}) = \left(1 - \frac{w^2}{4N}\Box\right)^N \delta_{\vec{x},\vec{y}}, \tag{A.59}$$

where $\Box$ is the lattice version of the Laplacian

$$\Box(\vec{x},\vec{y}) = \sum_{i=1}^{3} \left(\delta_{\vec{x},\vec{y}-\hat{i}} + \delta_{\vec{x},\vec{y}+\hat{i}}\right). \tag{A.60}$$

(A.59) then approximates (A.58) in the limit $N \to \infty$, with the radius R being determined by w. Replacing $\Box$ with its covariant form

$$\Box(\vec{x},\vec{y};t) = \sum_{i=1}^{3} \left(U_i(\vec{x},t)\delta_{\vec{x},\vec{y}-\hat{i}} + U_i^{\dagger}(\vec{x}-\hat{i},t)\delta_{\vec{x},\vec{y}+\hat{i}}\right), \tag{A.61}$$

results in a gauge invariant operator, negating the requirement for gauge fixing. This choice of ϕ is called *gauge-invariant Gaussian smearing*.

We have utilised both a wall-smearing (denoted W) and a gauge-invariant Gaussian smearing (denoted G) in our study.

A.5.4 Gauge fixing

When constructing a correlator involving the gauge-dependent wall-smeared quark bilinear, we must fix the gauge on each configuration with which we wish to work. We fix to Coulomb gauge by generating a gauge-fixed gauge configuration from the original by maximising the quantity $\sum_{\mathbf{x}} \sum_{i=1}^{3} \mathrm{Re}\left(\mathrm{Tr}[U_i(\mathbf{x})]\right)$ which ensures the necessary gauge fixing condition $\partial_i A_i = 0$. The standard mechanism for achieving this on the lattice was described in [130] and the status of the topic was recently reviewed in [131].

A.6 Meson correlator phenomenology

A.6.1 Meson masses

We extract the meson masses from our theory by analysing correlators of the form (A.47) in the case where we consider source and sink operators with equal symmetries, i.e. $\Gamma = \Gamma'$, and so we shall write $f_{\Gamma\Gamma} = f_\Gamma$. We can write f_Γ explicitly as an expectation value on the vacuum state $|0\rangle$:

$$f_\Gamma(t) = \sum_{\vec{x}} \langle 0|\mathcal{O}_\Gamma^{\mathrm{SINK}\dagger}(\vec{x},t)\mathcal{O}_\Gamma^{\mathrm{SRCE}}(\vec{0},0)|0\rangle. \tag{A.62}$$

Labelling the energy eigenstates of the theory as $|n,\vec{p}\rangle$, we can write a complete set of states as

$$\sum_n \int \frac{d^3p}{(2\pi)^3 2E_n(\vec{p})} |n,\vec{p}\rangle\langle n,\vec{p}|. \tag{A.63}$$

We can insert this in f_Γ producing

$$f_\Gamma(t) = \sum_n \sum_{\vec{x}} \int \frac{d^3p}{(2\pi)^3 2E_n(\vec{p})} \langle 0|\mathcal{O}_\Gamma^{\mathrm{SINK}\dagger}(\vec{x},t)|n,\vec{p}\rangle\langle n,\vec{p}|\mathcal{O}_\Gamma^{\mathrm{SRCE}}(\vec{0},0)|0\rangle. \tag{A.64}$$

Translating $\mathcal{O}^{\mathrm{SINK}}(\mathbf{x})$ to the origin produces $e^{i\mathcal{P}\cdot\mathbf{x}}\mathcal{O}^{\mathrm{SINK}}(\mathbf{0})e^{-i\mathcal{P}\cdot\mathbf{x}}$ where the four-momentum operator $\mathcal{P} = \{\vec{\mathcal{P}}, \mathcal{H}\}$ giving

$$\langle 0|\mathcal{O}_\Gamma^{\mathrm{SINK}\dagger}(\vec{x},t)|n,\vec{p}\rangle = \langle 0|\mathcal{O}_\Gamma^{\mathrm{SINK}\dagger}(\mathbf{0})|n,\vec{p}\rangle e^{-i\mathbf{p}\cdot\mathbf{x}}, \tag{A.65}$$

where $\mathbf{p} = \{E_n(\vec{p}), \vec{p}\}$. As a result, the sum over the spatial position $\vec{x}$ collapses the sum onto zero-momentum

$$f_\Gamma(t) = \sum_n \frac{1}{2E_n} \langle 0|\mathcal{O}_\Gamma^{\mathrm{SINK}\dagger}(\vec{0},0)|n\rangle\langle n|\mathcal{O}_\Gamma^{\mathrm{SRCE}}(\vec{0},0)|0\rangle e^{-iE_n t}, \tag{A.66}$$

where we denote $|n,\vec{0}\rangle$ as $|n\rangle$ and $E_n(\vec{0})$ as E_n. The overlaps $\langle 0|\mathcal{O}(\mathbf{0})|n\rangle$ will vanish for all states except those with the same symmetries as $\mathcal{O}_\Gamma$ and we can see that at large Euclidean time $\tau = it$ the correlator is dominated by the lowest in energy of such states which we denote $|\Gamma\rangle$ with energy E_Γ which as we are at zero momentum equals the mass of the state $E_\Gamma = m_\Gamma$:

$$\begin{aligned} f_\Gamma(\tau) &\overset{\tau\to\infty}{\longrightarrow} \frac{1}{2m_\Gamma} \langle 0|\mathcal{O}_\Gamma^{\mathrm{SINK}\dagger}(\vec{0},0)|\Gamma\rangle\langle\Gamma|\mathcal{O}_\Gamma^{\mathrm{SRCE}}(\vec{0},0)|0\rangle e^{-m_\Gamma\tau} \\ &\equiv A_\Gamma e^{-m_\Gamma\tau}. \end{aligned} \tag{A.67}$$

On a lattice with finite temporal extent $0 < \tau < L_t$, this asymptotic behaviour is modified by the appearance of an extra term corresponding to a quark

propagating backward from source to sink through the anti-periodic boundary:

$$\begin{aligned} f_\Gamma(\tau) \rightarrow & A_\Gamma \left(e^{-m_\Gamma \tau} + e^{-m_\Gamma (L_t - \tau)} \right) \\ \equiv & A_\Gamma \mathrm{hc}(\tau, m_\Gamma, L_t). \end{aligned} \tag{A.68}$$

In this way we can extract the meson masses from the exponential behaviour of the f_Γ at large Euclidean time.

As in [59], we use the Prony method [132] to solve this system, to produce an "effective mass" $m_\Gamma(\tau)$ which as a function of the lattice temporal coordinate is expected to approach the desired mass in the limit of large times $m_\Gamma(t) \overset{\tau \rightarrow \infty}{\longrightarrow} m_\Gamma$. The meson mass is extracted by choosing a region around the centre of the temporal axis and fitting the effective mass to a constant in this region.

In our study we have considered the case $\Gamma = \gamma_5$, defining the *pseudoscalar* channel, with mass m_{PS} and the degenerate cases $\Gamma = \gamma_i$ $i \in \{1, 2, 3\}$, defining the *vector* channel with mass m_{V}. In practice the correlators f_{γ_i} are averaged to produce a single correlator for the vector channel. We call the resulting vector correlator f_{VV} and the pseudoscalar correlator f_{PP}.

The masses can be extracted identically from these correlators regardless of the smearing used. In practice it is found that correlators with a smeared source are preferred to local correlators for this purpose, in that they produce an improved signal to noise ratio for the masses. Correlators with smearing at both the source and sink are found to be disfavoured because of enhanced fluctuations.

A.6.2 Amplitudes

If local quark fields are used, $\mathcal{O}_\Gamma^{\mathrm{SRCE/SINK}}(\mathbf{x}) = \bar{\psi}_1(\mathbf{x}) \Gamma \psi_2(\mathbf{x}) = \mathcal{O}_\Gamma^{\mathrm{L}}(\mathbf{x})$. In the case of both the pseudoscalar and vector channels, we are interested in the quantity $|\langle 0 | \mathcal{O}_\Gamma^{\mathrm{L}}(\mathbf{0}) | \Gamma \rangle|$ although they have different meanings:

$$\begin{aligned} |\langle 0 | \mathcal{O}_{\gamma_5}^{\mathrm{L}}(\mathbf{0}) | \gamma_5 \rangle| \equiv & G_{\mathrm{PS}}, \\ |\langle 0 | \mathcal{O}_{\gamma_i}^{\mathrm{L}}(\mathbf{0}) | \gamma_i \rangle| \equiv & \epsilon_i F_{\mathrm{V}} m_{\mathrm{V}}, \end{aligned} \tag{A.69}$$

where ϵ_i is a polarisation tensor. We call G_{PS} the *pseudoscalar vacuum to meson amplitude* (or, more commonly, simply the psuedoscalar amplitude), and F_{V} is

the *vector decay constant*. We can easily construct effective observables for these quantities from the local correlators f^{L}_{PP} and f^{L}_{VV}:

$$\begin{aligned} G^{\mathrm{L}}_{\mathrm{PS}}(\tau) =& \sqrt{\frac{2m_{\mathrm{PS}}(\tau)f^{\mathrm{L}}_{\mathrm{PP}}(\tau)}{\mathrm{hc}(\tau, m_{\mathrm{PS}}(\tau), L_t)}}, \\ F^{\mathrm{L}}_{\mathrm{V}}(\tau) =& \sqrt{\frac{2f^{\mathrm{L}}_{\mathrm{VV}}(\tau)}{m_{\mathrm{V}}\mathrm{hc}(\tau, m_{\mathrm{V}}(\tau), L_t)}}. \end{aligned} \tag{A.70}$$

If we wish to use smeared operators to extract these quantities, the amplitudes in (A.67) are, in general, no longer related to the quantities of interest (A.69). However, if our correlator involves only a smearing at the source, with a local sink, we see that the sink amplitude in (A.67) is still of the correct form (A.69). We need cancel the other undesired amplitude, introduced by the smearing. We can do this by combining our local-smeared correlator (f^{LS}_{Γ}) with a smeared-smeared correlator (f^{SS}_{Γ}). Effective observables equivalent to (A.69) can be defined from smeared correlators as

$$\begin{aligned} G^{\mathrm{S}}_{\mathrm{PS}}(\tau) =& \sqrt{\frac{2m_{\mathrm{PS}}(\tau)}{\mathrm{hc}(\tau, m_{\mathrm{PS}}(\tau), L_t)}\frac{{f^{\mathrm{LS}}_{\mathrm{PP}}}^2(\tau)}{f^{\mathrm{SS}}_{\mathrm{PP}}(\tau)}}, \\ F^{\mathrm{S}}_{\mathrm{V}}(\tau) =& \sqrt{\frac{2}{m_{\mathrm{V}}\mathrm{hc}(\tau, m_{\mathrm{V}}(\tau), L_t)}\frac{{f^{\mathrm{LS}}_{\mathrm{VV}}}^2(\tau)}{f^{\mathrm{SS}}_{\mathrm{VV}}(\tau)}}. \end{aligned} \tag{A.71}$$

A.6.3 Quark Mass

As our simulation is based on the Wilson quark formulation, the physical quark mass in our simulation m is related to the bare quark mass which is an input to the simulation m_0 by an additive renormalisation, which being a non-perturbative quantity can not be calculated a priori. As such we must have a method of determining the physical quark mass in the simulation in order to determine our proximity to the chiral point $m = 0$ and to observe the scaling of mesonic observables with m.

The most straight-forward such method is via the *partially conserved axial current mass* or PCAC mass. We define the continuum non-singlet axial and

pseudoscalar currents as

$$A_\mu(\mathbf{x}) = \bar{\psi}_1(\mathbf{x})\gamma_\mu\gamma_5\psi_2(\mathbf{x}), \qquad P(\mathbf{x}) = \bar{\psi}_1(\mathbf{x})\gamma_5\psi_2(\mathbf{x}). \tag{A.72}$$

We see that these are continuum versions of our $\mathcal{O}^L_{\gamma_\mu\gamma_5}$ and $\mathcal{O}^L_{\gamma_5}$. From the Ward identity for the axial transformation $\psi \to e^{i\alpha\gamma_5}\psi$ we obtain for the divergence of the axial current

$$\partial_\mu A_\mu(\mathbf{x}) = -2mP(\mathbf{x}), \tag{A.73}$$

where m is the physical quark mass, as above. From this we obtain

$$\frac{\partial}{\partial t}\int d^3x\, \langle A_0(\vec{x},t)\mathcal{O}_{\gamma_5}\rangle = -2m\int d^3x \langle P(\vec{x},t)\mathcal{O}_{\gamma_5}\rangle, \tag{A.74}$$

where $\mathcal{O}_{\gamma_5}$ is any bilinear quark operator with the symmetries of a pseudoscalar current. Taking a lattice version of this, and choosing for $\mathcal{O}_{\gamma_5}$ any of the local or smeared lattice pseudoscalar currents we have previously constructed, we see we can define an effective PCAC quark mass via

$$m(\tau) = \frac{m_{\mathrm{PS}}}{\sinh(am_{\mathrm{PS}})}\frac{f^{\mathrm{LS}}_{\mathrm{AP}}(\tau-a) - f^{\mathrm{LS}}_{\mathrm{AP}}(\tau+a)}{4f^{LS}_{\mathrm{PP}}(\tau)}, \tag{A.75}$$

where we define f_{AP} to be $f_{\gamma_0\gamma_5,\gamma_5}$. The prefactor of $\frac{m_{\mathrm{PS}}}{\sinh(am_{\mathrm{PS}})}$ arises by a choice of the lattice finite difference operator which more accurately represents the continuum derivative on f_{AP}. The correlators f^{LS} are constructed with a local sink, and a source which can be local, or involve any smearing.

A.6.4 Pseudoscalar decay constant

Similarly to (A.67) the correlator f_{AP} has an asymptotic behaviour:

$$\begin{aligned} f_{\mathrm{AP}}(\tau) \overset{\tau\to\infty}{\longrightarrow} &\frac{1}{2m_{\mathrm{PS}}}\langle 0|\mathcal{O}^{\mathrm{SINK}\dagger}_{\gamma_0\gamma_5}(\vec{0},0)|\gamma_5\rangle\langle\gamma_5|\mathcal{O}^{\mathrm{SRCE}}_{\gamma_5}(\vec{0},0)|0\rangle e^{-m_{\mathrm{PS}}\tau} \\ \equiv &A_{\mathrm{AP}}e^{-m_{\mathrm{PS}}\tau}. \end{aligned} \tag{A.76}$$

In contrast to (A.68) however, the contribution to f_{AP} from propagation around the lattice comes with the opposite sign, so on a lattice with finite temporal

extent,

$$\begin{aligned} f_{\mathrm{AP}}(\tau) \rightarrow & A_{\mathrm{AP}} \left(e^{-m_{\mathrm{PS}}\tau} - e^{-m_{\mathrm{PS}}(L_t-\tau)} \right) \\ \equiv & A_{\mathrm{AP}} \mathrm{hs}(\tau, m_{\mathrm{PS}}, L_t). \end{aligned} \tag{A.77}$$

Now we define the *pseudoscalar decay constant* F_{PS} as

$$m_{\mathrm{PS}} F_{\mathrm{PS}} = \langle 0 | \mathcal{O}^{\mathrm{L}}_{\gamma_0\gamma_5}(\vec{0}, 0) | \gamma_5 \rangle. \tag{A.78}$$

Combining this with the Ward identity for f_{AP} we can define an effective observable for F_{PS} as

$$F^{\mathrm{S}}_{\mathrm{PS}}(\tau) = \frac{2m(\tau) G^{\mathrm{S}}_{\mathrm{PS}}(\tau)}{m^2_{\mathrm{PS}}(\tau)}. \tag{A.79}$$

The superscript S here indicates that this is valid for observables obtained from any smeared correlator, provided the corresponding definition of G_{PS} is used, from (A.70) or (A.71).

Bibliography

[1] W.N. Cottingham and D.A. Greenwood. An introduction to the standard model of particle physics. 2007.

[2] K. Nakamura et al. Review of particle physics. *J. Phys.*, G37:075021, 2010.

[3] U. Dore and D. Orestano. Experimental results on neutrino oscillations. *Rept. Prog. Phys.*, 71:106201, 2008, 0811.1194.

[4] Peter W. Higgs. Broken Symmetries and the Masses of Gauge Bosons. *Phys.Rev.Lett.*, 13:508–509, 1964.

[5] F. Englert and R. Brout. Broken Symmetry and the Mass of Gauge Vector Mesons. *Phys.Rev.Lett.*, 13:321–322, 1964.

[6] G.S. Guralnik, C.R. Hagen, and T.W.B. Kibble. Global Conservation Laws and Massless Particles. *Phys.Rev.Lett.*, 13:585–587, 1964.

[7] Nicola Cabibbo. Unitary Symmetry and Leptonic Decays. *Phys.Rev.Lett.*, 10: 531–533, 1963.

[8] Makoto Kobayashi and Toshihide Maskawa. CP Violation in the Renormalizable Theory of Weak Interaction. *Prog.Theor.Phys.*, 49:652–657, 1973.

[9] Hironari Miyazawa. Spinor Currents and Symmetries of Baryons and Mesons. *Phys.Rev.*, 170:1586–1590, 1968.

[10] Yu.A. Golfand and E.P. Likhtman. Extension of the Algebra of Poincare Group Generators and Violation of p Invariance. *JETP Lett.*, 13:323–326, 1971.

[11] J. Wess and B. Zumino. Supergauge Transformations in Four-Dimensions. *Nucl.Phys.*, B70:39–50, 1974.

[12] Luigi Del Debbio, Eoin Kerrane, and Rodolfo Russo. Mass corrections in string theory and lattice field theory. *Phys. Rev.*, D80:025003, 2009, 0812.3129.

[13] Joseph D. Lykken. Beyond the Standard Model. 2010, 1005.1676.

[14] Combination of higgs searches. 2011.

[15] Combination of the searches for the higgs boson in 1 fb1 of data taken with the atlas detector at 7 tev center-of-mass energy. Technical Report ATLAS-CONF-2011-112, CERN, Geneva, Aug 2011.

[16] Search for supersymmetry in all-hadronic events with missing energy. 2011.

[17] Search for w' (or techni-rho) to wz. 2011.

[18] D. J. Gross and Frank Wilczek. ULTRAVIOLET BEHAVIOR OF NON-ABELIAN GAUGE THEORIES. *Phys. Rev. Lett.*, 30:1343–1346, 1973.

[19] H. David Politzer. RELIABLE PERTURBATIVE RESULTS FOR STRONG INTERACTIONS? *Phys. Rev. Lett.*, 30:1346–1349, 1973.

[20] J. Gasser and H. Leutwyler. Chiral Perturbation Theory to One Loop. *Annals Phys.*, 158:142, 1984.

[21] J. Gasser and H. Leutwyler. Chiral Perturbation Theory: Expansions in the Mass of the Strange Quark. *Nucl.Phys.*, B250:465, 1985.

[22] H. Leutwyler. Principles of chiral perturbation theory. 1994, hep-ph/9406283.

[23] Kenneth D. Lane. Technicolor 2000. 2000, hep-ph/0007304.

[24] Christopher T. Hill and Elizabeth H. Simmons. Strong dynamics and electroweak symmetry breaking. *Phys. Rept.*, 381:235–402, 2003, hep-ph/0203079.

[25] Steven Weinberg. Implications of Dynamical Symmetry Breaking. *Phys. Rev.*, D13:974–996, 1976.

[26] Steven Weinberg. Implications of Dynamical Symmetry Breaking: An Addendum. *Phys.Rev.*, D19:1277–1280, 1979. (For original paper see Phys.Rev.D13:974-996,1976).

[27] Leonard Susskind. Dynamics of Spontaneous Symmetry Breaking in the Weinberg- Salam Theory. *Phys. Rev.*, D20:2619–2625, 1979.

[28] Savas Dimopoulos and Leonard Susskind. Mass Without Scalars. *Nucl.Phys.*, B155:237–252, 1979.

[29] Estia Eichten and Kenneth D. Lane. Dynamical Breaking of Weak Interaction Symmetries. *Phys.Lett.*, B90:125–130, 1980.

[30] Stuart Raby, Savas Dimopoulos, and Leonard Susskind. Tumbling Gauge Theories. *Nucl.Phys.*, B169:373, 1980.

[31] Michael Edward Peskin and Tatsu Takeuchi. A New constraint on a strongly interacting Higgs sector. *Phys. Rev. Lett.*, 65:964–967, 1990.

[32] Michael Edward Peskin and Tatsu Takeuchi. Estimation of oblique electroweak corrections. *Phys. Rev.*, D46:381–409, 1992.

[33] Tom Banks and A. Zaks. On the Phase Structure of Vector-Like Gauge Theories with Massless Fermions. *Nucl. Phys.*, B196:189, 1982.

[34] Estia Eichten and Kenneth Lane. Low-scale technicolor at the Tevatron and LHC. *Phys.Lett.*, B669:235–238, 2008, 0706.2339.

[35] Thomas Appelquist and Francesco Sannino. The Physical Spectrum of Conformal SU(N) Gauge Theories. *Phys. Rev.*, D59:067702, 1999, hep-ph/9806409.

[36] Masafumi Kurachi and Robert Shrock. Behavior of the S parameter in the crossover region between walking and QCD-like regimes of an SU(N) gauge theory. *Phys. Rev.*, D74:056003, 2006, hep-ph/0607231.

[37] Dennis D. Dietrich and Francesco Sannino. Walking in the SU(N). *Phys. Rev.*, D75:085018, 2007, hep-ph/0611341.

[38] A. Armoni, M. Shifman, and G. Veneziano. Exact results in non-supersymmetric large N orientifold field theories. *Nucl. Phys.*, B667:170–182, 2003, hep-th/0302163.

[39] A. Armoni, M. Shifman, and G. Veneziano. SUSY relics in one-flavor QCD from a new 1/N expansion. *Phys. Rev. Lett.*, 91:191601, 2003, hep-th/0307097.

[40] Francesco Sannino and Kimmo Tuominen. Orientifold theory dynamics and symmetry breaking. *Phys. Rev.*, D71:051901, 2005, hep-ph/0405209.

[41] N. Evans and F. Sannino. Minimal walking technicolour, the top mass and precision electroweak measurements. 2005, hep-ph/0512080.

[42] Edward Witten. An SU(2) anomaly. *Phys. Lett.*, B117:324–328, 1982.

[43] Dennis D. Dietrich, Francesco Sannino, and Kimmo Tuominen. Light composite Higgs from higher representations versus electroweak precision measurements: Predictions for LHC. *Phys. Rev.*, D72:055001, 2005, hep-ph/0505059.

[44] Roshan Foadi, Mads T. Frandsen, Thomas A. Ryttov, and Francesco Sannino. Minimal Walking Technicolor: Set Up for Collider Physics. *Phys. Rev.*, D76: 055005, 2007, 0706.1696.

[45] Jeppe R. Andersen, Tuomas Hapola, and Francesco Sannino. W' and Z' limits for Minimal Walking Technicolor. 2011, 1105.1433.

[46] Thomas A. Ryttov and Robert Shrock. Technicolor Models with Color-Singlet Technifermions and their Ultraviolet Extensions. 2011, 1107.3572.

[47] Ari J. Hietanen, Kari Rummukainen, and Kimmo Tuominen. Evolution of the coupling constant in SU(2) lattice gauge theory with two adjoint fermions. *Phys. Rev.*, D80:094504, 2009, 0904.0864.

[48] Francis Bursa, Luigi Del Debbio, Liam Keegan, Claudio Pica, and Thomas Pickup. Mass anomalous dimension in SU(2) with two adjoint fermions. *Phys. Rev.*, D81:014505, 2010, 0910.4535.

[49] Simon Catterall, Luigi Del Debbio, Joel Giedt, and Liam Keegan. MCRG Minimal Walking Technicolor. 2011, 1108.3794. * Temporary entry *.

[50] Simon Catterall and Francesco Sannino. Minimal walking on the lattice. *Phys. Rev.*, D76:034504, 2007, 0705.1664.

[51] Luigi Del Debbio, Agostino Patella, and Claudio Pica. Higher representations on the lattice: numerical simulations. SU(2) with adjoint fermions. *Phys. Rev.*, D81: 094503, 2010, 0805.2058.

[52] Simon Catterall, Joel Giedt, Francesco Sannino, and Joe Schneible. Phase diagram of SU(2) with 2 flavors of dynamical adjoint quarks. *JHEP*, 11:009, 2008, 0807.0792.

[53] Ari J. Hietanen, Jarno Rantaharju, Kari Rummukainen, and Kimmo Tuominen. Spectrum of SU(2) lattice gauge theory with two adjoint Dirac flavours. *JHEP*, 05:025, 2009, 0812.1467.

[54] L. Del Debbio, B. Lucini, A. Patella, C. Pica, and A. Rago. Conformal vs confining scenario in SU(2) with adjoint fermions. *Phys. Rev.*, D80:074507, 2009, 0907.3896.

[55] E. Shintani et al. S-parameter and pseudo-Nambu-Goldstone boson mass from lattice QCD. *Phys. Rev. Lett.*, 101:242001, 2008, 0806.4222.

[56] Peter A. Boyle, Luigi Del Debbio, Jan Wennekers, and James M. Zanotti. The S Parameter in QCD from Domain Wall Fermions. 2009, 0909.4931.

[57] Thomas Appelquist et al. Parity Doubling and the S Parameter Below the Conformal Window. *Phys. Rev. Lett.*, 106:231601, 2011, 1009.5967.

[58] Luigi Del Debbio, Biagio Lucini, Agostino Patella, Claudio Pica, and Antonio Rago. The infrared dynamics of Minimal Walking Technicolor. *Phys. Rev.*, D82: 014510, 2010, 1004.3206.

[59] Luigi Del Debbio, Biagio Lucini, Agostino Patella, Claudio Pica, and Antonio Rago. Mesonic spectroscopy of Minimal Walking Technicolor. *Phys. Rev.*, D82: 014509, 2010, 1004.3197.

[60] Luigi Del Debbio and Roman Zwicky. Hyperscaling relations in mass-deformed conformal gauge theories. *Phys. Rev.*, D82:014502, 2010, 1005.2371.

[61] Luigi Del Debbio and Roman Zwicky. Scaling relations for the entire spectrum in mass-deformed conformal gauge theories. 2010, 1009.2894.

[62] Francis Bursa, Luigi Del Debbio, Liam Keegan, Claudio Pica, and Thomas Pickup. Mass anomalous dimension and running of the coupling in SU(2) with six fundamental fermions. *PoS*, LATTICE2010:070, 2010, 1010.0901.

[63] Y. Iwasaki, K. Kanaya, S. Sakai, and T. Yoshie. Quark confinement and number of flavors in strong coupling lattice QCD. *Phys.Rev.Lett.*, 69:21–24, 1992.

[64] Y. Iwasaki, K. Kanaya, S. Kaya, S. Sakai, and T. Yoshie. Phase structure of lattice QCD for general number of flavors. *Phys.Rev.*, D69:014507, 2004, hep-lat/0309159.

[65] Thomas Appelquist, George T. Fleming, and Ethan T. Neil. Lattice study of the conformal window in QCD-like theories. *Phys.Rev.Lett.*, 100:171607, 2008, 0712.0609.

[66] Albert Deuzeman, Maria Paola Lombardo, and Elisabetta Pallante. The Physics of eight flavours. *Phys.Lett.*, B670:41–48, 2008, 0804.2905.

[67] M. Hayakawa, K.-I. Ishikawa, Y. Osaki, S. Takeda, S. Uno, et al. Running coupling constant of ten-flavor QCD with the Schródinger functional method. *Phys.Rev.*, D83:074509, 2011, 1011.2577.

[68] Thomas Appelquist, George T. Fleming, and Ethan T. Neil. Lattice Study of Conformal Behavior in SU(3) Yang-Mills Theories. *Phys.Rev.*, D79:076010, 2009, 0901.3766.

[69] A. Deuzeman, M.P. Lombardo, and E. Pallante. Evidence for a conformal phase in SU(N) gauge theories. *Phys.Rev.*, D82:074503, 2010, 0904.4662.

[70] Anna Hasenfratz. Conformal or Walking? Monte Carlo renormalization group studies of SU(3) gauge models with fundamental fermions. *Phys.Rev.*, D82: 014506, 2010, 1004.1004.

[71] Etsuko Itou, Tatsumi Aoyama, Masafumi Kurachi, C.-J.David Lin, Hideo Matsufuru, et al. Search for the IR fixed point in the Twisted Polyakov Loop scheme (II). *PoS*, LATTICE2010:054, 2010, 1011.0516.

[72] Anna Hasenfratz. Infrared fixed point of the 12-fermion SU(3) gauge model based on 2-lattice MCRG matching. 2011, 1106.5293. * Temporary entry *.

[73] Zoltan Fodor, Kieran Holland, Julius Kuti, Daniel Nogradi, and Chris Schroeder. Twelve massless flavors and three colors below the conformal window. *Phys.Lett.*, B703:348–358, 2011, 1104.3124. * Temporary entry *.

[74] Xiao-Yong Jin and Robert D. Mawhinney. Lattice QCD with 8 and 12 degenerate quark flavors. *PoS*, LAT2009:049, 2009, 0910.3216.

[75] Thomas Appelquist, George T. Fleming, Meifeng Lin, Ethan T. Neil, and David A. Schaich. Lattice Simulations and Infrared Conformality. *Phys.Rev.D*, 2011, 1106.2148. * Temporary entry *.

[76] Alexander Belyaev, Roshan Foadi, Mads T. Frandsen, Matti Jarvinen, Fracesco Sannino, et al. Technicolor Walks at the LHC. *Phys.Rev.*, D79:035006, 2009, 0809.0793.

[77] Yigal Shamir, Benjamin Svetitsky, and Thomas DeGrand. Zero of the discrete beta function in SU(3) lattice gauge theory with color sextet fermions. 2008, 0803.1707.

[78] Thomas DeGrand, Yigal Shamir, and Benjamin Svetitsky. Phase structure of SU(3) gauge theory with two flavors of symmetric-representation fermions. *Phys.Rev.*, D79:034501, 2009, 0812.1427.

[79] Thomas DeGrand. Volume scaling of Dirac eigenvalues in SU(3) lattice gauge theory with color sextet fermions. 2009, 0906.4543.

[80] Thomas DeGrand. Finite-size scaling tests for SU(3) lattice gauge theory with color sextet fermions. *Phys.Rev.*, D80:114507, 2009, 0910.3072.

[81] Thomas DeGrand, Yigal Shamir, and Benjamin Svetitsky. Running coupling and mass anomalous dimension of SU(3) gauge theory with two flavors of symmetric-representation fermions. *Phys.Rev.*, D82:054503, 2010, 1006.0707.

[82] Zoltan Fodor, Kieran Holland, Julius Kuti, Daniel Nogradi, and Chris Schroeder. Chiral properties of SU(3) sextet fermions. *JHEP*, 0911:103, 2009, 0908.2466.

[83] Zoltan Fodor, Kieran Holland, Julius Kuti, Daniel Nogradi, and Chris Schroeder. Chiral symmetry breaking in fundamental and sextet fermion representations of SU(3) color. 2011, 1103.5998. * Temporary entry *.

[84] Eoin Kerrane et al. Improved Spectroscopy of Minimal Walking Technicolor. *PoS*, LATTICE2010:058, 2010, 1011.0607.

[85] Francis Bursa, Luigi Del Debbio, David Henty, Eoin Kerrane, Biagio Lucini, et al. Improved Lattice Spectroscopy of Minimal Walking Technicolor. *Phys.Rev.*, D84: 034506, 2011, 1104.4301.

[86] Robert G. Edwards and Balint Joo. The Chroma software system for lattice QCD. *Nucl. Phys. Proc. Suppl.*, 140:832, 2005, hep-lat/0409003.

[87] Neal Madras and Alan D. Sokal. The Pivot algorithm: a highly efficient Monte Carlo method for selfavoiding walk. *J.Statist.Phys.*, 50:109–186, 1988.

[88] Julian S. Schwinger. On Quantum electrodynamics and the magnetic moment of the electron. *Phys. Rev.*, 73:416–417, 1948.

[89] D. Hanneke, S. Fogwell, and G. Gabrielse. New Measurement of the Electron Magnetic Moment and the Fine Structure Constant. *Phys. Rev. Lett.*, 100:120801, 2008, 0801.1134.

[90] S. Laporta and E. Remiddi. Status of the QED prediction of the electron (g - 2). *Nucl. Phys. Proc. Suppl.*, 181-182:10–14, 2008.

[91] G. W. Bennett et al. Final report of the muon E821 anomalous magnetic moment measurement at BNL. *Phys. Rev.*, D73:072003, 2006, hep-ex/0602035.

[92] Fred Jegerlehner and Andreas Nyffeler. The Muon g-2. *Phys. Rept.*, 477:1–110, 2009, 0902.3360.

[93] Masashi Hayakawa, Thomas Blum, Taku Izubuchi, and Norikazu Yamada. Hadronic light-by-light scattering contribution to the muon g-2 from lattice QCD: Methodology. *PoS*, LAT2005:353, 2006, hep-lat/0509016.

[94] T. Blum and S. Chowdhury. Hadronic contributions to g-2 from the lattice. *Nucl. Phys. Proc. Suppl.*, 189:251–256, 2009.

[95] F. Jegerlehner. Muon g - 2 update. *Nucl. Phys. Proc. Suppl.*, 181-182:26–31, 2008.

[96] Eduardo de Rafael. Hadronic contributions to the muon g-2 and low-energy QCD. *Phys. Lett.*, B322:239–246, 1994, hep-ph/9311316.

[97] T. Blum. Lattice calculation of the lowest order hadronic contribution to the muon anomalous magnetic moment. ((U)). *Phys. Rev. Lett.*, 91:052001, 2003, hep-lat/0212018.

[98] M. Gockeler et al. Vacuum polarisation and hadronic contribution to muon g-2 from lattice QCD. *Nucl. Phys.*, B688:135–164, 2004, hep-lat/0312032.

[99] T. Blum. Lattice calculation of the lowest order hadronic contribution to the muon anomalous magnetic moment: An update with Kogut-Susskind fermions. *Nucl. Phys. Proc. Suppl.*, 129:904–906, 2004, hep-lat/0310064.

[100] C. Aubin and T. Blum. Calculating the hadronic vacuum polarization and leading hadronic contribution to the muon anomalous magnetic moment with improved staggered quarks. *Phys. Rev.*, D75:114502, 2007, hep-lat/0608011.

[101] Michele Della Morte, Benjamin Jager, Andreas Juttner, and Hartmut Wittig. The leading hadronic vacuum polarisation on the lattice. 2010, 1011.5793.

[102] Xu Feng, Karl Jansen, Marcus Petschlies, and Dru B. Renner. Two-flavor QCD correction to lepton magnetic moments at leading-order in the electromagnetic coupling. 2011, 1103.4818.

[103] Peter Boyle, Luigi Del Debbio, Eoin Kerrane, and James Zanotti. Lattice Determination of the Hadronic Contribution to the Muon $g-2$ using Dynamical Domain Wall Fermions. 2011, 1107.1497.

[104] Shigemi Ohta. Nucleon structure from 2+1 flavor domain wall QCD at nearly physical pion mass. 2011, 1102.0551.

[105] RBC/UKQCD. Continuum Limit Physics from 2+1 Flavor Domain Wall QCD II.

[106] C. Allton et al. Physical Results from 2+1 Flavor Domain Wall QCD and SU(2) Chiral Perturbation Theory. *Phys. Rev.*, D78:114509, 2008, 0804.0473.

[107] Y. Aoki et al. Continuum Limit Physics from 2+1 Flavor Domain Wall QCD. 2010, 1011.0892.

[108] Vadim Furman and Yigal Shamir. Axial symmetries in lattice QCD with Kaplan fermions. *Nucl. Phys.*, B439:54–78, 1995, hep-lat/9405004.

[109] Michele Della Morte and Andreas Juttner. Quark disconnected diagrams in chiral perturbation theory. *JHEP*, 11:154, 2010, 1009.3783.

[110] K. G. Chetyrkin, Johann H. Kuhn, and M. Steinhauser. Three-loop polarization function and $O(\alpha(s)^2)$ corrections to the production of heavy quarks. *Nucl. Phys.*, B482:213–240, 1996, hep-ph/9606230.

[111] R. Arthur and P. A. Boyle. Step Scaling with off-shell renormalisation. *Phys. Rev.*, D83:114511, 2011, 1006.0422.

[112] M. A. Donnellan et al. Lattice Results for Vector Meson Couplings and Parton Distribution Amplitudes. *PoS*, LAT2007:369, 2007, 0710.0869.

[113] Andreas Juttner and Michele Della Morte. New ideas for g-2 on the lattice. *PoS*, LAT2009:143, 2009, 0910.3755.

[114] Ph. Hagler et al. Nucleon Generalized Parton Distributions from Full Lattice QCD. *Phys. Rev.*, D77:094502, 2008, 0705.4295.

[115] J. D. Bratt et al. Nucleon structure from mixed action calculations using 2+1 flavors of asqtad sea and domain wall valence fermions. *Phys. Rev.*, D82:094502, 2010, 1001.3620.

[116] Krzysztof Cichy, Gregorio Herdoiza, and Karl Jansen. Continuum Limit of Overlap Valence Quarks on a Twisted Mass Sea. *Nucl.Phys.*, B847:179–196, 2011, 1012.4412.

[117] David J. Antonio et al. Localization and chiral symmetry in 3 flavor domain wall QCD. *Phys. Rev.*, D77:014509, 2008, 0705.2340.

[118] Anna Hasenfratz and Francesco Knechtli. Flavor symmetry and the static potential with hypercubic blocking. *Phys. Rev.*, D64:034504, 2001, hep-lat/0103029.

[119] Kenneth G. Wilson. Confinement of Quarks. *Phys.Rev.*, D10:2445–2459, 1974.

[120] N. Metropolis, A.W. Rosenbluth, M.N. Rosenbluth, A.H. Teller, and E. Teller. Equation of state calculations by fast computing machines. *J.Chem.Phys.*, 21: 1087–1092, 1953.

[121] A. Zichichi. New Phenomena in Subnuclear Physics. Part A. Proceedings: First Half of the 1975 International School of Subnuclear Physics, Erice, Sicily, Jul 11-Aug 1 1975. 1977.

[122] Holger Bech Nielsen and M. Ninomiya. Absence of Neutrinos on a Lattice. 1. Proof by Homotopy Theory. *Nucl.Phys.*, B185:20, 1981.

[123] Paul H. Ginsparg and Kenneth G. Wilson. A Remnant of Chiral Symmetry on the Lattice. *Phys.Rev.*, D25:2649, 1982.

[124] Martin Luscher. Exact chiral symmetry on the lattice and the Ginsparg-Wilson relation. *Phys.Lett.*, B428:342–345, 1998, hep-lat/9802011.

[125] David B. Kaplan. A Method for simulating chiral fermions on the lattice. *Phys.Lett.*, B288:342–347, 1992, hep-lat/9206013.

[126] Yigal Shamir. Chiral fermions from lattice boundaries. *Nucl.Phys.*, B406:90–106, 1993, hep-lat/9303005.

[127] D.J. Antonio et al. First results from 2+1 Flavor Domain Wall QCD: Mass Spectrum, Topology Change and Chiral Symmetry with L(s) = 8. *Phys.Rev.*, D75:114501, 2007, hep-lat/0612005.

[128] Thomas A. DeGrand and Richard D. Loft. Wave function tests for lattice QCD spectroscopy. *Comput. Phys. Commun.*, 65:84–91, 1991.

[129] S. Elitzur. Impossibility of Spontaneously Breaking Local Symmetries. *Phys. Rev.*, D12:3978–3982, 1975.

[130] Jeffrey E. Mandula and Michael Ogilvie. Efficient gauge fixing via overrelaxation. *Phys.Lett.*, B248:156–158, 1990.

[131] Leonardo Giusti, M.L. Paciello, C. Parrinello, S. Petrarca, and B. Taglienti. Problems on lattice gauge fixing. *Int.J.Mod.Phys.*, A16:3487–3534, 2001, hep-lat/0104012.

[132] George T. Fleming, Saul D. Cohen, Huey-Wen Lin, and Victor Pereyra. Excited-State Effective Masses in Lattice QCD. *Phys. Rev.*, D80:074506, 2009, 0903.2314.

Publications

- Luigi Del Debbio, Eoin Kerrane, and Rodolfo Russo. Mass corrections in string theory and lattice field theory. *Phys. Rev.*, D80:025003, 2009, 0812.3129.
- Eoin Kerrane et al. Improved Spectroscopy of Minimal Walking Technicolor. *PoS*, LATTICE2010:058, 2010, 1011.0607.
- Francis Bursa et al. Improved Lattice Spectroscopy of Minimal Walking Technicolor. *Phys.Rev.*, D84:034506, 2011, 1104.4301.
- Peter Boyle, Luigi Del Debbio, Eoin Kerrane, and James Zanotti. Lattice Determination of the Hadronic Contribution to the Muon $g-2$ using Dynamical Domain Wall Fermions. 2011, 1107.1497.